Wireless Location:
From Theory to Practice

Lei Qiu

B.E. (Nanjing University of Posts and Telecommunications)
M.Phil. (The Australian National University)

October 2008

Department of Information Engineering
Research School of Information Sciences and Engineering
The Australian National University

Declaration

I declare that this thesis embodies my own research work and that it is composed by myself. Where appropriate, I have made acknowledgments to the work of others. The contents of this thesis have not been submitted for a higher degree to any other university or institution.

Much of the work in this thesis has been published or has been submitted for publication in refereed journals and conference proceedings. In some cases the conference papers contain material overlapping with the journal publications. The following is a list of these publications.
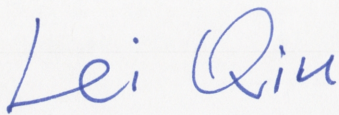
Journal Publications

1. L. Qiu and R. A. Kennedy, "Adaptive Prediction of Wireless Signal Spatial Distribution with application in WLAN location," in preparation for submitting to *International Journal of Adaptive Control and Signal Processing*, Wiley.

2. L. Qiu and R. A. Kennedy, "Limits of Dimensionality in Correlated Random Multipath Fields," in preparation for submitting to *IEEE* Trans. Signal Processing.

3. L. Qiu and R. A. Kennedy, "Optimal Sensor Positions for Complete Wavefield Reproduction," in preparation.

Conference Publications

1. L. Qiu, D. Jiang and L. Hanlen, "Neural Network Prediction of Radio Propagation," in *Proceedings of the 6th Australian Communications Theory Workshop*, pp. 252–257, Brisbane, Australia, Feb. 2005.

2. L. Qiu and R. A. Kennedy, "Spatial Correlation based Degrees of Freedom of Multipath," in *IEEE Information Theory Workshop (ITW)*, pp.663-667, Chengdu, China, Oct. 22 – 26, 2006.

3. L. Qiu, R. A. Kennedy and T. Betlehem, "Degrees of Freedom of Correlated Multipath," in *International Conference on Acoustics, Speech, and Signal Processing (ICASSP)*, Vol. 2, pp. 857-860, Honolulu, Hawai'i, U.S.A., Apr. 15 – 20, 2007.

4. L. Qiu and R. A. Kennedy, "Wireless Location Using Pattern Matching Techniques in Fixed Wireless Communication Networks," in *International Symposium on Communications and Information Technologies (ISCIT)*, pp. 1054–1059, Sydney, Australia, Oct. 17 – 19, 2007.

5. L. Qiu and R. A. Kennedy, "Multipath Richness of Random Multipath Wavefields," in preparation.

The research in this thesis has been performed jointly with Prof. Rodney A. Kennedy and Dr. Leif Hanlen. The majority, approximately 75%, of this work was my own.

Lei Qiu

Lei Qiu

October 2008

Department of Information Engineering

Research School of Information Science and Engineering

The Australian National University

Canberra ACT 0200

Australia

Acknowledgement

It is time to thank The Australian National University and National ICT Australia (NICTA). Without their support, I have no way to complete my Ph.D. study.

It is my great pleasure to acknowledge the many people who helped me to finish this thesis. I would like to express my gratitude to Professor Rodney A. Kennedy and Dr. Leif Hanlen for their enthusiasm, inspiration and insight in guiding and coaching me. With their patience and great efforts in explaining abstract mathematical concepts, they helped to turn mathematics into fun to me. Throughout my thesis writing, Professor Kennedy provided valuable feedback to me to improve my writing.

I would like to thank Dr. Danchi Jiang (now with University of Tasmania) who helped me a lot to the first publishing in my Ph.D. The first paper is very important to me; it breaks the ice and encourages me to go further in wireless communications research. I am grateful to Dr. Paul Malholm (NICTA) who illustrates the beauty of mathematics to me. From him, I got the chance to sip the principles of engineering from a mathematician's viewpoint. I wish to thank Dr. Terence Betlehem. We have had many fruitful and interesting talks which deserve special mention.

I am indebted to my many student colleagues for accompanying me the past a few years in Canberra. Specially, I spent happy times with Ming (Matt) Ruan, Ying Chen, Sandra(Xiaoqin) Chen, Hao Shen, Michael I. Y. Williams, Tharaka A. Lamahewa, Rasika R. Perera, Wen Zhang, Glenn N. Dickins, Lin Luo, Sanlin Xu and Huan Zhang.

I want to thank Debbie Pioch for her administrative support. It is always nice to talk to this lady.

I wish to thank my wife, Qin, and my son, Tianrui (Ricky), for their support in helping me going through the most difficult times.

Lastly and most importantly, I wish to thank my mother, Zhi'e Wang. She gave birth to me, raised me, cared me, taught me and loved me so much. I dedicate this thesis to her.

Abstract

Locating and tracking targets using wireless-waves can be traced back more than sixty years, with early applications in radar and sonar. Recently, the Federal Communications Commission (FCC), together with the European recommendation E112, required wireless communication systems to locate a E911/E112 caller's position to within tens of meters accuracy. This has stimulated research interest in how to achieve such high accuracy wireless location. In this thesis, we have endeavored to analyse wireless location problem in both the theoretical and practical aspects.

Improving location accuracy is a topic of great interest in wireless location research. Our objective, in the theoretical aspects of developing a wireless location system, is to determine the fundamental limits of wireless location accuracy and resolution. Towards this goal, we define "location signature" and "location resolution" in our research, using methods derived from wave propagation and functional representations including spherical harmonic decompositions for the 3D angular dependence. We investigate the performance limits (resolution) of a mobile terminal's location under such an arbitrary wireless wave propagation environment. In particular, we analyze the effect of multipath propagation, generally the bane of wireless communication, on the wireless location resolution. Curiously, our findings reveal that richer multipath in a wireless terminal's spatial region can be beneficial to improving the location resolution, assuming the incoming multipaths are correlated in angle.

In the practical aspects of developing a wireless location system, we begin with a "virtual" radio wave propagation model for the wireless environment. With this we can predict the spatial distribution of the radio signal. We proposed an adaptive algorithm to learn this "virtual" environment based on the wireless signal strength measured in actual field measurements. Also, we introduced a Channel Impulse Response (CIR) fingerprint location solution, which takes advantages of the features of fixed wireless network. Through pattern matching a practical solution is determined for the location problem.

Glossary of Notations

Abbreviations

AoA	Angle of Arrival
AP	Access Point
AWGN	Additive White Gaussian Noise
APS	Angular Power Spectrum
BPF	Bandpass Filter
BS	Base Station
CDMA	Code Division Multiplex Access
CIR	Channel Impulse Response
dB	decibel
DoA	Directional of Arrival
DoF	Degree of Freedom
EIRP	Equivalent Isotropically Radiated Power
FB	Fractional Bandwidth
E-OTD	Existing Observed Time Difference
FCC	Federal Communications Committee
FOBE	Fraction-out-of-band Energy
FWN	Fixed Wireless Network
GPS	Global Position System
ICI	Interchip Interference
IF	Intermediate Frequency
ISI	Intersymbol Interference
KLE	Karhunen-Loeve Expansion
KKT	Karush-Kuhn-Tucker (KKT)
LSC	Location Service Center
LPF	Lowpass Filter
LTI	Linear Time Invariant
MF	Matched Filter
MHT	Multi-hypothesis Tracking
MIMO	Multiple Input Multiple Output
ML	Maximum Likelihood
MLE	Maximum Likelihood Estimator
MMSE	Minimum Mean Squared Error
MP	Multipath Profile
MRC	Maximum Ratio Combining
MS	Mobile Subscriber
MSN	Maximum Scanning Number
MTI	Moving-Target Indication
NLOS	Non Line-of-Sight

NN	Nearest Neighbour
KNN	K Nearest Neighbour
KWNN	K Weighted Nearest Neighbour
OS	Operating System
OTDOA	Observed Time Difference of Arrival
pdf	probability density function
pmf	probability mass function
PN	Pseudo Noise (codes)
PSD	Power Spectral Density
RBF	Radial Basis Function
RF	Radio Frequency
RMS	Root Mean Square
RP	Reference Point
RPS	Radiowave Propagation Simulator
RSS	Radio Signal Strength
RSSDM	Radio Signal Spatial Distribution Map
RTLS	Real Time Localization System
SNR	Signal-to-Noise Ratio
SSS	Site Survey Solution
SVD	Singular Value Decomposition
SVM	Support Vector Machine
TDOA	Time Difference of Arrival
TOA	Time of Arrival
VPE	Virtual Propagation Environment
WCDMA	Wideband Code Division Multiplex Access
WLAN	Wireless Local Area Network
WSS	Wide-sense Stationary
WiMAX	World Interoperability for Microwave Access

Mathematical Symbols

$\lVert \cdot \rVert$	Norm
∇^2	Laplacian operator
$\otimes$	Convolution
$\mathbf{x}$	vector
$\mathbf{X}$	matrix
$(\cdot)^*$	Complex conjugate
$(\cdot)^T$	Transpose
$\mathcal{E}$	Expectation
$\mathcal{E}_x[f(x)]$	Expectation of function $f(x)$ with respect to x
Var	Variance
exp	Exponential function
$\text{diag}(\cdots)$	Diagonal matrix
a_ℓ	gain (including phase and magnitude) of the ℓ multipath
d	Differentiation
$\delta(\cdot)$	Dirac delta function
E_0	Electric Field (V/m)
f	Frequency
f_c	Center frequency
$h(t)$	Channel impulse response
$\jmath$	$\sqrt{-1}$, imaginary unit
$J_n(\cdot)$	integer order Bessel function of the first kind
κ	width of the von-Mises distribution
L	Number of multipath
$\mathcal{L}(\cdot,\cdot)$	Loss Function
λ	Wavelength of radio wave
$n(t)$	AWGN
$\mathcal{N}(\cdot,\cdot)$	Normally distributed random process
$\phi(k,\rho)$	Neural Network General Basis Function
∂	Partial differentiation
$p(\cdot)$	pdf for continuous variables and pmf for discrete variables
$\phi(\cdot)$	symbol correlation function
$\Pr(\cdot)$	Probability
$Q(\cdot)$	Complementary Gaussian cumulative distribution function
$\rho(\cdot)$	Spatial correlation function
$r(t)$	Received signal
σ_0^2	Variance of AWGN $n(t)$

sup	Supremum
t	Time
τ	Delay
$\mathbf{\Gamma}(\cdot)$	Covariance matrix
ε_0	Mean energy of the first arriving path in a multipath channel
$\varepsilon(\cdot)$	Normalised mean square error

Contents

List of Figures

List of Tables

Chapter 1

Introduction

1.1 Background

Wireless localization technology aims at determining and estimating the number of targets and their geometrical position and velocity with the aiding of one or multiple reference points (RP). The RPs' positions are generally known in a wireless location system. Location sensitive parameters of wireless waves traversing between the targets and RPs, such as time of arrival (TOA), time difference of arrival (TDOA), direction of arrival (DOA), signal strength, signal noise ratio/signal interference ratio [1,2], and even the message borne in wireless waves, are measured (sampled and stored) and available to help solve localisation problems. Such applications of localization based on wave propagation parameters are primarily, though not strictly, limited to radio waves and acoustic waves. The locating process could be implemented either at target side or at the RP side, and thereby categorised as either a target-side based system or a network-based system.

Among various location systems, radar is perhaps the most well known wireless localization system. The word "radar" is the abbreviation for "RAdio Detection And Ranging" which emphasizes the goal of localization. Early radar systems used radio frequency waveforms and directive antennas to transmit electromagnetic energy into the surrounding environment to detect target. Targets within a specific volume will reflect part of electromagnetic energy (echo) back to radar. The echo is detected by radar and used to extract the target's position information such as traverse time, incident azimuth, amplitude attenuation, phase and velocity, etc. These types of radar systems are called "active" systems since they send out radio wave energy actively. Other types are "passive" systems, which detect targets by electromagnetic waveforms emitted by the target. This type of radar system, such as most military radars, is "silent" without transmitting any waveform in a way

that protects its own position from detection.

1.2   Literature Review

Traditional radar systems demonstrate the principle of wireless localization which is to measure location sensitive parameters of the wireless waveform propagating between target and RP. Real or relative position of the target is estimated based on the measurement results.

Wireless location technology is becoming more and more relevant and popular in today's social daily life. Depending on different categorizing criteria, location systems could be grouped in cellular network versus ad hoc sensor network systems or indoor versus outdoor systems [3]. In a cellular network the mobile subscriber (MS) is the target and the Base Stations (BS) are acting as RPs. Cellular networks are generally characterised by large signal range coverage per BS and delicate device structures at both of MS/BS sides; in wireless Local Area (WLAN) networks, access points are RPs in general. It is assumed that RPs' position are known in a location system. Other standard wireless location systems include Loran-C system, Omega system, Global Position System (GPS), etc.

Time of Arrival (ToA) and Time Difference of Arrival (TDOA) are range measurement methods for wireless location using a time domain approach.

In order to measure TOA, the clock in the target and RPs must be synchronized. That means TOA needs a fully synchronized network. It is expensive for the operator to synchronize MS with all involved BSs fully [4]. Instead, it is more feasible to synchronize the BSs clock excluding the target. The target's clock bias is treated as a parameter when implementing TOA. One example is in GPS where only the satellites are accurately synchronized. TOA performance is affected by synchronization accuracy, chip rate and chip sample rate. In the two-dimension (2D) case, at least three RPs are necessary to produce an unique target position.

One solution to cut the implementation cost is to adopt Time Difference of Arrival (TDOA). In this scenario the MS clock bias with respect to the network can be neglected. Three or more BSs measure the transmitted signal from a target and calculate the arrival time difference between any two BSs pair-wisely. For any two BSs, the target is located geometrically on a hyperbola related with the observed time difference. The crossing points of multiple hyperbolas indicate the most probably target's location. An example is the GSM network using existing observed time difference (E-OTD) [5]. Since the GSM network is not synchronous it is required to compute the clock differences between involved BSs by the Location

Service Centre (LSC). In 2D location estimation E-OTD has accuracy from 50 ms to 500 ms.

Another variation is Observed TDOA (OTDOA) which is designed to operate in wideband-code division multiple access (WCDMA) networks. Due to the inherent characteristic of CDMA, OTDOA encounters challenges such as inband interference, the "Near-Far" problem, and unsynchronized BSs in FDD mode [6].

In the spatial domain, a wireless waveform's incoming angles are detected by smart antennas installed at BS in cellular network [7]. A smart antenna consists of a multiple sensor-elements array whose antenna elements are located in an aperture-limited receiver region. This makes it possible to detect incoming waveform's power and phase spatial distributions [8]. The target's position is determined by the intersection of at least two bearings. More than two BSs are necessary for calculating the target's position, especially in dense multipath propagation environments. The antenna elements are constrained in the receiver region. The authors in [9] demonstrate that the performance of a direction of arrival (DoA) estimator is intrinsically limited by the aperture of the region over which the incoming wavefield is measured. The principle is based on analyzing the information contained in the receiver region. This leads the research approach, for the problem of wireless localization, by considering the spatial aspects of the incoming wavefield coupled to the receiver region. More details will be presented in the first portion of this thesis.

Compared to cellular networks, Wireless Local Access Networks (WLAN) and Ad Hoc Sensor Networks have a much simpler system structure, with less system capacity and lower number of users. They can utilize economical localisaiton methods which suit their network structure. As we know, received Radio Signal Strength (RSS) is inverse proportional to the traversed distance from transmitter to receiver in free space. Thus range estimation is available through the RSS attenuation. The research in [10] is one of the first and most comprehensive studies of 801.11 localisation using RSS—theoretical prediction of the RSS and manual calibrations are considered. A correlation between orientation and measured signal strength was established. Several improved power attenuation models were introduced in [11] which considers wall and floor effects.

Another way to locate a MS in WLAN and/or sensor networks is to utilize a radio signal spatial distribution map (RSSDM). A RSSDM contains MS's radio signal spatial distribution characteristic when MS is at a certain position. For example, in WLAN, several access points (AP) can measure a MS's RSS when the MS is at a known position. The measured RSSs (of multiple APs) are recognized as the MS's location fingerprint at that particular position. The fingerprints at

multiple positions are recorded and thus set up a RSSDM. This is implemented during an offline training stage. In the online stage, when the MS comes in an unknown position, the measured RSS (possibly from multiple BSs) is used to search the database to find most probable position using a pattern matching technique [12, 13]. The fingerprint technique provides a method for mitigating the effects of non line-of-sight (NLOS) propagation, given an appropriate sample grid size during the offline training stage. The training process is generally a considerable amount of work typically due to the dense sample grid and size required.

When multiple RPs are lying on one line, solving the range estimation equation array is relatively simple. Optimized solutions are given in [14]. In reality the RP is randomly placed and this means solving a nonlinear equation array. Smith and Abel proposed a closed-form solution based on a spherical interpolation estimator in [14]. Taylor series method [15] is commonly used for improved accuracy. When the TDOA error is small, Chan's estimation for hyperbolic location [16] is an approximation of maximum likelihood (ML) estimator. Straight line of position represents range estimation replaces the normal circle in TOA in the method by Caffery [17]. This method has better anti-NLOS ability when statistical characteristic of measurement error is unknown.

In practical location systems, algorithms based on probabilistic models have better accuracy than deterministic models because they are able to account for uncertainty and inaccuracy. This is roughly analogous to performance improvements of decoder with soft-output comparing with hard-decision.

The maximum likelihood estimator (MLE) is a commonly employed (optimal) technique in case of limited prior knowledge: $\widehat{\theta}_{MLE} = \arg max_\theta f_z(z|\theta)$ where $\theta(x,y)$ is the position of MT, $\widehat{\theta}(\cdot)$ is the position estimation, z is measurement and $f_z(z|\theta)$ is the conditional probability density function (PDF) of z. MLE has difficulty in real applications since $f_z(z|\theta)$ is unknown. An estimated $\widehat{f}_z(z|\theta, P)$ can be given with the assistance of a propagation model P. Location estimation accuracy is dependent on the estimated PDF and propagation model. With prior knowledge, the optimal method is the Minimum Mean Square Error (MMSE) estimator:

$$\widehat{\theta}_{MMSE} = E(\theta|z)$$
$$= \int_S \theta f_\theta(\theta|z) \, d\theta \tag{1.1}$$

where $f_\theta(\theta|z)$ is the conditional PDF of position θ given measurement z, S is the region the MS resides in [18]. The term $f_\theta(\theta|z)$ dominates the estimation accuracy and relies on reliability of prior knowledge. Bayesian technique is applied where

RSSI path loss is predicted by the Okumura model.

Since it is hard to take perfect measurements of the location sensitive parameters and the multipath (reflection/diffraction) propagation characteristics of wireless waveforms, it is better to represent the uncertainty by localization algorithms and combine measurement results from different types of sensor. The Bayesian filtering technique is a strong candidate to manage measurement uncertainty and perform multi-measurement fusion, where Kalman filtering is the most widely applied variant of Bayesian filtering due to its computational simplicity. However, it requires the target evolves through a linear dynamic model and unimodal Gaussian distributed noise in state evolution and observation [19].

Multi-hypothesis tracking (MHT) extends Kalman filters to multi-modal beliefs [20]. MHT models the belief by combinations of multiple Gaussians. The prediction accuracy is considered as an indicator of the weight of a hypothesis. One apparent advantage of MHT compared to Kalman filter is the representing of multimodal belief.

Furthermore, sequential Monte Carlo methods known as particle filters, extends MHT's capacity to represent arbitrary distributions [21]. It is adopted in describing nonlinear state space with Gaussian or non-Gaussian noise. One of the key techniques in particle filter is sequential importance sampling with resampling. The disadvantage is its computational complexity increases exponentially with the dimensionality of the state space.

Traditional localization methods work well if the target is within the line-of-sight of the RP. This is not usually the case since in cellular and indoor environments propagation is often non line-of-sight (NLOS). In the NLOS scenario, the measured location parameters are biased, and mitigation algorithms need to develop in improving poorer location accuracy. In ToA estimation, the NLOS error is always significant. In the IS-95 CDMA network the error is studied and could be as large as 1300m [22]. In [22] a LOS-reconstructed algorithm is proposed while NLOS statistical knowledge and time history of received waveform are required. Better performance is achievable for this algorithm if the target is moving. The authors of [23] present a new algorithm by using a new variable to replace the square term and adding loose variables. This algorithm requires no prior knowledge with constrained estimation accuracy since it depends on the initial estimation value of Chan's algorithm [16]. This is similar to the simulation in [15] where an iterative linear method based on Taylor series is proposed. The method converges well if the initial guess is not far way from the true position. To overcome this constraint, [24] presents an approach to ameliorate the effect of the NLOS exploiting the redundant

time measurements in scenarios with more than the minimum number of RPs. A sound detection principle for the selection of the best hypothesis was proposed, instead of averaging the results of all hypothesis as in other approaches.

Besides using signal strength for building RSS, the channel impulse response (CIR) is adopted in labelling a target at a particular position [25]. Estimation of CIR is implemented by the demodulator of receiver for mitigating the effect imposed by wireless channel upon received radio signal.

One advantage of using CIR as location signature is it does not need any hardware modification on current existing wireless communication system. The only modification is to feed the CIR information from physical layer to location determination application. Since CIR contains information of multipath profile of wireless channel, it has stronger ability in determining a geographical position uniquely compared with RSS. In general, the advantages of CIR as location fingerprint makes it feasible to design a location system requiring less BSs.

In fixed wireless networks (FWN) each BS has a wide coverage. One example is in WiMax network, a BS covers a region with radius of almost 10 km. This makes it hard to estimate a MS's position with the information shared by multiple BSs. We would like to take advantage of a feature of FWN. There are numerous fixed users in FWN with their positions already known. The CIRs from these users are sample points to set up the RSSDM, which saves much working effort.

1.3   Design and Structure of Thesis

In this thesis we study and research on wireless localisation problems from both theoretical and practical aspects.

In theoretical aspect, we extend the normal research focus from location accuracy to location resolution. The concept of "location resolution" is proposed here and it is interpreted as the minimum detectable geometrical displacement of target. (It is feasible to classify location resolution as a mobility sensitivity detection problem.) We analyse the effect of multipath richness imposed on wireless location resolution. To address problems on wireless localisation and wavefield high fidelity reproduction, we articulate the essential number and optimal position of sensors for wavefields coupled to an aperture-limited region, from a spatial information theory viewpoint.

Following the theoretical work, we provide practical wireless location solutions focused on fingerprint technology. As we know, fingerprint technology is most widely adopted in existing location systems due to its simplicity and robustness.

It has no requirements for clock synchronisation between base stations when temporal parameters are measured and antenna elements' calibration when AoA is measured. Unlike other location techniques which need multiple base stations, single base station works well for fingerprint technology. It has stable location estimation performance and is robust to the impact of multipath propagation, channel fading condition and the relative positions of target and base stations. The successful example of fingerprint technology is Ekahau's Real Time Localization System (RTLS) and Site Survey Solutions (SSS). RTLS and SSS have been selected as Nortel, Simens, 3M and the London Clinic's provider of location tracking solutions. To contribute to fingerprint technology, in this thesis, we use an idea of building a "virtual propagation environment" for predicting radio signal strength in wireless LANs and exploit the already available channel impulse response of fixed wireless terminals as location fingerprints to assist wireless localisation in fixed wireless networks. (In this thesis, we apply adaptive radio signal prediction and pattern matching algorithms to improve wireless location accuracy.) In our work, radio wave real field measurements and propagation simulations are implemented to support the applied algorithms.

The thesis is structured as follows: the theoretical analysis part is composed of Chapter 2 and Chapter 3. and the practical solution part is composed of Chapter 4 and Chapter 5. In Chapter 2 a wavefield coupled to source-free space is modeled with the assistance of Hilbert space technique. Chapter 3 analyses the effect of multipath richness numerically by introducing an angular correlated spatial scattering model based on the general theoretical framework set up in Chapter 2. In the later part of Chapter 3 the essential number and optimal position of sensors for sampling a wavefield coupled to anaperture-limited region are addressed. Chapter 4 proposes an adaptive radio signal strength prediction method with its applications in Wireless LAN localisation. In Chapter 5, a novel pattern matching technique, using support vector machine, is applied in wireless location for fixed wireless communication networks. In the final chapter, Chapter 6, we summarise our work in this thesis and possible future research investigations are developed.

Chapter 2

Wavefields in a Spatial Bounded Region

Wireless signals rely on space as the physical medium to propagate and thus transfer information. The propagation is characterized by multipath due to reflection, diffraction, and scattering by obstacles in the propagation environment [26]. The spatial aspects of multipath have also drawn research attention from an information theory perspective [27,28]. These works inaugurated the study of the fundamental physical limits that space imposes on the dynamics of multipath wave propagation and wireless information transfer. Further work in [29] defined the intrinsic limits on the dimension or degrees of freedom for multipath fields when they are observed in, or coupled to, a source-free region of space. Multiple sensors are constrained to be placed in the region of space to sample the multipath field for communication or signal processing purposes.

In the literature, a central result in information theory relates to time-frequency concentration and the essential dimensionality of time-frequency signals governed by the Fourier Transform [28]. When constrained in both time and frequency there is a limit to the degree of concentration, as measure by fraction-out-of-band, of energy simultaneously possible in the two domains (FOBE). This is a form of uncertainty principle where the criterion for time-frequency concentration differs from the classical Heisenberg formulation which expresses signal concentration in terms of root mean square deviation (RMS). The FOBE criterion considers the minimization of energy outside some region and imposes no constraints on the energy distribution within the region. This type of criterion is more appropriate in engineering applications where, for example, signals need to be confined to independent frequency bands so as to not interfere with adjacent bands. In contrast, there is no advantage or meaning with the Heisenberg type concentration which

would favor concentrating the energy to the center of the band which is not likely to be an optimal use of the frequency resources.

Uncertainty principles and essential dimensionality results can be interpreted as the natural consequences of broad classes of operator equations where the operator is either self-adjoint, normal or unitary.

This thesis intends to analyse wireless location fundamental limits in relation to the use of free-space as an information bearing resource. Wireless communications involves the exploitation of space to achieve communication. The extent to which this is fundamentally possibly is constrained by the wave equation in free space. That is, the degree to which data, in an abstract sense, can be borne on information bearing wave-fields in space is limited by the essential dimensionality of such wave-fields [28]. In this thesis we develop the results for narrowband and in this regard frequency plays no role nor does the Fourier Transform. Specially we analyse the spatial diversity of multipath since the received multiple paths occupies a wide range of incident angles in azimuth and elevation. We also investigate the potential advantages and applications of this spatial diversity. This work provides a novel understanding of the impact of multipath on wireless localization.

As we know, a wavefield can be interpreted as the functional solution to the wave equation. It is convenient to analyse wavefield in Hilbert space since Hilbert space makes it feasible to treat sets of objects such as functions in a similar way as we do points and vectors as in Euclidean space and notions of orthogonality are well formulated. So we will adopt results from Hilbert space to address the spatial diversity of multipath wavefield. We review basic concepts and principles of Hilbert space in the next section prior to moving onto our original contributions.

2.1   Hilbert Space Representation

Hilbert space is a means to extend the experience of Euclidean concepts meaningfully beyond geometry into the idealised constructions of more abstract mathematics. In this case we are interested in functions as these will represent our wavefields that characterize signal propagation in physical space.

The elements of Euclidean geometry such as points, lines, vectors, distances and angles are abstracted in Hilbert space in a way that we can treat sets of objects such as functions in a similar manner as we do points, etc., in Euclidean space. Hilbert space is defined as a *complete* inner product space. To have a further more precise understanding, it is essential to address vector space, inner product and the adjective "complete". A (linear) vector space is a nonvoid set S for which addition

and scalar multiplication is defined. Addition is commutative and associative. Scalar multiplication is associative and distributive. A vector space encapsulates operations on its elements typically of the form

$$(x_1, \ldots, x_N) + \alpha(y_1, \ldots, y_N) = (x_1 + \alpha y_1, \ldots, x_N + \alpha y_N)$$

where α is a scalar (complex or real).

Let $\mathcal{H}$ be a complex vector space (by which we mean the scalars are complex). A function mapping $x \in \mathcal{H}$ into $\mathbb{R}$ is called a norm if it satisfies the following conditions:

$$\|x\| = 0 \quad \text{if and only if } x = 0 \tag{2.1}$$

$$\|\lambda x\| = |\lambda| \|x\| \quad \text{for every } x \in \mathcal{H} \text{ and } \lambda \in \mathbb{C} \tag{2.2}$$

$$\|x + y\| \le \|x\| + \|y\| \quad \text{for every } x, y \in \mathcal{H} \tag{2.3}$$

Let $\mathcal{H}$ be a complex vector space. A complex bilinear function/mapping $\langle \cdot, \cdot \rangle$: $\mathcal{H} \times \mathcal{H} \mapsto \mathbb{C}$ is called an *Inner Product* if for any $f, g, g_1, g_2 \in \mathcal{H}$ and $\alpha_1, \alpha_2 \in \mathbb{C}$ the following conditions are satisfied:

$$\langle f, g \rangle = \overline{\langle g, f \rangle}$$

$$\langle \alpha_1 f_1 + \alpha_2 f_2, g \rangle = \alpha_1 \langle f_1, g \rangle + \alpha_2 \langle f_2, g \rangle$$

$$\langle f, f \rangle \ge 0$$

$$\langle f, f \rangle = 0 \quad \text{implies } f = 0. \tag{2.4}$$

Given an inner product $\langle \cdot, \cdot \rangle$ in a vector space, the norm can be defined by

$$\|x\| = \langle x, x \rangle^{\frac{1}{2}} \tag{2.5}$$

or more succinctly $\| \cdot \| = \langle \cdot, \cdot \rangle^{\frac{1}{2}}$. That is, it is sufficient to have an inner product to define a norm.

Vector space, norm, inner product and completeness are the four pillars of Hilbert space. Further, the concept of *Cauchy Sequence* is helpful in understanding Hilbert space. It is defined as a sequence $\{x_n\}_{n=0}^{\infty}$ in a normed space is called a Cauchy sequence if $\forall \epsilon > 0, \exists N$ such that $\|x_m - x_n\| < \epsilon, \forall m, n > N$. A normed space $\mathcal{H}$ is called complete if every Cauchy sequence in $\mathcal{H}$ converges to a vector in $\mathcal{H}$. A complete normed space is called a *Banach space*. A vector space $\mathcal{H}$ with an Inner Product is called an Inner Product space or a Pre-Hilbert space. A complete inner product space is called a *Hilbert space.* Based on Hilbert space, the
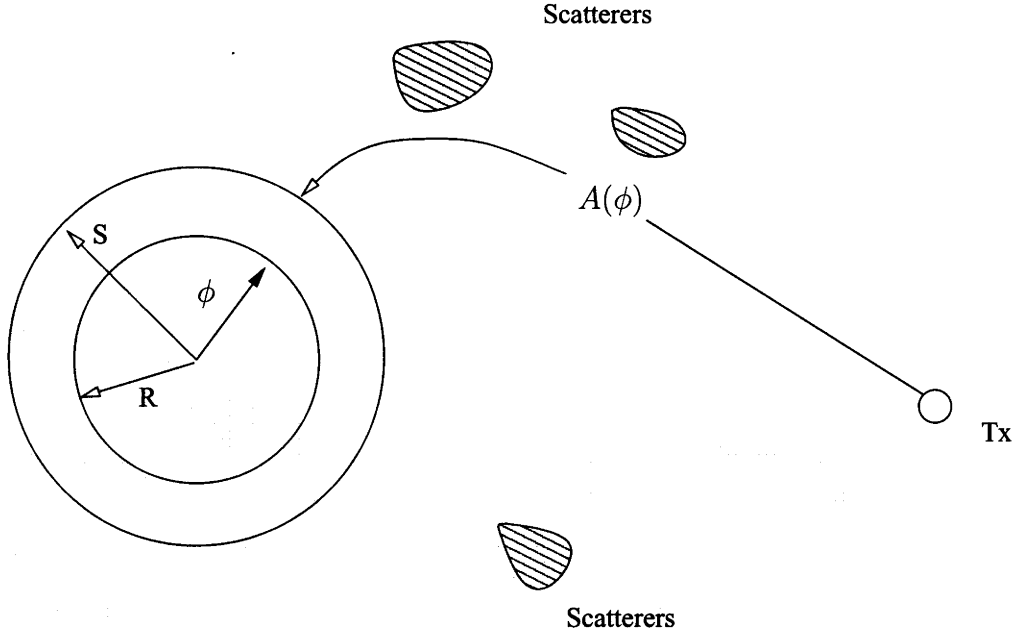
Figure 2.1: Wireless Wave Propagation Environment.

analysis in this thesis considers multipath fields as the function solutions to the wave equation [30].

The multipath fields are constrained in a region of interest. All scatterers are assumed to be beyond the region, that is, at a sufficient distance. This region can be thought of as the region bearing the receiver antenna elements. However, the notion of antenna elements is not strictly needed here because equally well the description holds true for hypothetical continuous sensors and more general distributions of sensors. As shown in Figure 2.1, all sources are assumed beyond the outer ball of radius S and receiver antenna elements are limited in the inner ball of radius $R < S$.

Let x represent a vector in $\mathbb{R}^3$ or $\mathbb{R}^2$ space, and let $r = \|x\|$ denote the Euclidean distance of x from the origin, which is the center of some region of interest. The unit vector in the direction of non-zero vector x is denoted $\widehat{x} \triangleq x/\|x\|$. In our case the region of interest is described by $\|x\| \leq R$. Furthermore, x with Cartesian coordinate (x, y, z) is denoted by spherical coordinate (r, θ, ϕ) as in Figure 2.2 and they are related by:

$$x = r \sin \theta \cos \phi$$
$$y = r \sin \theta \sin \phi$$
$$z = r \cos \theta \tag{2.6}$$

We denote the wavefield as $F(x, t)$ at position x and at time t. All source-free
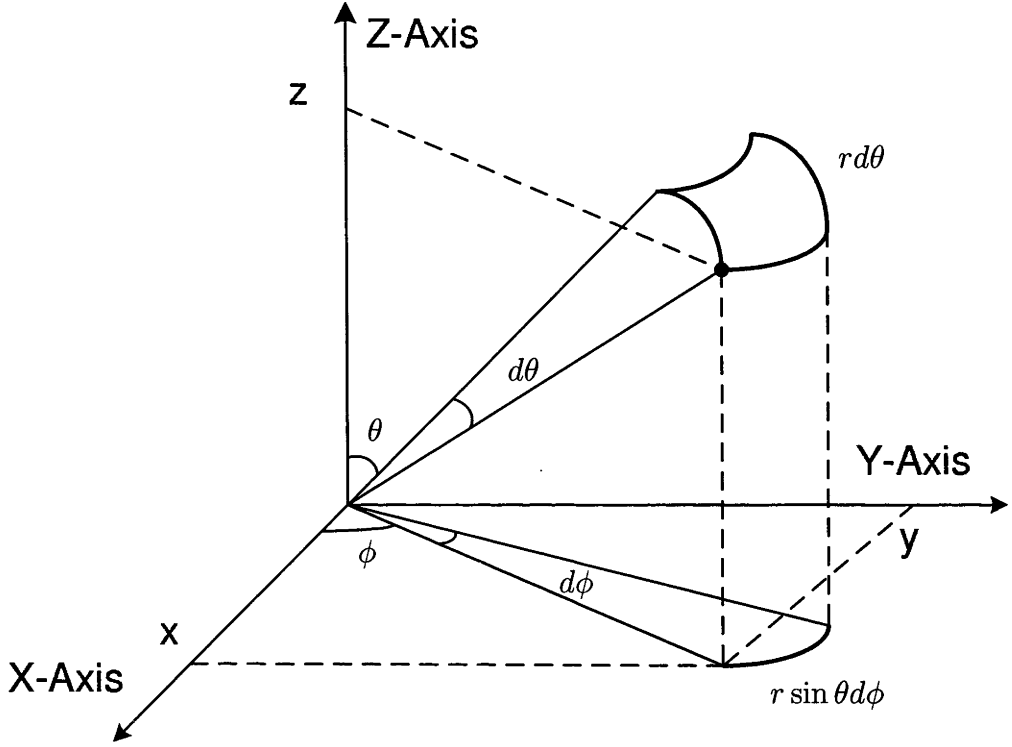
Figure 2.2: Relationship between Cartesian coordinate and Spherical coordiante.

wavefields in the source free ball of radius S satisfy the scalar wave equation [31]:

$$\nabla^2 F(\boldsymbol{x}, t) = \frac{1}{c^2} \frac{\partial^2 F(\boldsymbol{x}, t)}{\partial t^2} \tag{2.7}$$

where ∇^2 is the Laplacian operator and c is the propagation speed of the wave in a medium. ∇^2 can be expanded in the appropriate coordinate system, either in Cartesian or spherical system. We expand the Laplacian into spherical coordinates:

$$\nabla^2 F = \frac{1}{c^2} \frac{\partial^2 F}{\partial t^2} \frac{1}{r^2} \frac{\partial}{\partial r}(r^2 \frac{\partial F}{\partial r}) + \frac{1}{r^2 \sin\theta} \frac{\partial}{\partial \theta}(\sin\theta \frac{\partial F}{\partial \theta}) + \frac{1}{r^2 \sin\theta^2} \frac{\partial^2 F}{\partial \phi^2} \tag{2.8}$$

Applying the method of separation of variables, we assume the solution of (2.8) is

$$F(\boldsymbol{x}, t) = F(r, \theta, \phi, t) = R(r)\Theta(\theta)\Phi(\phi)T(t). \tag{2.9}$$

Solve the differential equation for the temporal variable, t, we have

$$\frac{1}{T(t)} \frac{1}{c^2} \frac{d^2 T(t)}{dt^2} = -k^2. \tag{2.10}$$

whose solution is

$$T(t) = T_1 e^{i\omega t} + T_2 e^{-i\omega t} \tag{2.11}$$

Here $\omega = 2\pi f = kc$ is the frequency. Since $e^{-i\omega t}$ denotes wave propagating back-

wards in time so

$$T(t) = T_1 e^{i\omega t} \tag{2.12}$$

Substituting (2.9) and (2.12) into (2.8) we have the so called Helmholtz equation

$$\nabla^2 F(\boldsymbol{x}) + k^2 F(\boldsymbol{x}) = 0, \quad \|\boldsymbol{x}\| < S. \tag{2.13}$$

The homogeneous Helmholtz equation is known as the reduced form of the complete Helmholtz equation. In the following we are mainly interested in the region of interest, that is, the field in $\|\boldsymbol{x}\| \leq R$. Two broad classes of representation of the solution to (2.13) will be considered. The first class is based on plane wave synthesis and is considered in Section 2.2.1. The second class is based on orthogonal solutions to the wave equation.

All solutions to (2.13) for a given source-free region define a linear subspace of functions which follows from the linearity and homogeneity of (2.13). That is, if $u_1(\boldsymbol{x})$ and $u_2(\boldsymbol{x})$ are solutions to (2.13) in a region then $\xi_1 u_1(\boldsymbol{x}) + \xi_2 u_2(\boldsymbol{x})$ is also a solution in the same region, where $\xi_1, \xi_2 \in \mathbb{C}$. We formalize and develop this interpretation as follows.

We begin with the complex separable Hilbert space of complex valued square integrable functions, $L^2(\mathbb{B}_S)$, defined in $\mathbb{B}_S$ for some radius S (which later will be identified with any radius that excludes all sources), equipped with inner product

$$\langle f, g \rangle_{\mathbb{B}_S} \triangleq \int_{\mathbb{B}_S} f(\boldsymbol{x}) \overline{g(\boldsymbol{x})} d\upsilon(\boldsymbol{x}) \tag{2.14}$$

with induced norm

$$\|f\|_{\mathbb{B}_S}^2 \triangleq \int_{\mathbb{B}_S} |f(\boldsymbol{x})|^2 d\upsilon(\boldsymbol{x}) \tag{2.15}$$

The volume element $d\upsilon(\boldsymbol{x})$ is given by

$$d\upsilon(\boldsymbol{x}) \triangleq r^2 \sin\theta \, d\theta d\phi dr \tag{2.16}$$

in three dimension space where ϕ and θ are the azimuth and elevation respectively; equivalently in two dimension space we have

$$d\upsilon(\boldsymbol{x}) \triangleq r \, d\phi dr \tag{2.17}$$

The solutions to (2.13) that form a strict linear subspace of $L^2(\mathbb{B}_S)$ is a separable

Hilbert Space and denoted

$$\mathcal{G}_S \triangleq \{f \in L^2(\mathbb{B}_S) : \nabla^2 f(\boldsymbol{x}) + k^2 f(\boldsymbol{x}) = 0\} \qquad (2.18)$$

Both $L^2(\mathbb{B}_S)$ and its subspace $\mathcal{G}_S$ have inner product (2.14). Since $\mathcal{G}_S$ is separable, there exist orthonormal sequences $\{\phi_p\}_{p=0}^{\infty}$, which are complete in $\mathcal{G}_S$, that is, for all $f \in \mathcal{G}_S$

$$f = \sum_{p=0}^{\infty} \langle f, \phi_p \rangle_{\mathbb{B}_S} \phi_p, \qquad (2.19)$$

where convergence is in the mean (strong convergence in the norm) and

$$\beta_p \triangleq \langle f, \phi_p \rangle_{\mathbb{B}_S} \qquad (2.20)$$

is the Fourier Coefficient. By completeness we have Parseval's Relation

$$\|f\|_{\mathbb{B}_S}^2 = \|\beta\|_{\ell^2}^2. \qquad (2.21)$$

So now we may apply this general theorem to study the spatial diversity of multipath wavefield by identifying elements of Hilbert space with wavefield.

2.2   2D Multipath Field Representation

2.2.1   Multiple Plane Wave Representation

A standard multipath model involves modeling every distinct path explicitly as a plane wave. That is,

$$F(\boldsymbol{x}) = \sum_p a_p e^{ik\boldsymbol{x}\cdot\widehat{\boldsymbol{y}}_p} \qquad (2.22)$$

where the plane wave of index p has complex amplitude $a_p \in \mathbb{C}$, the propagation direction is denoted by the unit vector $\widehat{\boldsymbol{y}}_p \equiv (1, \phi_p)$, and $\boldsymbol{x} \cdot \boldsymbol{y}$ denotes the scalar product between vectors $\boldsymbol{x}$ and $\boldsymbol{y}$. We interpret representation (2.22) as encoding the field with a countable number of pairs $\{a_p, \widehat{\boldsymbol{y}}_p\}$ enumerated by p.

A generalization that subsumes (2.22) is the supervision of plane waves from all azimuth directions ϕ as

$$F(\boldsymbol{x}) = \int_0^{2\pi} A(\phi) e^{ik\boldsymbol{x}\cdot\widehat{\boldsymbol{y}}(\phi)} d\phi, \quad \|\boldsymbol{x}\| \le R \qquad (2.23)$$

where $A(\phi)$ is the complex multipath scattering gain, the complex amplitude of a

multipath originating from each direction ϕ, $\widehat{\boldsymbol{y}}(\phi)$ is a unit vector in the direction ϕ. $A(\phi)$ implicitly represents a specific geometrical distribution of far-field scatterers.

2.2.2   Orthogonal Representation and Effect of Region Size

Equation (2.23) implicitly requires that any sources be in the farfield. In quantifying degrees of freedom a Fourier expansion of $F(\boldsymbol{x})$ is better suited than (2.23). With an orthonormal expansion (using the natural inner product defined over the region of interest $\mathbb{B}_R$) the degrees of freedom can be determined by the significant Fourier coefficients which we write as $\beta_{n;R}$, $n \in \mathbb{Z}$.

As we know an orthonormal sequence is required for determining the Fourier coefficients uniquely. One orthogonal sequence in 2D disk of radius R ($\mathbb{B}_R$) is given for its best finite dimensional approximation as follows:

$$i^n J_n(k\|\boldsymbol{x}\|)e^{in\phi(\boldsymbol{x})} \tag{2.24}$$

$J_n(\cdot)$ is the integer order Bessel function of the first kind [32].

The spatial normalisation of this sequence in 2D disk region $\mathbb{B}_R$ is implemented by introducing the factor $\sqrt{2\pi \mathscr{J}_n(R)}$ into (2.24) where

$$\mathscr{J}_n(R) \triangleq \int_0^R \left(J_n(kr)\right)^2 r\, dr \tag{2.25}$$

is a normalizing term for the region of interest $\mathbb{B}_R$. Thus we have the natural orthonormal basis functions defined as:

$$\Phi_{n;R}(\boldsymbol{x}) \triangleq \frac{i^n J_n(k\|\boldsymbol{x}\|)e^{in\phi(\boldsymbol{x})}}{\sqrt{2\pi \mathscr{J}_n(R)}}. \tag{2.26}$$

To verify $\Phi_{n;R}$'s orthonormality we note that

$$\int_0^{2\pi}\int_0^R \Phi_{n;R}\, r\, d\phi\, dr = \int_0^{2\pi}\int_0^R \Phi_{n;R}(\boldsymbol{x})\Phi_{m;R}(\boldsymbol{x})^*\, r\, dr\, d\phi = \delta(m-n). \tag{2.27}$$

So, we rewrite (2.23) as

$$F(\boldsymbol{x}) = \sum_{n=-\infty}^{\infty} \beta_{n;R}\, \Phi_{n;R}(\boldsymbol{x}), \quad \|\boldsymbol{x}\| \le R \tag{2.28}$$

where $\beta_{n;R}$ is calculated according to inner product of (2.14). In a simpler method, we combine the field expression (2.23), natural basis functions (2.26) and Jacobi-

Anger expansion [30, p. 32],

$$e^{i\boldsymbol{x}\cdot\widehat{\boldsymbol{y}}} = \sum_{n=-\infty}^{\infty} i^n J_n(k\|\boldsymbol{x}\|)e^{in(\phi(\boldsymbol{x})-\phi(\widehat{\boldsymbol{y}}))}, \tag{2.29}$$

and comparing with (2.28) we find

$$\beta_{n;R} = \sqrt{2\pi \mathcal{J}_n(R)}\,\alpha_n \tag{2.30}$$

where $\alpha_n \in \mathbb{C}$ is the nth Fourier series coefficient of $A(\phi)$ defined as

$$\alpha_n = \int_0^{2\pi} A(\phi)e^{-in\phi}d\phi. \tag{2.31}$$

and

$$A(\phi) = \sum_{n=-\infty}^{\infty} \frac{\alpha_n}{2\pi}e^{in\phi}. \tag{2.32}$$

In quantifying the degrees of freedom a Fourier expansion of $F(\boldsymbol{x})$ is better suited than (2.23). With an orthonormal expansion (using the natural inner product defined over the region of interest $\mathbb{B}_R$) the degrees of freedom can be determined by the significant Fourier coefficients which we write as $\beta_{n;R}$, $n \in \mathbb{Z}$ in (2.28). A natural set of basis functions for multipath (which are optimal only in the special case of isotropic multipath) is introduced in (2.26), which is helpful to characterize the influence of region size on degrees of freedom. The properties of (2.25) capture precisely the low pass, albeit non-ideal, action in the angular domain. Increasing R increases the effective bandwidth of the low pass action increasing the DoF. The equivalent filtered multipath scattering gain $A(\phi)$, (2.31), yields an effective multipath scattering gain,

$$A_R(\phi) \triangleq \frac{1}{\sqrt{2\pi}} \sum_{n=-\infty}^{\infty} \sqrt{\mathcal{J}_n(R)}\alpha_n e^{in\phi} \tag{2.33}$$

which is directly amenable to standard degree of freedom analysis [29]. The erosion of the Fourier coefficients with decreasing region size, R, directly decreases the degrees of freedom. We conclude the effect of the region, parameterized by radius R, is equivalent to a filtering (convolution) of $A(\phi)$. In the transform domain this is given by the multiplication (2.30). To conclude, (2.33) is a key equation which theoretically determines the effect of the size of a circular region on the degrees of freedom. It is shown that the effect of changing the radius of the region is equivalent to filtering the angular multipath distribution, $A(\phi)$, with a specific non-ideal

low pass filter. In summary, the key equations in this section also include (2.28) and (2.30). Given the natural orthonormal basis functions of a region of aperture R, $\Phi_{n;R}(\boldsymbol{x})$, the couple wavefiled is uniquely represented by the Fourier coefficients $\beta_{n;R}$, where $n = -\infty, \ldots, \infty$. We note the basis functions are functions of the region only and contained no intrinsic information of the wavefield. All information of the wavefield is represented by $\beta_{n;R}$ completely. Next, we extend the deterministic equations (2.28) and (2.30) to describe multipath fields in a uncertain (stochastic) representative style.

2.2.3   Random Multipath Fields

It is better to represent the wavefields in a random way. The main reason is accurate information about scatterers that generate the multipath field $F(\boldsymbol{x})$ is usually limited. Therefore, it is reasonable to represent multipath field $F(\boldsymbol{x})$ as a random process.

Referring to (2.23), the scattering gain $A(\phi)$ is random and so is α_n in (2.31). The angular power spectrum (APS) is given by

$$P'(\varphi) = \mathcal{E}\{A(\varphi)A^*(\varphi)\}, \tag{2.34}$$

Under the APS limited measurement case the only available information is APS defined in (2.34). This indicates we have no information regarding the phase term of $A(\varphi)$. The APS can be thought of as describing in which directions and at what strength the multipath power is coming from (without regard for phase information). Hence the APS has a direct physical interpretation. However, in this section we shall see there is a second physical interpretation in terms of spatial correlation in the region of interest and this relates closely to the normalized APS.

The normalised APS is given by

$$P(\varphi) \equiv \frac{\mathcal{E}\{A(\varphi)A^*(\varphi)\}}{\int_0^{2\pi} \mathcal{E}\{A(\varphi)A^*(\varphi)\}d\varphi}. \tag{2.35}$$

The spatial correlation is defined in [33] as

$$\begin{aligned}
\rho(\boldsymbol{x}_1, \boldsymbol{x}_2) &\equiv \frac{\mathcal{E}\{F(\boldsymbol{x}_1)F^*(\boldsymbol{x}_2)\}}{\mathcal{E}\{F(\boldsymbol{x}_1)F^*(\boldsymbol{x}_1)\}} \\
&= \frac{\int_0^{2\pi}\int_0^{2\pi} \mathcal{E}\{A(\varphi)A^*(\varphi')\}e^{ik\boldsymbol{x}_1\cdot\widehat{\boldsymbol{y}}(\varphi)}e^{-ik\boldsymbol{x}_2\cdot\widehat{\boldsymbol{y}}(\varphi')}d\varphi d\varphi'}{\int_0^{2\pi}\int_0^{2\pi} \mathcal{E}\{A(\varphi)A^*(\varphi')\}e^{ik\boldsymbol{x}_1\cdot\widehat{\boldsymbol{y}}(\varphi)}e^{-ik\boldsymbol{x}_1\cdot\widehat{\boldsymbol{y}}(\varphi')}d\varphi d\varphi'}.
\end{aligned} \tag{2.36}$$

With the assumption that $A(\varphi)$ and $A(\varphi')$ are uncorrelated in (2.36), we have

$\mathcal{E}\{A(\varphi)A^*(\varphi')\} = \delta(\varphi - \varphi')$, where $\delta(\cdot)$ is the Kronecker Delta function. Thus

$$\rho(\boldsymbol{x}_2, \boldsymbol{x}_1) = \rho(\boldsymbol{x}_2 - \boldsymbol{x}_1) = \int_0^{2\pi} P(\varphi)e^{ik(\boldsymbol{x}_2-\boldsymbol{x}_1)\cdot\widehat{\boldsymbol{y}}(\varphi)} \, d\varphi. \tag{2.37}$$

where $\widehat{\boldsymbol{y}}(\varphi)$ is the unit vector in the direction of φ, shows the spatial correlation is spatially stationary (under the uncorrelatedness assumption). So $\rho(\boldsymbol{x}_2 - \boldsymbol{x}_1)$ is the only information available from the receiver region in the 2D disc of radius R. Furthermore, the Jacobi-Anger expansion [30, p.32] states

$$e^{i\boldsymbol{x}\cdot\widehat{\boldsymbol{y}}} = \sum_{n=-\infty}^{\infty} i^n J_n(k\|\boldsymbol{x}\|)e^{in(\varphi(\boldsymbol{x})-\varphi(\widehat{\boldsymbol{y}}))} \tag{2.38}$$

where $\varphi(\boldsymbol{x})$ and $\varphi(\widehat{\boldsymbol{y}})$ are the angles of $\boldsymbol{x}$ and $\widehat{\boldsymbol{y}}$, respectively. By substituting (2.38) into (2.37) we obtain

$$\rho(\boldsymbol{x}_2 - \boldsymbol{x}_1) = \sum_{n=-\infty}^{\infty} i^n\gamma_n J_n(k\|\boldsymbol{x}_2 - \boldsymbol{x}_1\|)e^{in\varphi_{21}}. \tag{2.39}$$

where φ_{21} in the difference in angles between $\boldsymbol{x}_2$ and $\boldsymbol{x}_1$, and

$$\gamma_n = \int_0^{2\pi} P(\varphi)e^{-in\varphi}d\varphi. \tag{2.40}$$

In (2.37) $\boldsymbol{x}_2$ and $\boldsymbol{x}_1$ are two arbitrary points within the 2D disc of radius R. Thus $\boldsymbol{z} = \boldsymbol{x}_2 - \boldsymbol{x}_1$ can take values in any direction but is restricted to separations of $2R$ (being the maximum separation of two point in a disk of radius R). This suggests a countable set of orthonormal basis function over the 2D disc of radius $2R$ given by

$$\Phi_{n;2R}(\boldsymbol{z}) \equiv \frac{i^n J_n(k\|\boldsymbol{z}\|)e^{in\varphi(\boldsymbol{z})}}{\sqrt{2\pi\mathcal{J}_n(2R)}}, \quad \|\boldsymbol{z}\| \leq 2R. \tag{2.41}$$

We can rewrite (2.39) in its orthonormal expansion form

$$\rho(\boldsymbol{z}) = \sum_{n=-\infty}^{\infty} \gamma_{n;R}\Phi_{n,2R}(\boldsymbol{z}). \tag{2.42}$$

where $\gamma_{n;R}$ is defined as $\sqrt{2\pi\mathcal{J}_n(2R)}\gamma_n$.

To model angular *correlated* multipath we can augment the APS, (2.34), by introducing an angular correlation function $\rho(\phi_1, \phi_2)$ between two incoming multi-

path directions ϕ_1 and ϕ_2:

$$\rho(\phi_1, \phi_2) \equiv \frac{\mathcal{E}\{A(\phi_1)A^*(\phi_2)\}}{\sqrt{\mathcal{E}\{|A(\phi_1)|^2\}\mathcal{E}\{|A(\phi_2)|^2\}}}. \qquad (2.43)$$

To summary, we consider the spatial scatterer gain $A(\phi)$ is random and so is $\beta_{n:R}$ in (2.30). We note that in (2.28) a sequence of Fourier coefficients $\beta_{n:R}$ of infinite length is required to represent the wavefield $F(\boldsymbol{x})$. But, is it possible to represent the wavefield by finite elements of the sequence $\beta_{n:R}$ without significant information losing of the wavefield? This leads the concepts of Degree of Freedom and multipath richness of wavefield in the next section.

2.3   Degrees of Freedom of Multipath Wavefield

A wavefield in a bounded region of interest in space can be accurately described with a small number of parameters. These parameters capture the notion of degrees of freedom (DoF). As shown in Figure 2.1 the inner part is a circular region for our bounded region

$$\mathbb{B}_R = \{\boldsymbol{x} \colon \|\boldsymbol{x}\| \leq R\}$$

where R is the radius, $\boldsymbol{x}$ represents the 2D vector of spatial variables an $\|\cdot\|$ is the Euclidean norm. This special shaped region admits a simpler formulation and can be regarded as a natural 2D analog of either the time interval, $[0, T]$, or the frequency interval, $[-W, W]$, used in the bandlimited waveform channel case. Alternatively, an arbitrary bounded shape can be contained within such a circular region and the DoF thereby bounded. For antenna arrays such a continuous region is better suited to bounding the performance of circular arrays than linear arrays.

If all wavefields in the region of interest $\mathbb{B}_R$ can be accurately expressible with a finite number of parameters $\{\beta_n\}_{n=-N}^{N}$ multiplying some orthonormal basis functions $\Phi_n(\boldsymbol{x})$, we say the wavefield possesses $2N + 1$ *DoF with respect to that basis*. Such a basis and coefficients can be regarded as truncation of a generalized Fourier Series representation.

Previously we qualitatively linked DoF with the number of significant Fourier coefficients. Here we make the connect explicit. Consider a particular realization $F(\boldsymbol{x})$ of a random wavefield. Let $F_N(\boldsymbol{x})$ be the N truncation of wavefield, (2.28), retaining the $2N+1$ lowest order terms. The normalized mean square error between

$F(\boldsymbol{x})$ and $F_N(\boldsymbol{x})$ over $\mathbb{B}_R$ can be written

$$\epsilon(N, R) = \frac{\int_{\mathbb{B}_R} |F(\boldsymbol{x}) - F_N(\boldsymbol{x})|^2 d\boldsymbol{x}}{\int_{\mathbb{B}_R} |F(\boldsymbol{x})|^2 d\boldsymbol{x}} = \frac{\sum_{|n|>N} |\beta_{n;R}|^2}{\sum_{n=-\infty}^{\infty} |\beta_{n;R}|^2} \qquad (2.44)$$

where the denominator is the total energy in the receiver region. We define the DoF as the number of parameters required for which the error between truncated and actual wavefields is below an acceptable threshold level ϵ_0:

$$\mathrm{DoF} = 2 \times \arg\min_N \{\epsilon_{N,R} \leq \epsilon_0\} + 1 \qquad (2.45)$$

Conventionally one takes $\epsilon_0 = 0.01$. DoF measures the number of parameters with respect to *the natural basis functions* (2.26). A stochastic notion of degrees of freedom can be obtained by inserting expectations around the numerator and denominator of (2.44) and estimated by averaging over a number of trials.

In [29] an upper bound is derived on the MSE sense of multipath field truncation error when the field is represented by the natural choice of orthonormal basis in (2.26). The authors show that a general dimensionality of 2D multipath coupled to a disk with radius R, is

$$D_R^{2D} = 2N + 1 = 2\lceil \pi R e / \lambda \rceil + 1, \qquad (2.46)$$

regardless of stochastic scattering characteristics.

Referring back to (2.45) it is interesting to consider the question of what choice of basis leads to the least number of parameters. This question is answered in the next section and captures the notion of multipath richness.

2.4 Degrees of Freedom of APS Limited Multipath Wavefield

When restricting the knowledge of a multipath wavefield to a region of interest, this is equivalent to restricting knowledge of the spatial correlation. With this spatial correlation the question arises as to whether it can be well approximated by a limited (finite) number of terms as this will characterize the degrees of freedom. The approximate spatial correlation $\rho_N(\boldsymbol{x}_2 - \boldsymbol{x}_1)$ is defined by the finite sum

$$\rho_N(\boldsymbol{x}_2 - \boldsymbol{x}_1) = \sum_{n=-N}^{N} i^n \gamma_n J_n(k\|\boldsymbol{x}_2 - \boldsymbol{x}_1\|) e^{in\varphi_{21}}. \qquad (2.47)$$

The error between the approximate and real spatial correlation is given by

$$\epsilon_N(\boldsymbol{z}) = |\rho(\boldsymbol{z}) - \rho_N(\boldsymbol{z})|$$
$$= |\sum_{|n|>N} i^n \gamma_n J_n(k\|\boldsymbol{z}\|)e^{in\varphi(\boldsymbol{z})}|, \quad \|\boldsymbol{z}\| \leq 2R \tag{2.48}$$

Since $|\gamma_n| \leq 1$ in (2.48)[2], then

$$\epsilon_N(\boldsymbol{z}) \leq \sum_{|n|>N} |J_n(k\|\boldsymbol{z}\|)| = 2\sum_{n>N} |J_n(k\|\boldsymbol{z}\|)| \tag{2.49}$$

As shown in [27],

$$|J_n(k\|\boldsymbol{z}\|)| \leq \frac{q(N,2R)^n}{\sqrt{2\pi(N+1)}}, \quad n > N, \ \|\boldsymbol{z}\| \leq 2R \tag{2.50}$$

where

$$q(N,2R) = \frac{2\pi eR/\lambda}{(N+1)}.$$

We can obtain a bound on the error for given values of N and $2R$

$$\epsilon_N(\boldsymbol{z}) \leq \sqrt{\frac{2}{(N+1)\pi}} \frac{q(N,2R)^{N+1}}{1 - q(N,2R)}$$

The restriction on $q(N,R)$ provides an upper bound on n, given by N, such that the error is small and exponentially decreasing with n increasing. The critical bound is given by

$$N > (\pi e)2R/\lambda - 1.$$

and $2\lceil(\pi e)2R/\lambda - 1\rceil + 1$, the number of terms in (2.47), is taken as the dimensionality of the region interest whose radius in R based on APS limited measurements only. Note that since the APS limited case is less restricted than the deterministic case which needs to satisfy the homogeneous Helmholtz equation then the degrees of freedom are higher. This less restricted case results in a factor of 2 increase in the degrees of freedom.

2.5   Multipath Richness

In a random wavefield, each wavefield coefficient $\beta_{n;R}$ is a random variable. In [29] an upper bound is derived on the MSE of multipath field truncation error when

---

[2]Note that $\gamma_n = \int_0^{2\pi} P(\varphi)e^{-in\varphi} \, d\varphi$ and $|\gamma_n| \leq \gamma_0 = 1$.

the field is represented by the natural choice of orthonormal basis in (2.26). The authors show that a general dimensionality of 2D multipath coupled to a disk with radius R, is $D_R^{2D} = 2N + 1 = 2\lceil \pi Re/\lambda \rceil + 1$, regardless of stochastic scattering characteristics.

Depending upon the statistical class of wavefield, the wavefield coefficients are generally correlated (which represents redundancy). The intrinsic reasons are limited angle of arrival of wavefield and angular correlation of the spatial scatterer gain.

It is possible in this case to express the wavefield in a different set of basis functions with a lesser number of parameters that are uncorrelated (to the same truncation accuracy).

The optimal representation (in terms of covariance) of a wavefield is given by the Karhunen-Loeve (KL) expansion

$$F(x) = \sum_{n=1}^{\infty} \sqrt{\lambda_n} \zeta_n \ \Psi_n(x), \tag{2.52}$$

(which can be truncated to the desired finite number of terms) where the orthonormal basis (eigen-)function set $\{\Psi_n\}$ represents the optimal set for a stochastic multipath field, $\lambda_n > 0$ represents an eigenvalue associated with eigenfunction $\Psi_n(x)$ and ζ_n are new uncorrelated wavefield coefficients (random variables) of unit variance. In the 2D case given the spatial correlation in (2.36) we have

$$\int_0^{2R} \int_0^{2\pi} \rho(x_1, x_2) \Psi_n(x_1) r_1 dr_1 d\phi_1 = \lambda_n \Psi_n(x_2)$$

where $x_i \triangleq (r_i, \phi_i)$, for $i = 1, 2$.

We define multipath richness in analogy to (2.44) as follows. Assume indexes n are arranged in descending order of λ_n. The field in $\mathbb{B}_R$ is said to have a *multipath richness* of N when the normalized eigenvalue residual is less than some threshold ϵ_0:

$$\frac{\sum_{n>N} \lambda_n}{\sum_{n=0}^{\infty} \lambda_n} < \epsilon_0. \tag{2.53}$$

Again conventionally one takes $\epsilon_0 = 0.01$. Under this framework, given the ℓ_2 formulation, the N in (2.53) tightly lower bounds the N in (2.44) for the same error threshold and, thereby, the richness is a tight lower bound on the degree of freedom for any basis.

Systematic Numerical Method for Eigenvalue Calculation

Algorithm

Systematic Numerical Calculation of λ_n in (2.52):

1. Based on (2.46), truncate the random sequence $\sqrt{2\pi \mathcal{J}_n(R)}\alpha_n$ with truncation length $N \geq \lceil e\pi R/\lambda \rceil$, to obtain the random vector

$$\boldsymbol{v} = \left[\sqrt{2\pi \mathcal{J}_{-N}(R)}\alpha_{-N} \cdots \sqrt{2\pi \mathcal{J}_N(R)}\alpha_N \right]$$

2. Using (2.64), form the covariance matrix for the random vector $\boldsymbol{v}$ defined as $\Gamma_{2N+1} = \mathcal{E}\{\boldsymbol{v}\boldsymbol{v}^H\}$.

3. The eigenvalue of the covariance matrix Γ_{2N+1} give the first $2N+1$ eigenvalues of the spatial correlation $\rho(\boldsymbol{x}_1, \boldsymbol{x}_2)$. $\qquad\square$

To calculate the elements in the covariance matrix Γ_{2N+1}, it is critical to calculate $\mathcal{E}\{\alpha_n \alpha_{n'}^*\}$, $n, n' = -N, \ldots, N$. We define γ_{m-n} as the $(m-n)$th Fourier series coefficients of the normalised APS $P(\phi)$:

$$\gamma_{m-n} \triangleq \int_0^{2\pi} P(\phi)e^{-i(m-n)\phi}d\phi \tag{2.54}$$

Substituting (2.31) into (2.54) and assuming that $A(\phi)$ is angular non-correlated, we have

$$\gamma_{m-n} = \frac{\mathcal{E}\{\alpha_m \alpha_n^*\}}{\mathcal{E}\{\alpha_n \alpha_n^*\}} \tag{2.55}$$

$$= \frac{\mathcal{E}\{\alpha_m \alpha_n^*\}}{\int_0^{2\pi} \mathcal{E}\{A(\phi)A(\phi)^*\}d\phi} \tag{2.56}$$

Thus

$$\mathcal{E}\{\alpha_m \alpha_n^*\} = \gamma_{m-n} \int_0^{2\pi} \mathcal{E}\{A(\phi)A(\phi)^*\}d\phi \tag{2.57}$$

We note that $\int_0^{2\pi} \mathcal{E}\{A(\phi)A(\phi)^*\}d\phi$ is a constant for determined $A(\phi)$. In case of angular non-correlated $A(\phi)$, the definition

$$\mathcal{E}\{\alpha_n \alpha_{n'}^*\} = \mathcal{E}\{\int_0^{2\pi} A(\phi)e^{-in\phi}d\phi \int_0^{2\pi} A^*(\varphi)e^{in'\varphi}d\varphi\}$$

$$= \int_0^{2\pi} \int_0^{2\pi} \mathcal{E}\{A(\phi)A^*(\varphi)\}e^{-in\phi}e^{in'\varphi}d\phi d\varphi \tag{2.58}$$

From (2.43) it is straightforward that

$$\mathcal{E}\{A(\phi)A^*(\varphi)\} = \mathcal{A}\sqrt{P(\phi)}\sqrt{P(\varphi)}\rho(\phi,\varphi)$$

where $\mathcal{A} \triangleq \int_0^{2\pi} \mathcal{E}\{|A(\phi)|^2\}d\phi$. In this way we have

$$\mathcal{E}\{\alpha_n\alpha_{n'}^*\} = \mathcal{A}\int_0^{2\pi}\int_0^{2\pi}\sqrt{P(\phi)}\sqrt{P(\varphi)}\rho(\phi,\varphi)e^{-in\phi}e^{in'\varphi}d\phi d\varphi. \qquad (2.59)$$

In addition, we would like to consider the mth Fourier series coefficient of $\sqrt{P(\phi)}$ defined through

$$\sqrt{P(\phi)} = \frac{1}{2\pi}\sum_{m=-\infty}^{\infty}\iota_m e^{im\phi} \qquad (2.60)$$

and

$$\iota_m = \int_0^{2\pi}\sqrt{P(\phi)}e^{-im\phi}d\phi. \qquad (2.61)$$

We also consider the double Fourier expansion

$$\rho(\phi_1,\phi_2) = \frac{1}{(2\pi)^2}\sum_{m=-\infty}^{\infty}\sum_{m'=-\infty}^{\infty}\xi_{mm'}e^{i(m\phi_1-m'\phi_2)}, \qquad (2.62)$$

$$\xi_{mm'} = \int_0^{2\pi}\int_0^{2\pi}\rho(\phi_1,\phi_2)e^{-i(m\phi_1-m'\phi_2)}d\phi_1 d\phi_2 \qquad (2.63)$$

By substituting (2.61) (2.63) into (2.59) we have the explicit form:

$$\mathcal{E}\{\alpha_n\alpha_{n'}^*\} = \frac{\mathcal{A}}{(2\pi)^2}\sum_{m=-\infty}^{\infty}\sum_{m'=-\infty}^{\infty}\iota_m\iota_{m'}\xi_{(n-m)(n'+m')} \qquad (2.64)$$

Equations (2.57) and (2.64) are essential equations to provide a straight forward solution to calculate multipath richness as far as angular correlated or non-correlated spatial scatterer gain are concerned. We will give out numerical results of DoF and multipath richness regarding to specified APS in next chapter. DoF and multipath richness lay theoretical foundations for analysing the effect of multipath richness on wireless localisation.

2.6 Contributions

The technical contributions of this chapter were:

1. To theoretically determine the effect of the size of a circular region on the degrees of freedom. It is shown that the effect of changing the radius of the region is equivalent to filtering the angular multipath distribution with a specific non-ideal low pass filter.

2. To provide an explicit solution to calculate multipath richenss as far as angular correlated or non-correlated spatial scatterer gain are concerned. This lays theoretical foundation for analysing the effect of multipath richness on wireless localisation resolution.

3. To theoretically determine the degrees of freedom for APS limited wavefield. Since the APS limited case is less restricted than the deterministic case which must satisfy the homogeneous Helmholtz equation, the degrees of freedom is increased by a factor of 2.

Chapter 3

Effect of Multipath Richness on Wirless Location Resolution

As we know wireless signals propagate in space through a multipath environment due to the presence of reflectors and scatterers. It is widely reckoned that wireless communication systems are adversely affected by this multipath propagation because of the various levels of synchronization and high estimation accuracy requirements to keep track of the random variations of propagation complex gains of multipath.

On the other hand, multipath provides a form of spatial diversity since the incident waves occupy multiple incoming angles. Therefore, it is less likely that different points in space have similar fading characteristics. This raises the question of whether this spatial diversity of multipath could be beneficial to wireless localisation. This motivates us to address this question through an appropriate analytical framework.

We think it is feasible to consider wavefield as a function in Hilbert space. In Hilbert space, the multipath wavefield is regarded as an extended "vector" object as in Euclidean space. We have identified elements of Hilbert space with multipath wavefield in Chapter 2. Specially, the multipath wavefield is studied as solutions to the wave equation in an infinite-dimensional vector space as in (2.28). This provides a feasible solution to describe the wavefield by a limited number of parameters with tolerable information loss.

In this chapter we start by introducing the concept of *wireless location resolution* with the notion of "location signature". A model of $A(\phi)$ is proposed for simplifying introduction of angular correlation. Then we demonstrate the impact of multipath richness on wireless location resolution numerically. We base our study on the spatial aspects of multipath: the degrees of freedom (DoF) and multipath richness

in spatial multipath coupled to a aperture limited, source-free region of space (2D or 3D). We consider two cases: firstly we assume either we have complete knowledge of the spatial scatterer gain $A(\phi)$, both the amplitude and phase terms or we have statistical knowledge of $A(\phi)$ only, which is the expectation of the amplitude $|A(\phi)|$.

Our research results demonstrate richer multipath has a tendency to decrease the DoF of wavefields coupled to an aperture limited region. This indicates energy is more likely concentrated among the lower order Fourier coefficients (the energy is more isotropic) of the wavefield when the incoming multipath waves become richer. This energy concentration to lower order coefficients phenomenon provides insight to demonstrate positive effect multipath can have on wireless location resolution.

3.1   Location Signature

Before defining the concept of wireless location resolution, we introduce the notion of a *location signature.*

We assume a target of interest stays at a certain position for a time and the far-field scatterers have a specific geometrical distribution. The distribution is described by a specific $A(\phi)$ in (3.1):

$$F(\boldsymbol{x}) = \int_0^{2\pi} A(\phi) e^{ik\boldsymbol{x} \cdot \widehat{\boldsymbol{y}}(\phi)} d\phi, \quad \|\boldsymbol{x}\| \leq R \qquad (3.1)$$

The propagation scenario is shown in Figure 3.1 where each position has an unique spatial scatterer gain $A(\phi)$ observed from the region:

$$\mathbb{B}_R = \{\boldsymbol{x} \colon \|\boldsymbol{x}\| \leq R\}.$$

Since all sensors are constrained in region R, the target's location is completely determined by the information contained by the wavefield $F(\boldsymbol{x})$ in (3.1) where $\|\boldsymbol{x}\| \leq R$. We emphasize that $F(\boldsymbol{x})$ contains *all* information available to us.

In this scenario *location signature* is based on information contained in receiver region R, as shown in Figure 3.1. We may select a set of natural basis functions as (3.2):

$$\Phi_{n;R}(\boldsymbol{x}) \triangleq \frac{i^n J_n(k\|\boldsymbol{x}\|) e^{in\phi(\boldsymbol{x})}}{\sqrt{2\pi \mathcal{J}_n(R)}}. \qquad (3.2)$$
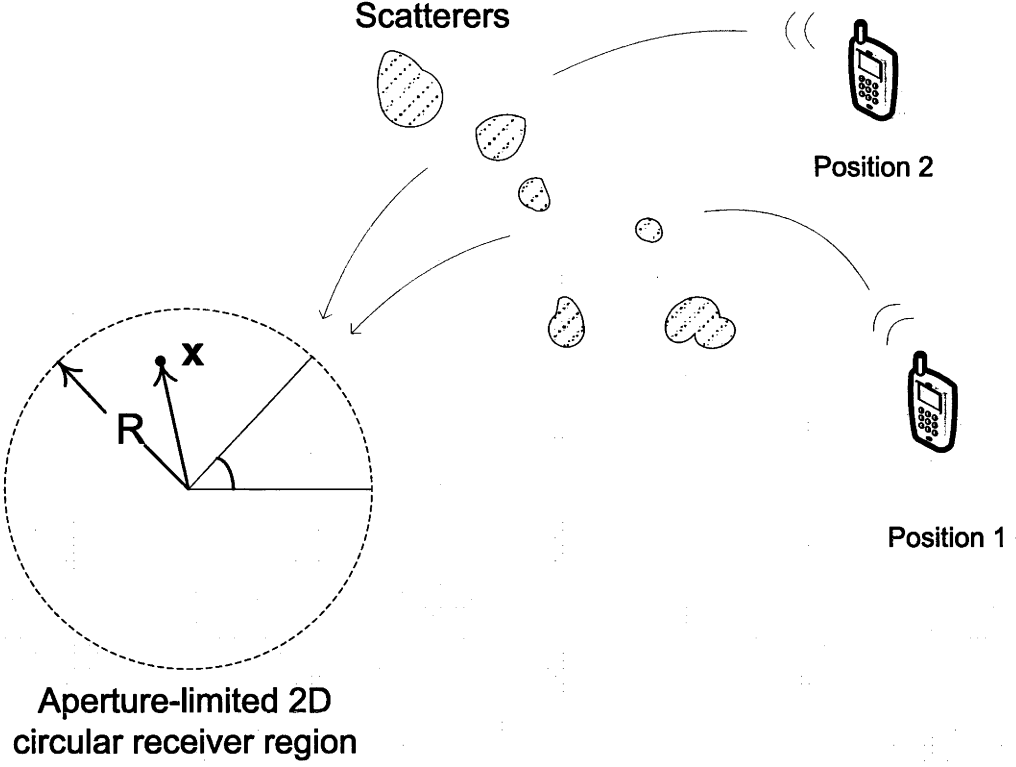
Figure 3.1: Propagation Scenario

to decompose $F(\boldsymbol{x})$ and we have:

$$F(\boldsymbol{x}) = \sum_{n=-\infty}^{\infty} \beta_{n;R}\, \Phi_{n;R}(\boldsymbol{x}), \quad \|\boldsymbol{x}\| \leq R \qquad (3.3)$$

where the set of Fourier coefficients $\{\beta_{n,R}\}$ is defined in (3.4).

$$\beta_{n;R} = \sqrt{2\pi \mathcal{J}_n(R)}\alpha_n. \qquad (3.4)$$

The set of basis functions is related with the region of space only and has relationship with $A(\phi)$. The $\{\beta_{n,R}\}$ sequence captures the properties of $A(\phi)$ by component α_n and the spatial filtering effect of the region by $\mathcal{J}_n(R)$.

It is straightforward that the natural basis functions have no contribution in determining a target's position when the region of space is determined. On the other hand, $\{\beta_{n;R}\}$ holds complete information on location of the target since for every $A(\phi)$ there exists a unique $\{\beta_{n;R}\}$ sequence. This makes it feasible to identify the position of the target by the information in the Fourier sequence, namely $\{\beta_{n;R}\}$. Hence $\{\beta_{n;R}\}$, corresponding to a specified $A(\phi)$, is defined as *location signature* of the target. Different positions of the target has a corresponding location signature. The above discussion is based on comprehensive knowledge of the wavefield coupled

to the circular region. In case of APS limited wavefield, sequence $\{\gamma_{n;R}\}$ in (3.5) takes the role of $\{\beta_{n;R}\}$.

$$\rho(\boldsymbol{z}) = i^n J_n(k\|\boldsymbol{z}\|)e^{in\varphi(\boldsymbol{z})}\gamma_n$$

$$= \sum_{n=-\infty}^{\infty} \gamma_{n;R}\Phi_{n;2R}(\boldsymbol{z}). \tag{3.5}$$

where $\gamma_{n;R}$ is defined as $\sqrt{2\pi\mathcal{J}_n(2R)}\gamma_n$ and the orthonormal basis function over the 2D disc of radius $2R$ is given by

$$\Phi_{n;2R}(\boldsymbol{z}) \equiv \frac{i^n J_n(k\|\boldsymbol{z}\|)e^{in\varphi(\boldsymbol{z})}}{\sqrt{2\pi\mathcal{J}_n(2R)}}, \quad \|\boldsymbol{z}\| \leq 2R. \tag{3.6}$$

The *location signature* determines a target's position uniquely in the far field observed from the region of interest. There is a specified spatial scatterer gain $A(\phi)$ corresponding to the target when it stays at a certain position. If the target has a position displacement in space, the incident $A(\phi)$ observed from the region of interest changes. This leads to the discussion of wireless location resolution in the next section.

3.2   Wireless Location Resolution

In the literature, location accuracy has attracted significant interest and much effort. Improved location accuracy and accuracy lower bound analysis are most frequently studied. In this framework researchers are focussed on determining the real position of target with low estimation error.

In some scenarios it is hard to locate the transmitter accurately. For example, it is expected to have large location estimation error in a dense multipath environment without LOS component. Instead of seeking way to know the unreliable estimation of the position of the target, we intend to study the mobility detection of target. We could have knowledge of a target's approximate location and we are more interested in detecting the target's mobility. In wireless localisation research, *location resolution* is a different concept to location accuracy. In RADAR technologies this is referring as moving-target indication (MTI) problem. MTI radar is a type of simple pulse doppler radar. It uses low doppler pulse repetition rate (e.g., 300 Hz) to distinguish moving targets from stationary clutter based on accurate range measurement.

Note in our case the target is assumed to have the tendency of moving to
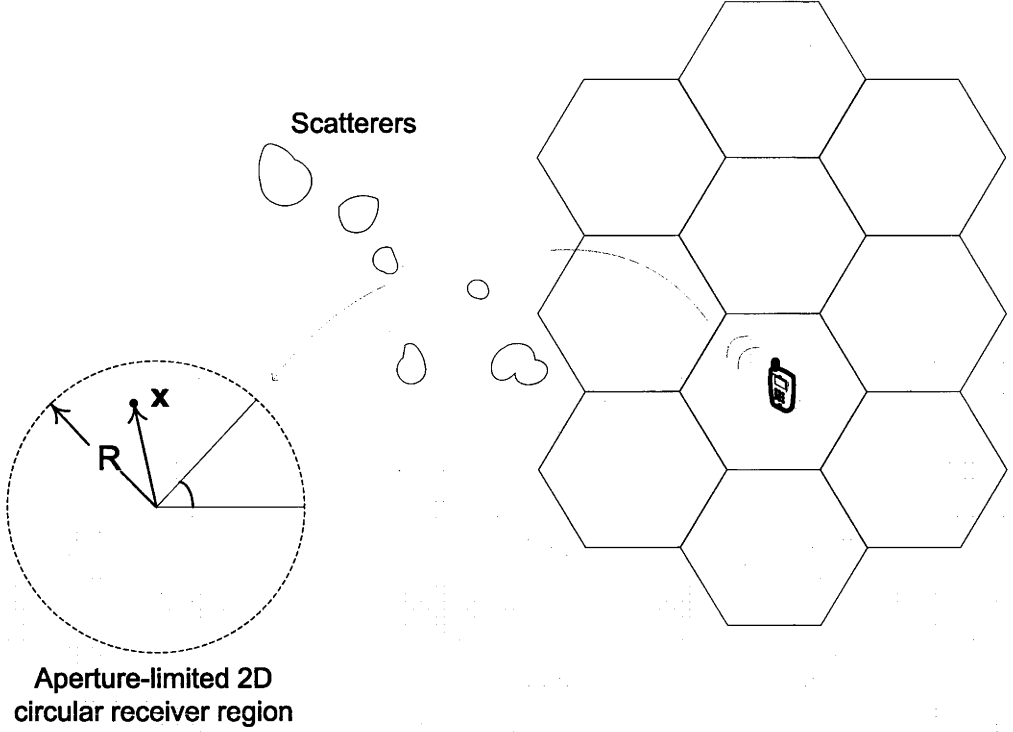
Figure 3.2: Location Resolution Cell

another position with slow speed.[1] Another signature is available regarding to
the new location. We make comparison of the two location signatures. If the
comparison result is larger than a threshold ϵ_{LR}, we consider the target has a
significant geographical displacement.

Suppose there is a target moving from position 1 to 2 then we have the corre-
sponding location signatures of $\{_1\beta_{n;R}\}$ and $\{_2\beta_{n;R}\}$. The decision of the target's
displacement is made based on whether

$$\sum_n |_1\beta_{n;R} - _2\beta_{n;R}|^2 \leq \epsilon_{LR}.$$

That is, once the signature difference reaches ϵ_{LR}, the target's current position is
distinguishable from previous one. The threshold ϵ_{LR} has significant impact on
location resolution for the given receiver region aperture and system noise. As
shown in Figure 3.2, the location signature difference is smaller than ϵ_{LR} if the
target (mobile handset) is roaming within one cell. In the case when the target has
shifted to other cell, it must have a new distinguishable location signature which
has a difference larger than ϵ_{LR} compared with the original cell. To summarise,
ϵ_{LR} determines the size of the cell with a positive proportion relation.

---

[1]In this thesis we will not consider Doppler effect on location signature.
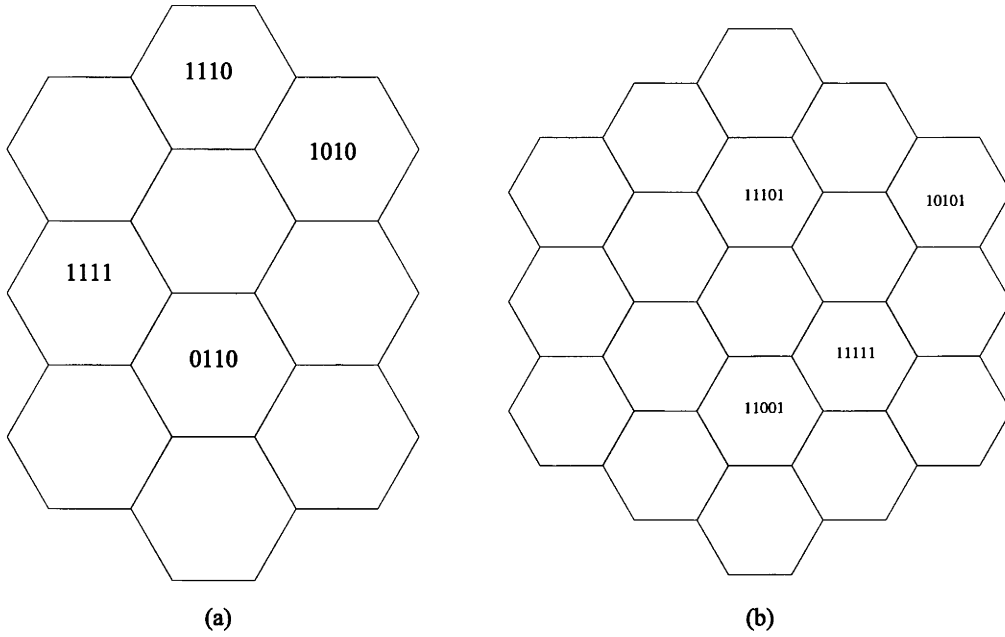
Figure 3.3: Location Resolution

With the assistance of the *location signature*, we can separate an arbitrary region in space into cells as shown in Figure 3.3(a), each with a digital label. The region is divided into cells with appropriate size decided by ϵ_{LR}, receiver region aperture R and system noise level. Comparing Figure 3.3(a) with Figure 3.3(b), fewer number of cells are required to label the region completely relative to the bigger cell size. Subsequently, each cell's label requires less number of digits to identify it.

A smaller cell size defines a finer *location resolution*, which determines the target's position with less ambiguity. We may ask if there are other factors influencing cell's size. This leads to our study on achieving finer location resolution for fixed ϵ_{LR}, receiver region aperture R and system noise level. In next section we analyse the effect of multipath richness imposed by the DoF which is determined through the Fourier sequence, either $\{\gamma_{n;R}\}$ or $\{\beta_{n;R}\}$. With the concept of *location signature* it becomes feasible to address the problem of the effect of multipath richness on wireless location resolution.

3.3   Effect of Multipath Richness on DoF of APS Limited Wavefield

The degrees of freedom relate closely with the notion of multipath richness and related concepts [29]. We focus our attention on how energy is distributed over the

coefficients in an expansion representation of multipath or equivalently the spatial correlation. Towards this end we formulate the following problem.

3.3.1   Problem Statement

As we know spatial correlation $\rho(z)$ where $z = x_2 - x_1$ is the only information available from the region region of radius R for APS limited wavefield. We refer to equations (3.5) (3.6) to study energy distribution over the coefficients in the serial expansion representation of spatial correlation. The effect of multipath richness on DoF is exposed by studying the energy contained by the total $2N + 1$ components in (3.5) while the total energy in the receiver region is assumed constant. Since different angular power spectrum dominates multipath richenss, we need to find the angular power spectrum, $P(\varphi)$, for fixed value of N. This achieves

$$\sup \frac{\sum_{n=-N}^{N} i^n \gamma_n J_n(k\|x_2 - x_1\|)e^{in\varphi_{21}}}{\sum_{n=-\infty}^{\infty} i^n \gamma_n J_n(k\|x_2 - x_1\|)e^{in\varphi_{21}}}$$

$$= \sup \frac{\sum_{n=-N}^{N} i^n \gamma_n J_n(k\|z\|)e^{in\varphi(z)}}{\sum_{n=-\infty}^{\infty} i^n \gamma_n J_n(k\|z\|)e^{in\varphi(z)}}$$

$$= \sup \frac{\sum_{n=-N}^{N} \sqrt{2\pi \mathcal{J}_n(2R)}\gamma_n \Phi_n(z)}{\sum_{n=-\infty}^{\infty} \sqrt{2\pi \mathcal{J}_n(2R)}\gamma_n \Phi_n(z)}. \tag{3.7}$$

3.3.2   Solution

According to Parseval's theorem, we can use the Fourier transform coefficients $\{\gamma_{n;R}\}$ to represent wavefield's energy. It is straightforward that (3.7) is well approximated by

$$\sup \frac{\sum_{n=-N}^{N} 2\pi \mathcal{J}_n(2R)|\gamma_n|^2}{\sum_{n=-\infty}^{\infty} 2\pi \mathcal{J}_n(2R)|\gamma_n|^2}. \tag{3.8}$$

where the natural orthogonal basis function $\Phi_{n;2R}(z)$ is dropped.

In this thesis we provide investigation into the notion of richness by numerical methods. We find that the concentration level of low-order modes of spatial correlation increases when multipath richness increases. This is demonstrated by the numerical simulation results that follow. We note the approach to mathematically quantify multipath richness is defined in [29].

3.3.3   Numerical Results

In our numerical simulation environment the receiver region is a 2D disk of $R = \lambda$. Some popular APS are selected to verify the effect of multipath on low-index modes

Figure 3.4: Numerical analysis of ratio $\frac{\sum_{n=-N}^{N} 2\pi \mathcal{J}_n(2R)|\gamma_n|^2}{\sum_{n=-\infty}^{\infty} 2\pi \mathcal{J}_n(2R)|\gamma_n|^2}$ for von-Mises APS with different multipath richness. The horizontal axis is the different truncation lengths N in (3.10). The receiver region is of $R = \lambda$.

concentration of spatial correlation in the receiver region. These APSs are von-Mises [34], extended Laplacian and extended Gaussian APS [33].

von-Mises APS

The von-Mises APS is described in (3.9):

$$P(\varphi) = \frac{1}{2\pi I_0(\kappa)} e^{\kappa \cos(\varphi - \varphi_0)}, \quad |\varphi - \varphi_0| \leq \pi \tag{3.9}$$

where we can tune the parameter κ to affect multipath richness (width of the von Mises distribution). With smaller value of κ the incoming waves should have richer multipath. The ratio of

$$\frac{\sum_{n=-N}^{N} 2\pi \mathcal{J}_n(2R)|\gamma_n|^2}{\sum_{n=-\infty}^{\infty} 2\pi \mathcal{J}_n(2R)|\gamma_n|^2}. \tag{3.10}$$

is shown in Figure 3.4.

From the results in the figure it appears N need to be as large as 8 in order for $\sum_{n=-N}^{N} 2\pi \mathcal{J}_n(2R)|\gamma_n|^2$ to contain more than 90% of the total energy of the spatial correlation fourier coefficients $\{\gamma_{n;R}\}$ when the incoming wave has multipath richness of 2. The total energy of the spatial correlation fourier coefficients $\{\gamma_{n;R}\}$ is $\sum_{n=-\infty}^{\infty} 2\pi \mathcal{J}_n(2R)|\gamma_n|^2$. This indicates $2N + 1 = 17$ components of $\{\gamma_{n;R}\}$ are

needed. If the incoming wave has multipath richness of 4 and 6, N is expected to be no less than 5 and 3, which requires 11 and 7 components of $\{\gamma_{n;R}\}$, respectively. In case that multipath richness is 14, only 3 ($N = 1$) components of $\{\gamma_{n;R}\}$ are needed.

Modified Laplacian APS

The Modified Laplacian APS is

$$P(\varphi) = \frac{Q}{\sqrt{2}\sigma}e^{-\sqrt{2}|\varphi-\varphi_0|/\sigma}, \quad |\varphi - \varphi_0| \leq \pi \tag{3.11}$$

for normalization constant Q, σ determines the angular width and φ_0 is the direction of the peak. The ratio of

$$\frac{\sum_{n=-N}^{N} 2\pi \mathcal{J}_n(2R)|\gamma_n|^2}{\sum_{n=-\infty}^{\infty} 2\pi \mathcal{J}_n(2R)|\gamma_n|^2}. \tag{3.12}$$

is shown in Figure 3.5. N needs to be as large as 10 in order for

$$\sum_{n=-N}^{N} 2\pi \mathcal{J}_n(2R)|\gamma_n|^2$$

to contain more than 90% of the total energy of the spatial correlation fourier coefficients $\{\gamma_{n;R}\}$ when the incoming wave has multipath richness of 2. This indicates $2N + 1 = 21$ components of $\{\gamma_{n;R}\}$ are needed. If the incoming wave has multipath richness of $4, 6, 8, 10$ and 12, N is expected to be no less than $9, 8, 7, 6$ and 5, which requires $20, 17, 15, 13$ and 11 components of $\{\gamma_{n;R}\}$ respectively. In case that multipath richness is 14, 5 ($N = 2$) components of $\{\gamma_{n;R}\}$ are needed.

Modified Gaussian APS

The Modified Gaussian APS is described in (3.13):

$$P(\varphi) = \frac{Q}{\sqrt{2\pi}\sigma}e^{-(\varphi-\varphi_0)^2/2\sigma^2}, \quad |\varphi - \varphi_0| \leq \pi \tag{3.13}$$

where σ is the angular variance, φ_0 is the direction of the peak/mean, and Q is a normalization to account for the finite truncation of the Gaussian distribution (which is normally of infinite support).

The ratio of

$$\frac{\sum_{n=-N}^{N} 2\pi \mathcal{J}_n(2R)|\gamma_n|^2}{\sum_{n=-\infty}^{\infty} 2\pi \mathcal{J}_n(2R)|\gamma_n|^2}. \tag{3.14}$$
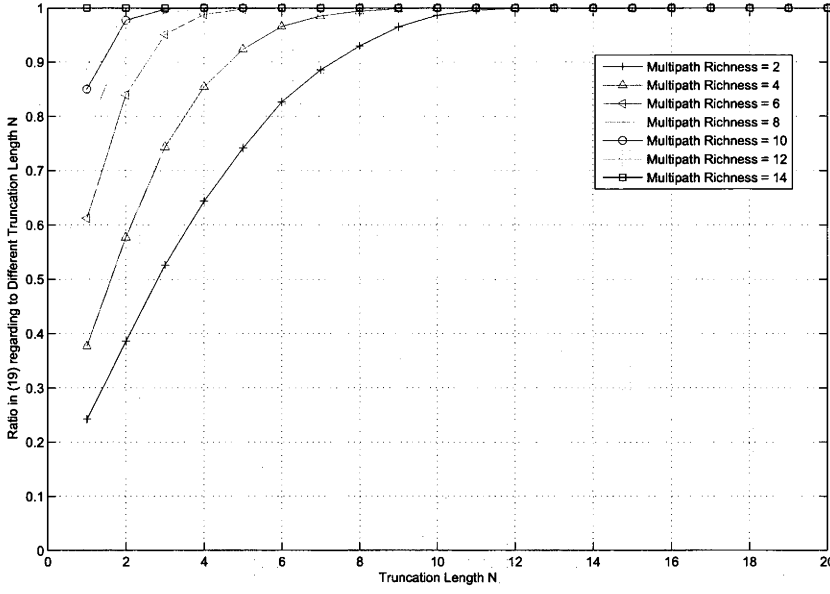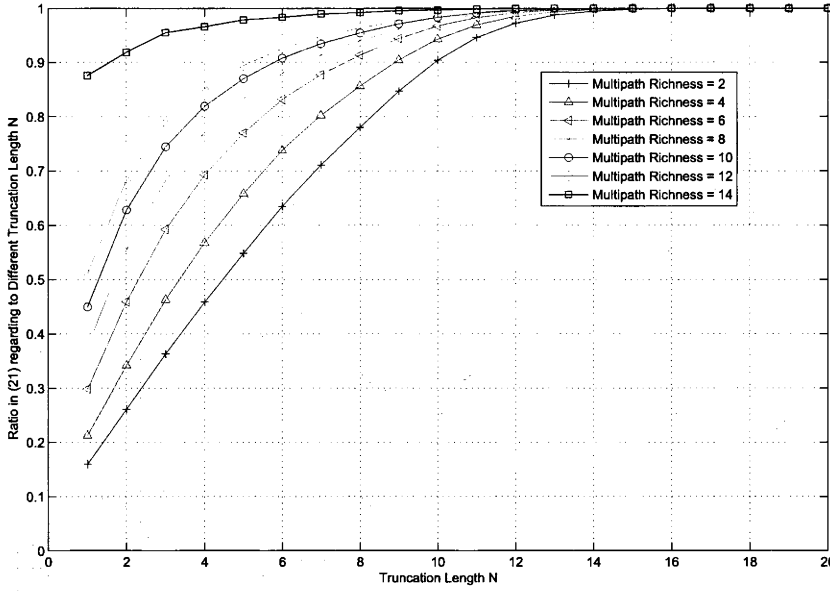
Figure 3.5: Numerical analysis of ratio $\frac{\sum_{n=-N}^{N} 2\pi \mathcal{J}_n(2R)|\gamma_n|^2}{\sum_{n=-\infty}^{\infty} 2\pi \mathcal{J}_n(2R)|\gamma_n|^2}$ for modified Laplacian APS with different multipath richness. The horizontal axis is the different truncation lengths N in (3.12). The receiver region is of $R = \lambda$.

is shown in Figure 3.6. N needs to be as large as 10 in order for

$$\sum_{n=-N}^{N} 2\pi \mathcal{J}_n(2R)|\gamma_n|^2$$

to contain more than 90% of the total energy of the spatial correlation fourier coefficients $\{\gamma_{n;R}\}$ when the incoming wave has multipath richness of 2. This indicates $2N + 1 = 21$ components of $\{\gamma_{n;R}\}$ are needed. If the incoming wave has multipath richness of $4, 6, 8, 10$ and 12, N is expected to be no less than $6, 4, 3, 2$ and 2, which requires $13, 9, 7, 5$ and 5 components of $\{\gamma_{n;R}\}$ respectively. In case that multipath richness is 14, 3 ($N = 1$) components of $\{\gamma_{n;R}\}$ are needed.

3.4　Effect of Multipath Richness on DoF

We address the problem of effect of multipath richness in the cases of uncorrelated spatial scatterers and correlated environments.
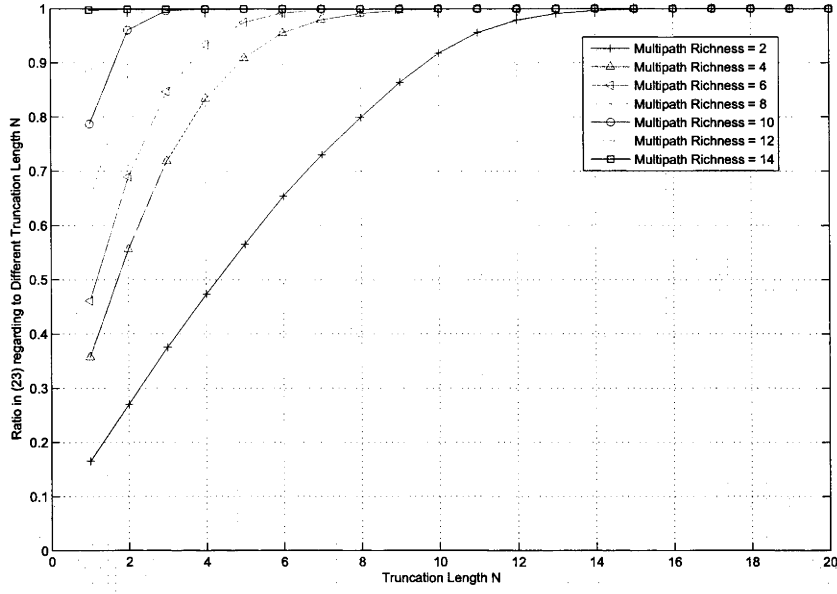
Figure 3.6: Numerical analysis of $\sum_{n=-N}^{N} 2\pi \mathcal{J}_n(2R)|\gamma_n|^2 / \sum_{n=-\infty}^{\infty} 2\pi \mathcal{J}_n(2R)|\gamma_n|^2$ for modified Gaussian APS with different multipath richness. The horizontal axis is the different truncation lengths N in (3.14). The receiver region has radius $R = \lambda$.

3.4.1   DoF in Uncorrelated Spatial Scatterer Environment

In an uncorrelated spatial scatterer environment we have

$$\mathcal{E}\{A(\phi_1)A^*(\phi_2)\} = \mathcal{E}\{|A(\phi_1)|^2\}\delta(\phi_1 - \phi_2).$$

We use a statistical method to study the effect of multipath richness on DoF. To introduce uncorrelated scattering, for a prescribed APS $P(\phi)$, we propose a model (which is not unique) by assuming $A(\phi)$ is circularly complex Gaussian and generated according to

$$A(\phi) = \sqrt{\frac{P(\phi)}{2}}\, x(\phi) + i\sqrt{\frac{P(\phi)}{2}}\, y(\phi) \tag{3.15}$$

where $x(\phi)$ and $y(\phi)$ are independent stationary Gaussian random processes of zero mean and variance one. Note that, $P(\phi)$ shapes the angular distribution independent of the component process correlations.

In our statistical method, we work with a sampled version of (3.15) which simplifies the introduction (in the next Section) of the angular correlation of $A(\phi)$. Evaluating $A(\phi)$ at a number of angles ϕ_1, ϕ_2, $\cdots$, ϕ_n, define the vectors of correlated Gaussian random variables $\boldsymbol{x} = [x(\phi_1), \cdots, x(\phi_n)]^T$ and $\boldsymbol{y} = [y(\phi_1), \cdots,$

Table 3.1: Relation of κ and Multipath Richness with angular uncorrelated $A(\phi)$, namely $\sigma_S = 0$

κ	0.1	2	3	3.5	5.5	11.5	64
Multipath Richness	14	12	10	8	6	4	2
DoF	15	15	15	15	15	15	15

$y(\phi_n)]^T$. Sequences $\boldsymbol{x}$ and $\boldsymbol{y}$ both have the same $n \times n$ identity covariance matrix.

A circular region whose radius $R = \lambda$ is adopted as receiver region. Discrete samples of $A(\phi)$ at angles ϕ_1, ϕ_2, $\cdots$, ϕ_n are generated and the Fourier sequence $\{\beta_{n,R}\}$ is calculated through numerical integration. This process is repeated for a large number of trials and the final statistical DoF is achieved according to (2.44) and (2.45). We may change the angular spread of APS to tune multipath richness of the wavefield. For a uni-modal APS $P(\phi)$ the von-Mises power distribution is the most common choice:

$$P(\phi) = \frac{1}{2\pi I_0(\kappa)} e^{\kappa \cos(\phi - \phi_0)}, \quad |\phi - \phi_0| \leq \pi, \qquad (3.16)$$

where κ describes the angular spread of multipath power, ϕ_0 is the central angle of arrival and $I_0(\kappa)$ is the modified Bessel function of the first kind. Given an uncorrelated $A(\phi)$ environment, the multipath richness is determined by κ, which is shown in Table 3.1. From our simulation results, the circular region with radius $R = \lambda$ has DoF of 15, which is irrelevant with what the multipath richness is because of the lack of angular correlation in the model.

3.4.2   DoF in Correlated Spatial Scatterer Environment

A. Correlated Scatterers Model

To introduce correlated scattering, for a prescribed APS $P(\phi)$, we propose a simple model by assuming $A(\phi)$ is circularly complex Gaussian and generated according to

$$A(\phi) = \sqrt{\frac{P(\phi)}{2}}\, x(\phi) + i\sqrt{\frac{P(\phi)}{2}}\, y(\phi) \qquad (3.17)$$

where $x(\phi)$ and $y(\phi)$ are independent stationary Gaussian random processes of zero mean and variance one. Note that, $P(\phi)$ shapes the angular distribution independent of the component process correlations.

We shall work with a sampled version of (3.17) which simplifies introduction of the correlation. Evaluating $A(\phi)$ at a number of angles ϕ_1, ϕ_2, $\cdots$, ϕ_n, define the vectors of correlated Gaussian random variables $\boldsymbol{x} = [x(\phi_1), \cdots, x(\phi_n)]^T$ and

$$\boldsymbol{y} = [y(\phi_1), \cdots, y(\phi_n)]^T.$$

Sequences $\boldsymbol{x}$ and $\boldsymbol{y}$ both have the same $n \times n$ covariance matrix $\boldsymbol{\rho}$ where a component at the ith row and j^{th} column is identified with $\rho(\phi_i, \phi_j)$. $\boldsymbol{\rho}$ can be decomposed by Cholesky factorization [35]

$$\boldsymbol{\rho}_{n \times n} = \boldsymbol{L}\boldsymbol{L}^T$$

where $\boldsymbol{L}$ is a lower triangular matrix.

We generate a vector of independent standard normal random variables $\boldsymbol{z} = [z(\phi_1), \cdots, z(\phi_n)]^T$ then define

$$\boldsymbol{x} = [x(\phi_1), \cdots, x(\phi_n)]^T = \boldsymbol{L}\boldsymbol{z}.$$

Here $\boldsymbol{x}$ is correlated Gaussian random vector with covariance matrix $\boldsymbol{\rho}$. In a similar way we can generate correlated random vector $\boldsymbol{y}$. Generating such correlated random vectors is standard, e.g., as given in [36, p. 215].

In a real multipath environment we expect that there should be correlation whenever the two angles ϕ_i and ϕ_j are close because they are likely to be coming from the same physical scatterer illuminated by the same source. Further, as the separation between the angles increases we expect decreasing correlation and so we adopt a simple model

$$\rho(\phi_i, \phi_j) = e^{-(\phi_i - \phi_j)^2 / 2\sigma_S^2}, \quad i, j = 1, 2, \ldots, n \tag{3.18}$$

where $\sigma_S \geq 0$ is a correlation spread factor, another important system parameter. Varying σ_S changes the amount of multipath correlation and hence the DoF. This correlation modeling is made independently of the APS $P(\phi)$.

For a uni-modal APS $P(\phi)$ the von-Mises power distribution is the most common choice

$$P(\phi) = \frac{1}{2\pi I_0(\kappa)} e^{\kappa \cos(\phi - \phi_0)}, \quad |\phi - \phi_0| \leq \pi, \tag{3.19}$$

where κ describes the angular spread of multipath power and ϕ_0 is the central angle of arrival.

Decreasing σ_S increases the level of correlation between close angles in the phase of $A(\phi)$. In Figure 3.7 and 3.8 we verify our model exhibits correlation. Plotted are samples of $A(\phi)$ at $\phi = 0°$ and $\phi = 5°$ which show greater concentration for lesser σ_S.
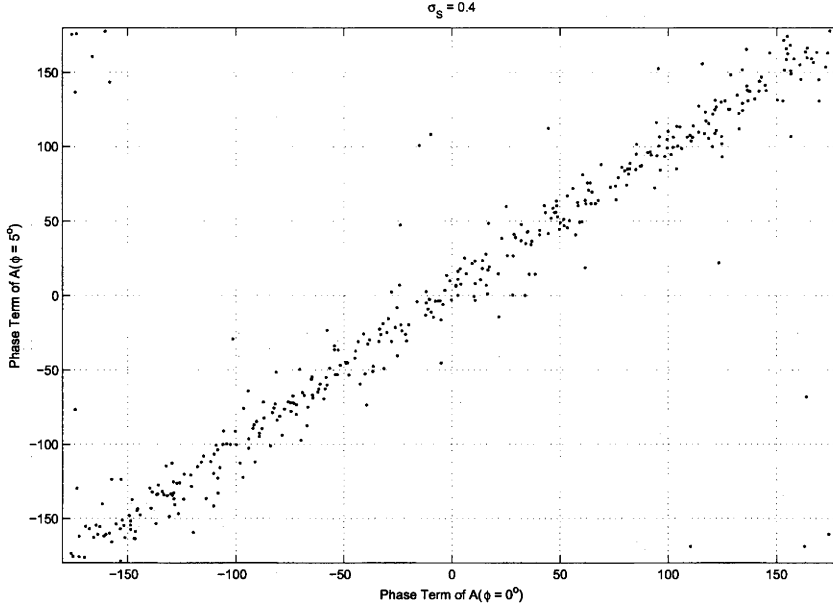
Figure 3.7: Plot of phase term of $A(\phi)$ at $\phi = 0°$ versus $\phi = 5°$ for $\sigma_S = 0.4$.

B. DoF in Correlated Spatial Scatterer Environment

With angular correlation of $A(\phi)$ as shown in (3.18) the random wavefield is more constrained (relative to the uncorrelated case) and, therefore, this reduces the degrees of freedom we can expect. As shown in Table 3.1, 3.2 and 3.3, angular correlation not only decreases the degrees of freedom but also reduces richness. In uncorrelated wavefield, richness is 14 and DoF is 7 when $\kappa = 0.1$. In a slight correlated wavefield ($\sigma_S = 0.4$), richness turns to be 11 and DoF is 5 given same APS angular spread ($\kappa = 0.1$). If we continue to augment the angular correlation by setting $\sigma_S = 1$, richness is only 5 and DoF is reduced to 3 only.

In detail, Figure 3.9 demonstrates the effect of multipath richness showing the ratio $\frac{\sum_{n=-N}^{N} |\beta_{n,R}|^2}{\sum_{n=-\infty}^{\infty} |\beta_{n,R}|^2}$ in our specific receiver region. The horizontal axis is the truncation length N. We see the ratio intends to increase as richness increases. The energy of the wavefield concentrates to low-order coefficients of $\{\beta_{n,R}\}$ sequence with richer multipath. The DoF is decreased correspondingly. We further increase the angular correlation by increasing σ_S from 0.4 in Figure 3.9 to 1.0 in Figure 3.10. With a stronger correlated $A(\phi)$, $\{\beta_{n,R}\}$ sequence indicates a more intense concentration to low-order Fourier coefficients. In this situation, each unit richness increase brings more percentage energy concentration, though the range of richness is more constrained.

We conclude that richer multipath has a tendency to concentrate its energy in the low-order modes of its corresponding Fourier sequence $\{\beta_{n,R}\}$, given an angular
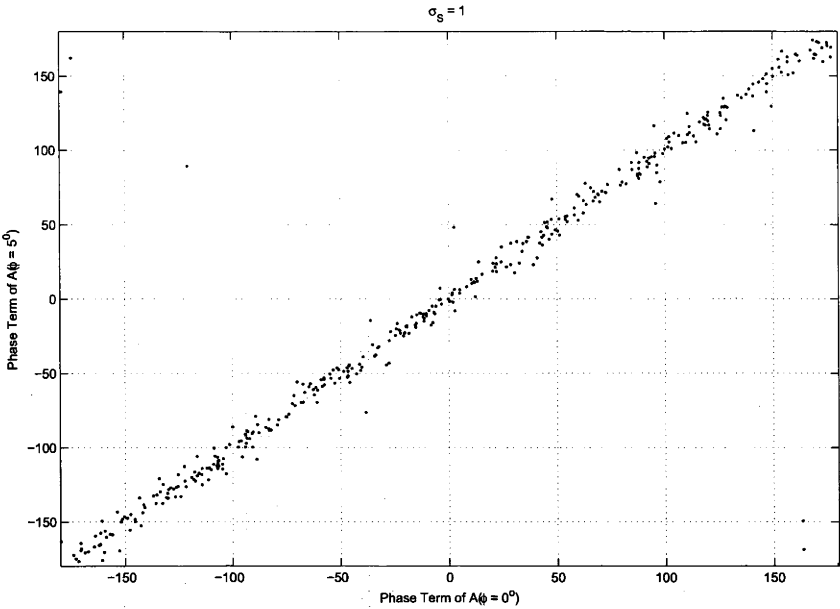
Figure 3.8: Plot of phase term of $A(\phi)$ at $\phi = 0°$ versus $\phi = 5°$ for $\sigma_S = 1.0$.

Table 3.2: Relation of κ, multipath richness and DoF with angular correlated $A(\phi)$ where $\sigma_S = 0.4$

κ	0.1	2	3	4	11
Multipath Richness	11	9	7	5	3
DoF	11	11	11	11	13

correlated spatial scatterer gain $A(\phi)$. This discovery has direct application in addressing wireless location resolution. We will discuss this application in the next section in detail.

Table 3.3: Relation of κ, multipath richness and DoF with angular correlated $A(\phi)$ where $\sigma_S = 1$

κ	0.1	3	4	8.5
Multipath Richness	5	4	3	2
DoF	7	7	9	9

Figure 3.9: Numerical analysis of ratio $\frac{\sum_{n=-N}^{N} |\beta_n|^2}{\sum_{n=-\infty}^{\infty} |\beta_n|^2}$ for von-Mises APS with different multipath richness. $\sigma_S = 0.4$. X-axis is different truncation length N in (2.45). The receiver region is of $R = \lambda$.

3.5 Applications

Using the noise model in [9] the optimal estimator of the Fourier coefficients $\widetilde{\beta}_{n;R}$ will be a normally distributed random process:

$$\widetilde{\beta}_{n;R} \sim \mathcal{N}\left(\beta_{n;R}, \frac{N_0 \pi R^2}{4\pi \mathcal{J}_n(R)}\right).$$

The noise term in $\widetilde{\beta}_{n;R}$ is spatial white and independent of the term index n. The target's position information is contained in the Fourier sequence $\{\beta_{n;R}\}$. As we demonstrated in previous section, $\{\beta_{n;R}\}$ will have low-order modes concentration with richer incoming multipath wavefields. This indicates the ratio of the energy of $\{\beta_{n;R}\}$ to noise power can be increased by richer multipath.

The assumption is that location resolution is related with the above ratio value in a noisy case. In a noise free case, low-order modes concentration will also contribute to finer location resolution. The point is to demonstrate how the magnitude of $\{\beta_{n;R}\}$ or the ratio affects location resolution.
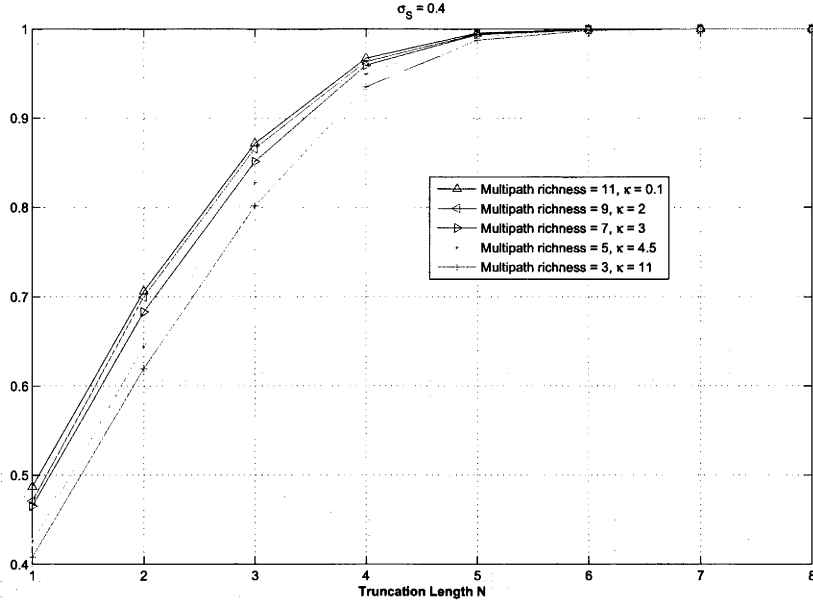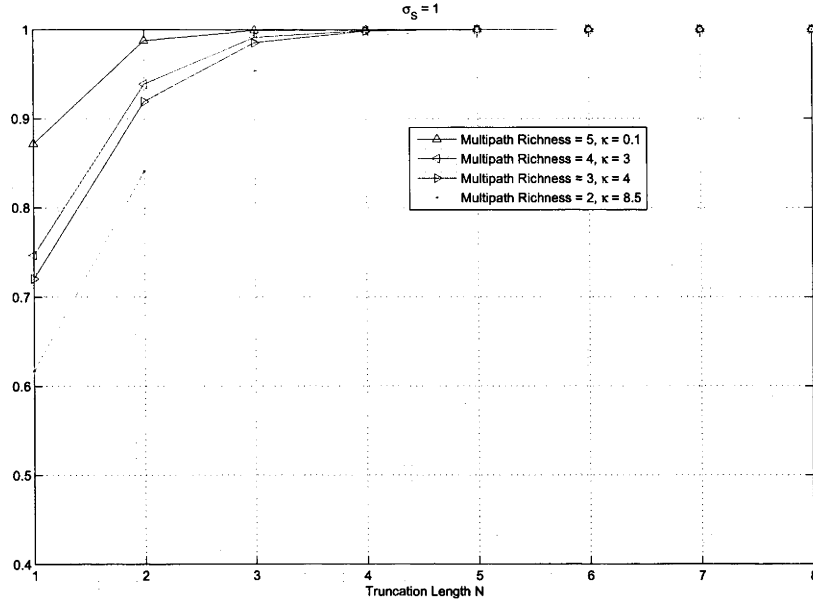
Figure 3.10: Numerical analysis of ratio $\frac{\sum_{n=-N}^{N} |\beta_n|^2}{\sum_{n=-\infty}^{\infty} |\beta_n|^2}$ for von-Mises APS with different multipath richness. $\sigma_S = 1$. X-axis is different truncation length N in (2.45). The receiver region is of $R = \lambda$.

3.6   Contributions

The technical contributions of this chapter were:

1. To theoretically determine the effect of angular correlation for a given angular power spectrum on the degrees of freedom and multipath richness.

2. To develop a model for generating random wavefields according to a given angular correlation characteristic which permits a numerical investigation into the effects of correlation modeling.

3. To theoretically determine the effect of multipath richness on wireless location resolution.

Chapter 4

Adaptive Radio Signal Prediction and Application

4.1 Introduction

In this and the next chapter, we provide practical wireless location solutions focused on fingerprint technology. As we know, fingerprint technology is most widely adopted in existing location systems due to its easy deployment and cost-efficiency. It operates over Wi-Fi infrastructure without the need for any additional proprietary hardware. It has no requirements for system clock synchronisation between base stations when temporal parameters are measured and antenna elements calibration when AoA is measured. Unlike other location techniques where multiple base stations are necessary, single base station even works well for fingerprint technology. It has accurate location estimation performance (enabled location of assets or people with up to 1 to 3 meter accuracy in Wi-Fi infrastructure) and is robust to the impact of multipath propagation, non line-of-sight propagation, channel fading condition and the relative positions of target and base stations. One of the successful application examples of fingerprint technology is Ekahau's Real Time Localization System (RTLS) and Site Survey Solutions (SSS). RTLS and SSS have been selected as Nortel, Simens, 3M and the London Clinic's provider of location tracking solutions. To contribute to fingerprint technology, in this chapter, we use an idea of building a "virtual propagation environment" (VPE) for predicting radio signal strength in Wireless LAN. Radio signal strengths at a number of (relatively sparse) sample points are measured and utilised to build VPE. In return, VPE provides a fingerprint database with finer resolution of spatial radio signal distribution. This advantage could be taken by WLAN localisation system to improve location accuracy. To verify and analyse the impact of finer spatial sample resolu-

tion on location accuracy, radio signal real field measurements are implemented in our work. Before addressing radio propagation prediction and its applications, we list the technical contributions of this chapter:

1. To adopt the concept of VPE to predict radio signal strength spatial distribution in WLAN.

2. VPE is applied in improving localisation accuracy in WLAN.

3. A novel "stochastic position" method is applied in real field radio signal strength measurement for mitigating small scale fading.

In the next chapter, we will exploit the already available channel impulse response of fixed wireless terminals as location fingerprint to assist wireless localisation in fixed wireless networks. (In this thesis, we apply adaptive radio signal prediction and pattern matching algorithms to improve wireless location accuracy.) In our work, radio wave real field measurements and propagation simulations are implemented to support the applied algorithms.

As we know, prediction of radio propagation in indoor environments is a difficult problem, due to reflection, diffraction and scattering of radio waves. Numerous statistical and deterministic radio propagation models are available for predicting wireless signal spatial and temporal distributions [37–40]. The performance of these models is unsatisfactory due to their accuracy and/or computational complexity, especially in propagation environments with dense multi-path such as indoor scenarios.

Many predictive methods use ray-tracing as a foundation [26]. Ray-tracing is a well known, and widely used radio propagation model, based upon the approximation of wireless signals as linear rays emanating from a point-like source. The rays are straight lines, perpendicular to the wavefront, possibly augmented with reflections and/or scattering [26, 41]. The model has been used in several scenarios, for example [37, 42] and takes its intuition from physical optics. Although ray-tracing is an effective tool for indoor/outdoor wireless environments [43], a fine spatial resolution of propagation environment is required for accurate prediction. The cost of computation increases with increasing sample resolution and the electromagnetic details of structures along radio propagation path are critical to final prediction results.

At high resolution, ray-tracing typically incorporates so-called "small scale" fading which varies on the order of a few wavelengths. However, for point-like receivers small scale fading is essentially not predictable for ranges beyond half-

wavelength [44]. Moreover, including small-scale fading does not provide useful predictive information.

For these reasons, we develop a ray-tracing like model which attempts to accurately match *large-scale* fading effects in the channel. We define large-scale fading as variations which are temporally and spatially coherent over a non-negligible range. Specifically, for a "position" in space-time $\{r, t\}$, we expect that the fading at a "nearby" position $\{r + \delta, t\}$ will have similar characteristics, for $\delta \gg \lambda$. Monte Carlo integration is adopted in averaging the received signal strength over this range. A corresponding field measurement based on Monte Carlo integration is developed.

The detail of the idea is to produce a "virtual propagation environment" to implement radio signal prediction based on sampled radio signal in the real environment. The idea comes from the intuition that key features of the real environment are contained in the radio signal samples and hence details of the real environment are not necessary for prediction. Instead, the "virtual propagation environment" will be built whose features are consistent to what is contained by the radio signal samples. In detail, dominant environment features such as reflective walls and scattering bodies in VPE are manipulated as model parameters according to the radio signal samples and relative geometrical displacement between transceivers. We apply adaptive nonlinear least square algorithm and feature based neural network to "learn" features of the real environment and predict radio signal distribution as a function of position r.

To illustrate the concept of VPE, two radio propagation models are given in section 4.2 as preliminaries. Section 4.3 and 4.4 present a feature based neural network and adaptive nonlinear least square algorithm for building VPE based on radio signal samples in a WLAN environment. Section 4.5 introduces the implementation of fingerprint technology in detail, such as nearest neighbor method and kernel method. To support our analysis, we build a WLAN localisation system based on a PC laptop running Linux. Details of the system is described in 4.6, where the normal static and the novel "stochastic position" measurement methods are also discussed. Section 4.7 presents three experimental results. The first experiment shows the advantage of the "stochastic position" method compared with the normal "static method". The second aims to demonstrate the prediction performance of VPE using one-dimensional radio signal samples. Without loss of generality, VPE trained by feature based neural network is shown. The last experiment demonstrates the location accuracy improvement achieved by the application of VPE while two-dimensional radio signal samples are provided.

4.2   Radio Propagation Models

We introduce two radio propagation models in this section, non-coherent and co-herent power component models. Consider a frequency-flat fading environment, where the channel is given by

$$y = ax + n$$

and y is the receive symbol, x is the transmit symbol with (complex scalar) channel gain a and AWGN sample n. The channel comprises L paths, and the signal received is a weighted sum of signals from each path without ISI. This is the well-known discrete model for multipath channels [45, 46], such that

$$a = \sum_{i=1}^{L} |\alpha_i| \, e^{-j\phi_i}$$

For any channel model, we must trade off prediction reliability with computa-tion expense, and measurement resolution. In our case, we are limited to signal strength (real power) measurements. We consider two simple models for the power received at a particular point r in space.

- Propagation model 1: the *signal* received is a phasor sum of complex signals, which result in a particular real power. In this way, the common phasor model for electric signals provides a hidden model for the received power.

- Propagation model 2: all received power is assumed to be a weighted sum of coherent power blocks (no phasor component) – so the underlying electrical source of the power measurement is ignored. The name "coherent power" reminds the reader that the underlying signals are effectively all in phase.

4.2.1   Propagation Model 1: electric signal

Consider a single path, of a multi-path environment. An electric signal arrives at the receiver with phase (and amplitude) determined by path length and reflection characteristics. The electric field with distance d_i to transmitter at time t is given by [26]

$$E_i(d_i, t) = \Gamma_i \frac{E_0 d_0}{d_i} \cos\left(\frac{2\pi d_i}{\lambda}\right) x(t) \tag{4.1}$$

where E_0 is the electric field (V/m) at a reference point with distance d_0 to trans-mitter, λ is the wavelength of the radio wave. The constant Γ_i is the reflected

field strength, in the case that the wave is reflected. For multiple waves the total electric field at a position is the scalar sum of all the components (LOS and/or NLOS) given by

$$E(\boldsymbol{r}) = \sum_i E_i(\boldsymbol{r}) \tag{4.2}$$

The corresponding received signal power at the position $\boldsymbol{r}$ is [26]

$$P(\boldsymbol{r}) = \frac{|E(\boldsymbol{r})|^2 G_r \lambda^2}{480\pi^2} \text{ Watts} \tag{4.3}$$

This model includes small scale fading, as is typically used for scattering models. Note that the power P is the "model parameter" which will be measured, not E.

4.2.2 Propagation Model 2: coherent power

Prediction of small-scale fading statistics is known to be an ill-posed problem [44]. Given the power measurements available at the receiver, we wish to estimate the value of a "large-scale" fading process: ie, one which may be modeled *without recourse to phase information*. For a multi-path signal, each path contributes to the power at receive location $\boldsymbol{r}$. The power contributed by the kth path is [43]

$$P_k(\mathbf{r}) = \frac{\alpha P_0}{l_k(\mathbf{r})^2} \prod_i \sigma_i \tag{4.4}$$

where $P_k(\mathbf{r})$ is given directly from signal-strength measurements. Here α is a constant, related to the antenna pattern, carrier frequency and initial path direction, P_0 is the transmitter power, $l_k(\mathbf{r})$ is the length of the unfolded path from transmitter to location $\mathbf{r}$ via path k, σ_i is the transmission or reflection coefficient of the ith wall along the path. We assume only a single reflection per path in this thesis, so the total power at a position is given by

$$P(\mathbf{r}) = \sum_k^L P_k(\mathbf{r}) = \sum_{k=1}^L \frac{\alpha P_0}{l_k(\mathbf{r})^2} \sigma_k \tag{4.5}$$

Model 2 assumes no phasor effects in the field received: all signals arrive at the receiver coherently. We conjecture model 2 may be arranged to perform equally well with the full phasor sum of model 1, under the relaxation that σ may take on negative values.

Given the above two propagation models, it is feasible to build VPE using either the feature based neural network or adaptive nonlinear least square algorithm which

are introduced in the following sections.

4.3   Neural Networks and Learning Algorithms

Artificial neural networks are well-developed for learning functional relationships, see [47], and comprehensive reviews exist, such as [48]. Artificial neural networks arise from imitations of biological neural systems, providing a simple application of parallel computation and have been extended to solve system learning and optimization problems [49, 50].

Any function may be approximated by a piece-wise linear function, which we shall denote as a "basis function". Let $\phi(k, \rho)$ be the general basis function used for approximation, where k is the index of the function and ρ is the state. We may consider the state in terms of function samples, where the function is evaluated at a finite set of "states" ρ_i, $i = 1, 2, \ldots$. Where there is no ambiguity, we shall interchange the state ρ_i and in index i. A function $J(\rho)$ can be approximated by a basis:

$$\widetilde{J}(i, r) = \sum_{k=0}^{K} r_k \phi_k(i), \tag{4.6}$$

where $r = \{r_1, \ldots r_K\}$ are the weights associated with the basis set $\{\phi_0(i), \ldots, \phi_K(i)\}$. The best approximation, in an MMSE sense, for a given set of basis functions may be obtained via solving:

$$r = \arg \min_{r \in R^{K+1}} \sum_i \left| J(i) - \widetilde{J}(i, r) \right|^2 . \tag{4.7}$$

Equation (4.6) represents a *single layer* neural network. For more complex (or higher dimensional) functions, multiple layers may be used. Such multi-layer neural networks are said to contain "hidden layers" which are composites of two or more single layer networks such as:

$$\widetilde{J}(i, r) = \sum_{k=1}^{K} r(k) \sigma \left(\sum_{l=1}^{L} r(k, l) x_l(i) \right), \tag{4.8}$$

where the base function $\sigma(s)$ is a smooth monotonic function taking values in $(0, 1)$ or such a function taking values in $(-1, 1)$. i.e., $\frac{1}{1+e^{-s}}$ or $\tanh(s)$.

Sometimes, there are functions of the state known to be important or useful in the prediction. In these cases, intermediate functions, called features, are introduced to capture the important aspects of the current state. Let the feature vector

associated with state i be denoted as $f(i)$, the single layer network now can be written as $\widetilde{J}(i, r) = \sum_k r(k)\phi_k(f(i))$. Features can be obtained by prior-knowledge of the network or heuristic policies. In this thesis, the radio propagation models are used as feature functions.

4.3.1 Feature-Based Network Design

Both generic and kernel-based neural networks have been applied to the study of signal strength measurement and prediction issues, see for example [51, 52]. However, previous work has focussed on the application of generic learning methods to the special class of the signal strength of wireless communication. In this paper, we use the feature-based learning method, which incorporates the special feature of the signal strength model under consideration. Rather than choose the usual sigmoidal function, as the basis, we use either radio propagation model 1 or model 2 instead. As such, the neural network itself has a strong physical meaning. In addition, because the neural network basis is selected closely with the real model, it is expected the resulted method can be more efficient and effective.

At the off-line stage we measure the received signal at given positions and use this data to train the feature weights of the neural network, which are in the the hidden layer. The features are the position and reflection coefficient of reflectors (walls) or scatters. The output layer is the Neural Network cost function J, the difference between the measured power distribution and the estimated power distribution.

The parameters of walls are adjusted according to the given power distribution map of a certain area, which has a certain grid size. In the one dimensional case, $P(m)$ is the power at position r_m where $m = 1, 2, \ldots, M$. There are M known positions stored in database, and each r_m is a labeling of a physical location. Since m uniquely specifies r_m we may consider P as a function of m. We assume we know the position and reflection coefficient of N ideal walls, either from an iteration or an initial guess.

Each wall will reflect its incident wave and contribute a signal component to a certain position r_m. We either use propagation model 1 or model 2 to calculate the estimated power distribution $\overline{P}(m, \mathbf{R})$ at the position r_m. Here $\mathbf{R}$ is the array of the parameters of the N walls. The cost function J is defined as

$$J = \frac{1}{2} \sum_{m=1}^{M} \left| P(m) - \overline{P}(m, \mathbf{R}) \right|^2 \tag{4.9}$$

and minimized by the fixed point equation:

$$\mathbf{R}_{k+1} = \mathbf{R}_k - \gamma \frac{\partial J}{\partial \mathbf{R}_k} \tag{4.10}$$

We set a threshold ϵ for the cost function J, and for $J < \epsilon$ the fixed point iterations are terminated.

4.4 Adaptive Nonlinear Least Square Algorithms

Given m radio signal samples $(\boldsymbol{r}_m, \overline{P}(m, \boldsymbol{R}))$, $\quad m = 1, \dots, M$, where m is the sample (position) index, we wish to find the parameter matrix $\boldsymbol{R}$ that best fits in the least square sense to the propagation model, either model 1 or model 2. This leads the nonlinear least square algorithm. In detail, the residual vector function $\boldsymbol{s}(\boldsymbol{R})$ is defined as $[s_1(\boldsymbol{R}) \ s_2(\boldsymbol{R}) \ \dots \ s_M(\boldsymbol{R})]^T$ where

$$s_m(\boldsymbol{R}) = \overline{P}(m, \boldsymbol{R}) - P(\boldsymbol{r}_m), \quad m = 1, \dots, M.$$

We intend to minimize the cost function defined as $g(\boldsymbol{R}) = \frac{1}{2} \boldsymbol{s}^T(\boldsymbol{R}) \boldsymbol{s}(\boldsymbol{R})$. *Gauss-Newton method* is applied in solving this problem by introducing the gradient vector and Hessian matrix of $g(\boldsymbol{R})$:

$$\nabla g(\boldsymbol{R}) = \boldsymbol{J}^T(\boldsymbol{R}) \boldsymbol{s}(\boldsymbol{R})$$

and

$$\boldsymbol{H}_g(\boldsymbol{R}) = \boldsymbol{J}^T(\boldsymbol{R}) \boldsymbol{J}(\boldsymbol{R}) + \sum_{m=1}^{M} s_m(\boldsymbol{R}) \boldsymbol{H}_m(\boldsymbol{R}).$$

Note that $\boldsymbol{J}(\boldsymbol{R})$ is the Jacobian matrix of $\boldsymbol{s}(\boldsymbol{R})$ and $\boldsymbol{H}_m(\boldsymbol{R})$ denotes the Hessian matrix of the component function $s_m(\boldsymbol{R})$. Suppose at an iteration k we have $\boldsymbol{R}_k$ as an approximate solution which is not far from the true value, the Newton step $\boldsymbol{n}_k$ is given by the linear system

$$[\boldsymbol{J}^T(\boldsymbol{R}_k) \boldsymbol{J}(\boldsymbol{R}_k) + \sum_{m=1}^{M} s_m(\boldsymbol{R}_k) \boldsymbol{H}_m(\boldsymbol{R}_k)] \boldsymbol{n}_k = -\boldsymbol{J}^T(\boldsymbol{R}_k) \boldsymbol{s}(\boldsymbol{R}_k) \tag{4.11}$$

Appropriate $\boldsymbol{R}_k$ prompts that the fit of the model function to the sample data is reasonably good. This case leads that the residual component function s_m is small, which makes it an reasonable approximation to drop the second-order term in the left-hand-side of (4.11). This approximation avoids the expensive and inconvenient computation of the m Hessian matrices $\boldsymbol{H}_m$. This motivates the *Gauss-Newton*

method for solving the nonlinear least squares problem and we have the linear system

$$\boldsymbol{J}^T(\boldsymbol{R}_k)\boldsymbol{J}(\boldsymbol{R}_k)\boldsymbol{n}_k = -\boldsymbol{J}^T(\boldsymbol{R}_k)\boldsymbol{s}(\boldsymbol{R}_k)$$

The approximate Newton step $\boldsymbol{n}_k$ at iteration k is for updating $\boldsymbol{R}_{k+1}$ at next iteration, namely $\boldsymbol{R}_{k+1} = \boldsymbol{R}_k + \boldsymbol{n}_k$. The iteration process is repeated until convergence criteria is satisfied or maximum iteration number has reached.

In principle, the Gauss-Newton method solves a sequence of linear least squares problems whose solutions converge to the solution of the original nonlinear problem. In case of large residual component function s_m, the approximation in Gaussian-Newton method is not accurate and this could cause slow convergence rate or convergent not to global minimum. It is better to consider a robust nonlinear minimization method which takes into account of the Hessian Matrix in (4.11).

4.5 Applications in Wireless LAN Localization

The feature based neural network and nonlinear least square algorithm lay the foundation for building VPE from the measured radio signal samples. In this section, we show how measured radio signal is applied in wireless LAN localization. The popular technology is mostly based on fingerprint technology. Target's location is estimated by searching in the training database set up during offline stage. The most robust and simple algorithms are nearest neighbour (NN), K nearest neighbour (KNN) and K weighted nearest neighbour (KWNN) [53].

By NN the vector difference between measured radio signal and items in database is calculated. The position of the nearest neighbour in the database is reckoned as the target position. For KNN, we like to take into account more neighbours around the nearest neighbour, the estimate of the MS position is the averaged coordinates of the total K neighbours, as in (4.12):

$$\widehat{\mathbf{X}}_T = \frac{\sum_{i=1}^{N} \mathbf{X}_i}{N} \tag{4.12}$$

where $\mathbf{X}_i$ ($i = 1, \ldots, N$) are the N neighbours. KNN is a special case of KWNN, with the weight to each neibhbour is equal to each other.

In KWNN, the MS position is estimated by the weighted average of the coordinates of the K neighbours (4.13).

$$\widehat{\mathbf{X}}_T = \frac{\sum_{i=1}^{N} w_i \mathbf{X}_i}{\sum_{i=1}^{N} w_i} \tag{4.13}$$

The weight is selected according to certain rule to achieve better performance. In our case the weight is equal to inverse of the radio signal vector/matrix distance.

In the kernel method a probability mass function is described by a "kernel" regarding to each of the observations in the training data set. The resulting probability estimation for observed signal strength o on position l, denoted as $p(o|l)$ is a combination of all probability mass functions of the available observations on l. We assume that there are N observations at l, namely $o_1, o_2, \ldots, o_N$. Then it is reached that

$$p(o|l) = \frac{1}{N} \sum_{i=1}^{N} K(o; o_i) \tag{4.14}$$

where $K(\cdot; o_i)$ denotes the kernel function. In this thesis the most widely Gaussian kernel function is used with definition in (4.15):

$$K(o; o_i) = \frac{1}{2\pi\sigma^2} \exp(-\frac{(o - o_i)^2}{2\sigma^2}) \tag{4.15}$$

where σ is a parameter dominating the width of the kernel function.

The above listed methods are not accurate models. The "radio signal distance" between the target and a RP has no linear relation with their geographical distance. The hidden relationship is dominant by the specified radio wave propagation environment. As we know, the principle of fingerprint technology is that the geographical space, where the target is inside, is partitioned into cells consisting of all points closer to a given training point r' than to any other training points. All points is thus labeled by the category of the training point. The cells are called Voronoi cells in two dimensions location space. In three dimensions, the cells are three-dimensional and the decision boundary resembles the surface of a crystal. From the above analysis, it comes that the aperture of the cells dominates location resolution, or accuracy. It provides a solution to improve location accuracy by decreasing aperture of the cells. It can predict radio signal strength at points other than the training points. This means it has denser training points thus decreases aperture of the cells. Thus the location accuracy is improved, which is verified by our real field measurement results in the follow. In the literature, Motley-Keenan propagation model [54]:

$$P_{received}(d)[dBm] = P_{received}(d_0)[dBm] - 10\alpha \log(\frac{d}{d_0}) \tag{4.16}$$

and the improved wall attenuation model [10]:

$$P_{received}(d)[dBm] = P_{received}(d_0)[dBm] - 10\alpha \log(\frac{d}{d_0}) - nW \times WAF \qquad (4.17)$$

have been applied in radio signal prediction and WLAN localisation. However, their performance is not satisfactory since they cannot cover details of the propagation environment. The VPE method describes the properties of the propagation environment by fitting its model parameters to training radio signal samples.

4.6 Experimental Measurement Setup

To support our analysis, we build a WLAN localisation system based on a PC laptop running Linux. Details of the system is described in this section, where the normal static and the novel "stochastic position" measurement methods are also discussed. For field measurements a Compaq Evo N800C laptop installed with Lucent ORiNOCO Gold 802.11b WLAN adaptor [55] was used as a measurement device. The Operating System (OS) for the laptop was Redhat 9.0 with kernel updated to 2.4.27. The adaptor driver version is 0.13-d [56] patched the scanning patch by Pavel Roskin [57,58], *Wireless Extension* and *Wireless tools* [59] provide the received signal strength from different APs. The laptop uses Wireless Tools v.26 and Wireless Extensions v.16. The field measurements were taken at the National ICT Australia Canberra Node.

4.6.1 Static Method

The receiver was placed at a position and the distance between receiver and transmitter measured. Then we ran a TCL/TK script to scan all the available APs in the neighborhood and store their signal strengths in database. After one second, we repeated the scanning again until the Maximum Scanning Number (MSN) is reached. The mean and maximum values of the MSN signal strengths at each position was stored. During the measurement cycle, the receiver position was held fixed.

In the static measurement experiment small scale fading is observed. In Figure 4.1 we take $MSN = 20$ samples at a position. T/R distance means the distance between the transmitter and receiver. The unit of received signal power at the receiver is dBm. The measurement step size within distance from $380cm$ to $550cm$ is $5cm$. Experiment results show the signal strength is stable in the temporal scale while suffering severe (and unpredictable) fading in the spatial scale. This is
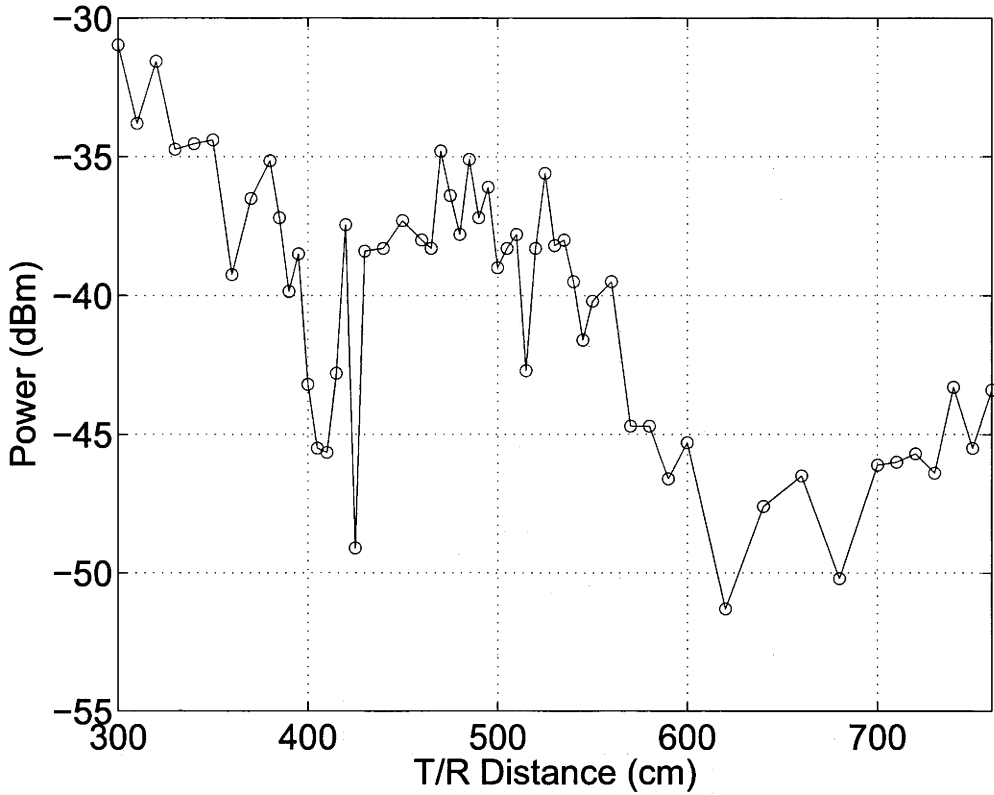
Figure 4.1: Small scale fading, from measured data along corridor. Note scale is in cm. $\lambda \approx 12cm$

because small scale fading is typically due to phase effects and occurs on spatial scales smaller than a wavelength ($\lambda \approx 12cm$). In dense multi-path, prediction of the fading characteristics is ineffective for extrapolation beyond approximately one wavelength λ [44], under the experimental setup used. Similar observations have been made in the temporal case [60]

4.6.2 Large-scale Fading Signal Measurement Based on Monte Carlo Method

In WLAN localisation system, in order to make an unique fingerprint of a certain location, small-scale fading is helpful. But it is hard to repeat the same signal pattern even at the same position. It is much easier to repeat the same patter at the same position using large-scale faded signal. However, in this case, the uniqueness is not well enough. In order to solve this dilemma, one solution based on Monte Carlo integration method is "fuzzy"z measurement, which is discussed here.

Monte Carlo methods are defined as statistical simulation methods, where sta-

tistical simulation is defined in quite general terms to be any method that utilizes sequences of random numbers to perform the simulation [61]. One application of Monte Carlo methods is Monte Carlo integration. For example, the integration of an arbitrary function in a closed variable range from a to b can be approximated by drawing numerous samples in the variable space $[a, b]$. This idea is brought into WLAN localisation to measure large scale fading in this thesis.

Given only simple power measurements, a metric is desirable which estimates the *large scale* fading characteristics of the field, without inappropriate emphasis on the small scale, local effects. A natural (statistical) approach would be to take a number of samples within a nearby region and to perform an averaging over the samples. We may ask *"Why ignore small scale fading?"* the answer to this comes from well known results in extrapolation of functions, such as the Nyquist sampling result, and [44]: if we wish to predict small scale fading, we must sample at well above the maximum rate of change in the fade, which requires *known calibration points at a sampling density greater than* $\lambda/2$. However, large scale fading is dominated by the free-space distance loss in power, and thus has a much lower rate of change over a local area, by comparison, $|E(r)|$ is (approximately) wavelength invariant, and varies at a rate of $-2d^{-3}$.

For each calibration position r, we apply the Monte Carlo integration method and measure the received signal strength at a set of positions in the near neighborhood of a sample point by simply moving the receiver within a nearby region during the MSN scanning process. We use the area-averaged signal strength as the fingerprint of the position. It is called "stochastic" method. Note that the position is not a point but a small area.

With our PC-based WLAN location system, we design three experiments to support our analysis and demonstrate the points in WLAN location. The follow section presents three experimental results. The first experiment shows the advantage of the "stochastic position" method compared with the normal "static method".

4.7 Experiments Results and Analysis

4.7.1 Experiment 1

Three Access Points (AP) were deployed in the office, which are shown in Figure ?? as red dots. The right one in the middle is the first AP, simply as AP1. There are 7 measurement points along the yellow line. Point 1 to 7 have approximately 6, 8, 9, 10, 11, 12, 14 meters from AP1. At every point, we measured radio signal

Table 4.1: Neighbor Distance

Method / Pos	6 m	8 m	9 m	10 m	11 m	12 m	14 m
StaMean	7.2	13.9	14.0	6.9	8.5	3.7	9.0
StaMax	7.6	10.4	13.9	5.7	8.8	4.6	11.0
FuzMean	8.3	7.9	7.4	1.3	2.5	4.0	3.3
FuzMax	3.7	10.6	10.6	2.2	1.4	1.4	2.4

strength from the three APs, using normal (static) and fuzzy (dynamic) method. The MSN is set as 30. The standard data set collected at a position looks like:

$$
\begin{bmatrix}
SS1_1(1) & SS1_1(2) & SS1_1(3) \\
SS1_2(1) & SS1_2(2) & SS1_2(3) \\
\cdots & & \\
SS1_{MSN}(1) & SS1_{MSN}(2) & SS1_{MSN}(3)
\end{bmatrix}
$$

where $SSx_y(z)$ means received signal strength at position x from AP z during the yth scanning.

Regarding to each data set collected by the two methods, we either select the averaged or the maximum signal strength value vector from the three APs as the fingerprint for the position. This stage is called off-line training stage in WLAN localization system. In this stage radio signal distribution at known positions are recorded in database and processed as the fingerprints for these positions. In the online stage, radio signal from different APs at an unknown position are received, which has the format as

$$
\begin{bmatrix}
SSx_1(1) & SSx_1(2) & SSx_1(3) \\
SSx_2(1) & SSx_2(2) & SSx_2(3) \\
\cdots & & \\
SSx_{MSN}(1) & SSx_{MSN}(2) & SSx_{MSN}(3)
\end{bmatrix}.
$$

Comparing this signal with fingerprints stored in database, the nearest neighbor is decided as the most possible position (MPP). In our experiment, radio signal at 10 meter is measured as the unknown position. Euclidean distance is used in comparing newly measured signal with fingerprints in database. Totally there are four models existing, which are mean value with with static method (Model 1), maximum value with static method (Model 2), mean value with fuzzy method (Model 3)and maximum value with fuzzy method (Model 4). The distances are calculated and shown in Table 4.1:

Model 1 shows point 6 has closest distance to this unknown point, which is 2

Table 4.2: Model combinations

	Small scale model 1 (static)	Large scale model 2 (fuzzy)
Reflective walls	Ia	IIa
Scattering bodies	Ib	IIb

meters away from the true location. Model 2 shows the same calculation result. Model 3 indicates that point 4 has closest distance, which is the truth. Model 4 suffers from selecting one best candidate from point 4, 5, 6, 7. From Table 4.1 it is shown that Model 3 has better performance in finding nearest neighbor, which is consistent with our previous analysis. We will use Model 3 measurement method in the following experiments.

The next experiment aims to show the prediction performance of VPE. Without loss of generality, VPE trained by feature based neural network is shown.

4.7.2 Experiment 2

In this experiment, a single Lucent ORiNOCO AP-1000 Access Point (AP) was deployed as the transmitter. The transmitter was located at the end of a corridor and measurements were taken along the length of the corridor. Our objective in this section is to evaluate several model combinations, toward providing a robust and sufficiently accurate modeling procedure. We have four combinations, which we summarize in Table 4.2. In each case the neural network was trained with measurement data at a collection of data points, and the resulting prediction compared with additional points.

Propagation Model 1 results

Firstly we use reflectors as the neural network nodes in the hidden layer. The statically measured signal is shown in Figure 4.2. The transmitter is deployed at the origin. The measurements are performed at distances of $1m, 1.5m, 2m, \ldots, 16m$ from the transmitter, among which the step size is $0.5m$. We use the first radio propagation model with eight reflectors. The circles are the training signal strength at known positions, namely at positions with distances of $1m, 2m, \ldots, 16m$ from the transmitter. The position of the ith reflector is represented by $a_i X + b_i Y + c_i = 0$. Including the reflection coefficient σ_i, the weight vector of the ith reflector is defined as $[a_i \ b_i \ c_i \ \sigma_i]$. All weight vectors constitute the weight matrix for the neural
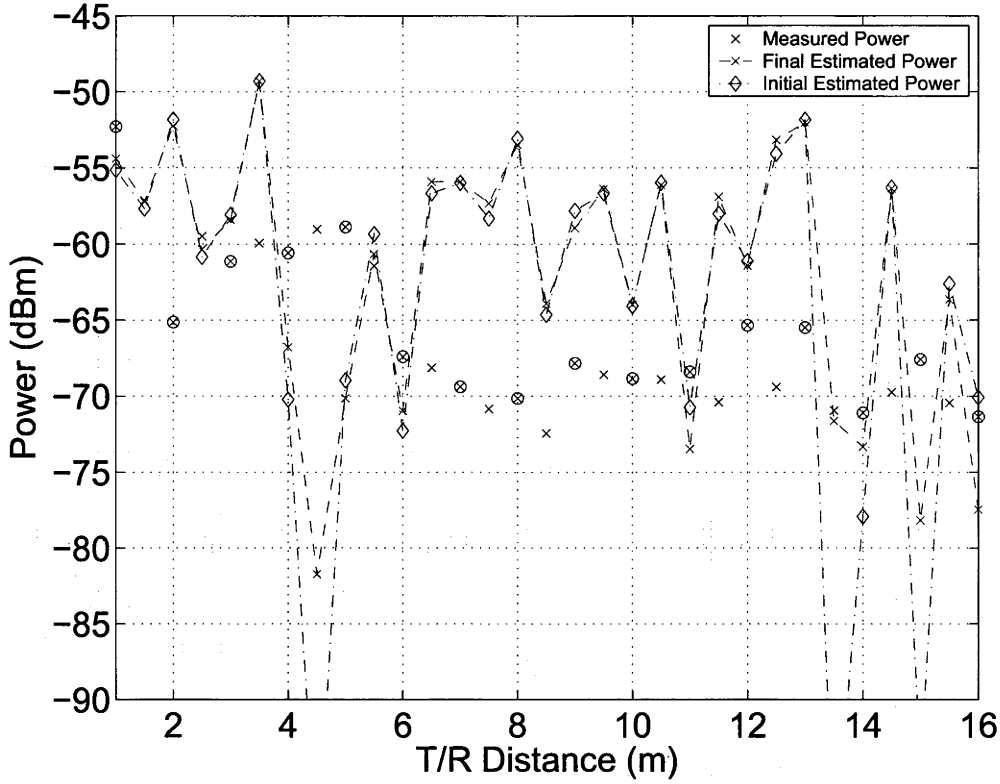
Figure 4.2: 8 Reflectors with Propagation Model 1. Crosses denote measurements, circled crosses mark training points.

network. With knowledge of position of the reflector, we can calculate the unfolded length from the transmitter to the receiver, based on image theory. Here we only consider simple one-bounce scenario.

In the training process, the converging is rather slow when the cost function is approximately equal to 650. The cost function is bounded above 640 as shown in Figure 4.6. It is shown in Figure 4.2 that the final estimated power distribution doesn't match the measured power well. It differs little with the initial estimated power distribution.

Given the same measured signal power distribution, we use sixteen scatterers as the hidden nodes. For each node the weight vector is $[a_i \ b_i \ \sigma_i]$, where (a_i, b_i) is the X-Y axis of the scatter and σ_i is the reflection coefficient of the scatter. With phase term included in propagation model, this neural network is efficient in decreasing cost function, which demonstrates the first propagation model has strong capability in fitting the training data. In order to prevent overfitting, the cost function in Figure 4.3 is 18, though this neural network can converge its cost function close to zero. This figure shows that while the phasor addition model can be easily matched to the trained data, it suffers from wild fluctuations away from
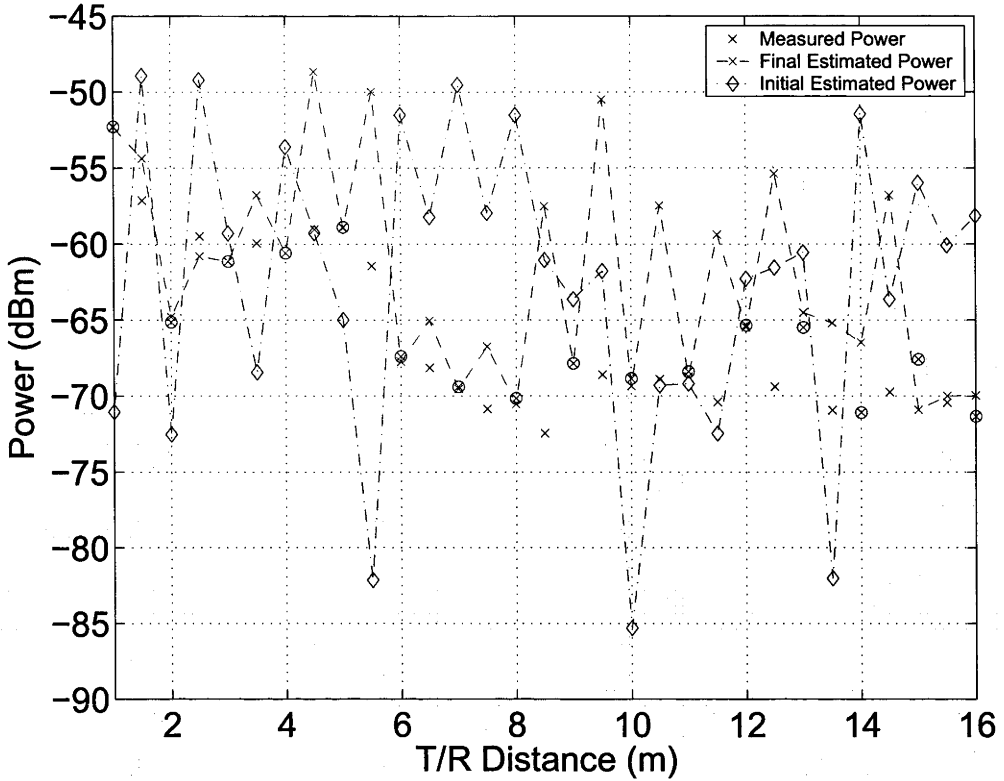
Figure 4.3: 16 Scatterers with Propagation Model 1. Crosses denote measurements, circled crosses mark training points. Note dominance of small-scale fading.

the measured data when used to predict signal strength. The reason is simple: small scale fading is highly reliant on local channel parameters, and thus sampling *must* be performed at or above the Nyquist sampling rate. Sadly, the sampling rate is *bounded from above by* $\lambda/2$ which requires a sampling density of greater than 3 samples per wavelength. Based on the learned features of the wireless propagation environment, it is possible to predict signal strength at other positions. We use measured signal strength distribution at $0.5m, 1.5m, \ldots, 15.5m$ to validate the predicted values. The prediction result matches the measured data well within a distance of 4 meters from transmitter as shown in Figure 4.3.

Propagation Model 2 results

The prediction accuracy with the second radio propagation model can be improved by using a "stochastic" measurement method. We apply the radio propagation model 2 in our algorithm to train the neural network until the cost function J is relatively small. Once the training process is finished, we apply the weight matrix to calculate signal strength distribution at unknown positions.

In Figure 4.4 four ideal reflectors are acting as the neural network hidden nodes
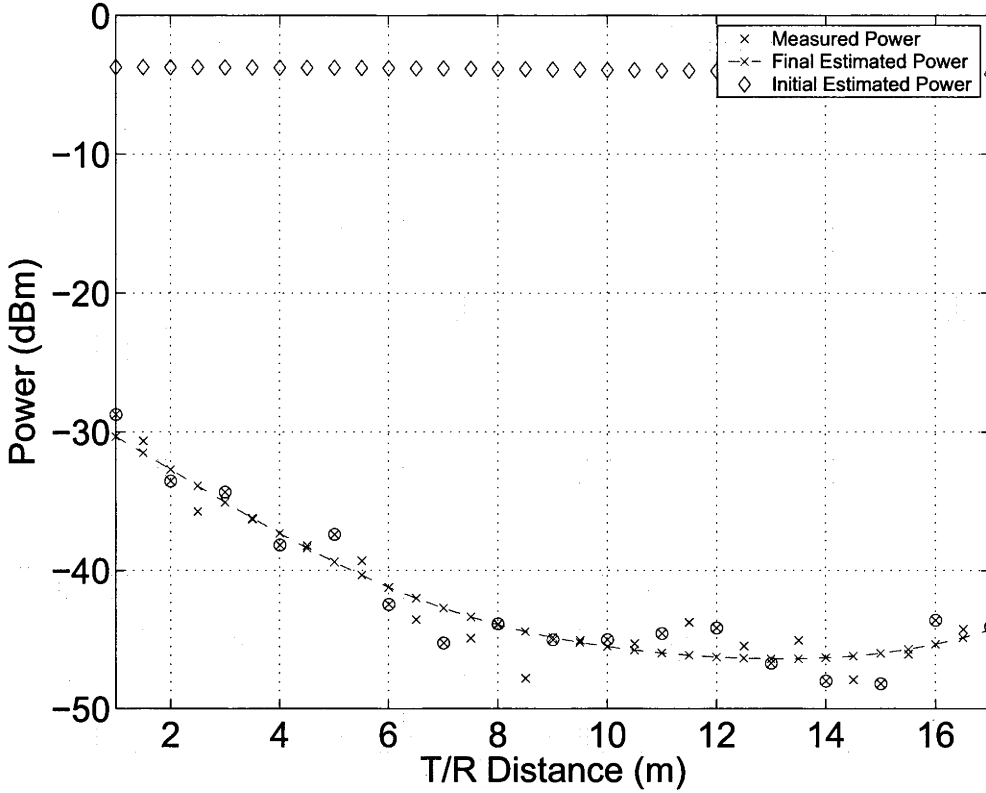
Figure 4.4: 4 Reflectors with Propagation Model 2. Crosses denote measurements, circled crosses mark training points.

with a final value of cost function around 17. Training signal strength is measured at positions with distances of $1m, 2m, \ldots, 17m$ to the transmitter. The signal fluctuates smoothly, comparing with Figure 4.3 and Figure 4.2. We estimate signal distribution at positions of $1.5m, 2.5m, \ldots, 15.5m$. The error between predicted values and measured values is reasonably small.

With the same training signal strength distribution, we used eight scatters as the hidden layer in Figure 4.5 giving eight nodes. In this figure the final value of cost function is around 14. The prediction can achieve the same level of accuracy as that by reflectors. In Figure 4.6 the computation complexity for the above four neural networks are given. Entry "Ia" in Table 4.2 suffers from the convergence bound of the cost function. "IIa" has similar problems but its bound is much smaller. "Ib" has good performance in converging to the training data but it is poor in signal prediction. "IIb" demonstrates its ability in predicting signal distribution with reasonable computation cost.

The last experiment will demonstrate the location accuracy improvement achieved by the aiding of VPE. According the results in Experiment 2, scatterer modeled neural network with propagation model 2 is adopted in the following WLAN loca-
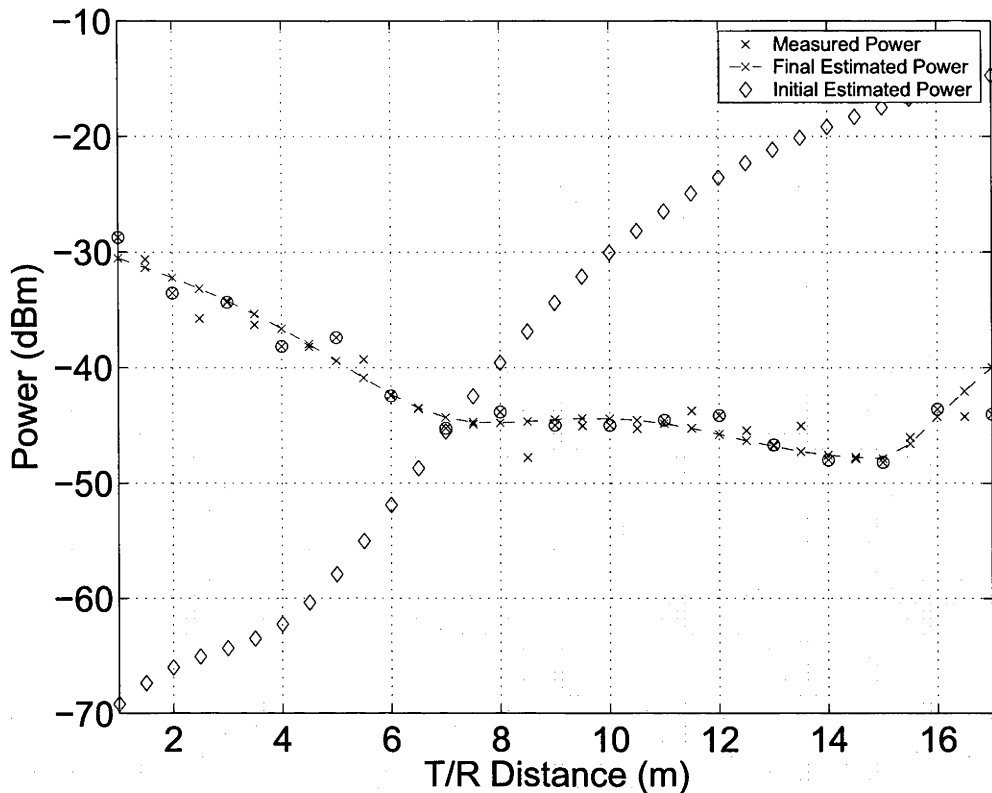
Figure 4.5: 8 Scatterers with Propagation Model 2. Crosses denote measurements, circled crosses mark training points.

tion implementation.

4.7.3 Experiment 3

This experiment aims to verify the practical applications of the virtual environment concept in WLAN localisation. The real filed radio signal measurement was implemented in NICTA's office. At the offline stage training data was measured at a grid size of 2 by $2m$. The approximate area of the available region is 250 square meters. Numerous testing data was measured randomly in the same measurement field. 3 weighted nearest neighbour (3WNN) and a Gaussian kernel method are utilised in calculating location error distance. As seen in Figure 4.7, the ninety percentage error distance is at about 6.5 m for the original $3WNN$ method while the average error is 3.50 m. With the aiding of the "learned" virtual environment, the ninety percentage error distance is around 6 m and the average error is 2.25 m. Figure 4.8 shows that the ninety percentage error distance is at about 5.8 m for the original Gaussian Kernel method while the average error is 3.00 m. With the aiding of the virtual environment, the ninety percentage error distance turns to be around 4.2 m and the average error is 2.50 m. The performance comparison between these two
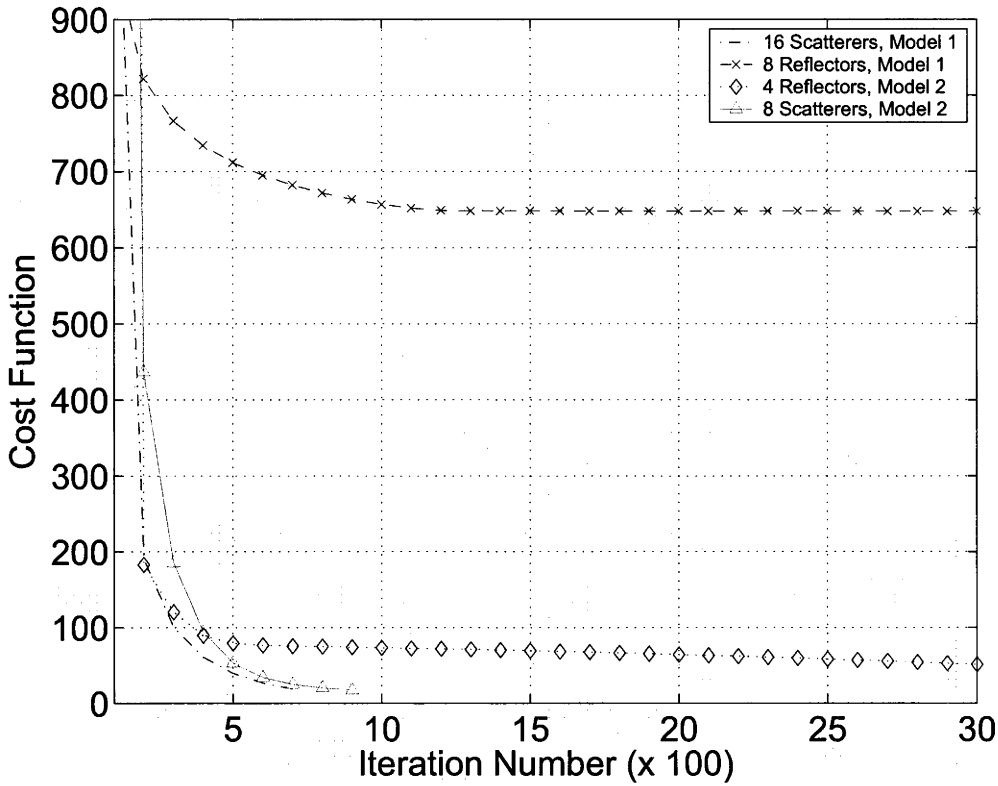
Figure 4.6: Mean square error compared with iteration number. Convergence occurs for cost function equal to zero. Model 1 does not converge as well as model 2, due to large variation. For reflectors (walls) model 1 did not always converge – note large final error for 8 reflectors, model 1.

figures indicates that the virtual environment works effectively in improving localisation accuracy in both the nearest neighbour and the Gaussian Kernel method. We note there is a performance cross-point in Figure 4.8. This demonstrates the VE could bring localisation accuracy degrading in small error distance range. This reminds us to utilise the VE method carefully in real applications.

4.8   Contributions

The technical contributions of this chapter were:

1. To develop new algorithms to predict wireless signal propagation environment, using feature-based neural network and adaptive nonlinear least square was presented. These algorithms constructed a virtual propagation environment which reasonably represented the real environment. Our experiment showed the VPE is helpful in improving WLAN localisation accuracy.

2. To apply a new method – "stochastic position" method – in real field sig-

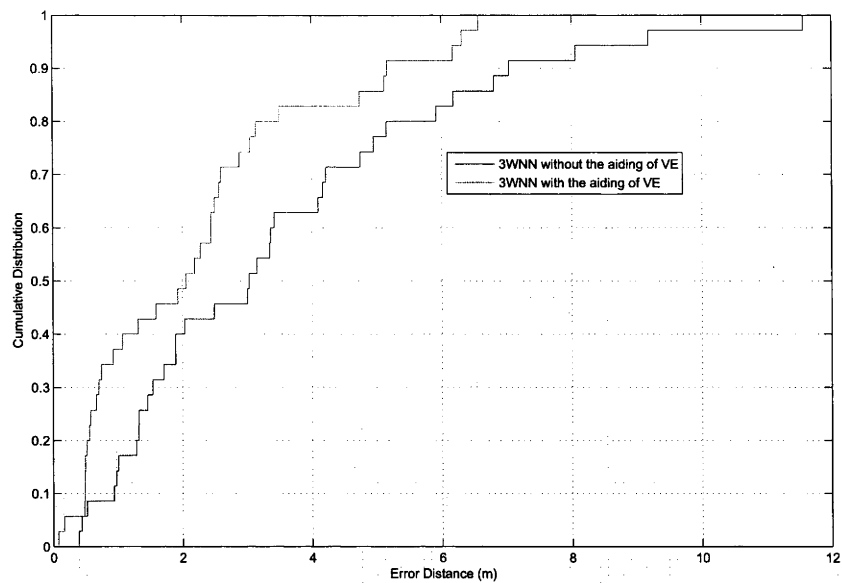Figure 4.7: Cumulative distribution of localization error using 3 Weighted Nearest Neighbour Method.

nal strength measurement, based on Monte Carlo method. This method mitigates the effect of small scale fading when examining signal strength values and has better performance in making radio fingerprint of a position in WLAN localization system.
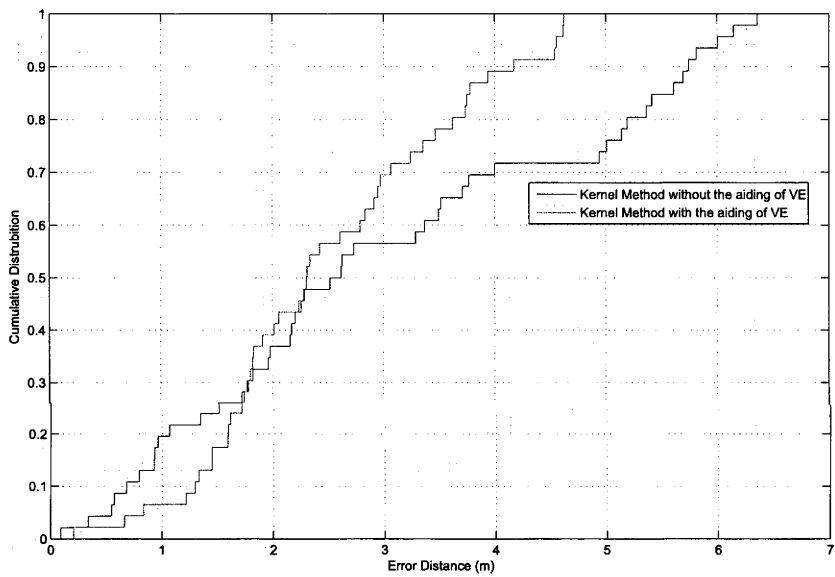
Figure 4.8: Cumulative distribution of localization error using Gaussian Kernel Method.

Chapter 5

Wireless Location Using Pattern Matching Techniques

5.1 Introduction

One popular technology to locate a MS in WLAN and/or sensor networks is to assist the localization with the aid of radio signal spatial distribution map (RSSDM). This is also known as fingerprint technology. RSSDM contains MS's radio signal spatial distribution characteristic when the MS is at a certain position. For example, in WLAN, several access points (AP) can measure a MS's radio signal spatial distribution when the MS is at a known position. The measured radio signal spatial distributions (of multiple APs) are recognized as the MS's location fingerprint at that particular position. The fingerprints at multiple positions are recorded and thus set up in a RSSDM database, which is implemented during an off-line training stage. In the online stage, when the MS goes to an unknown position, the measured RSS (possibly from multiple BSs) is used to search the database to find most probable position using pattern matching techniques [12] [13]. Normally the radio signal strength (RSS) is adopted in setting up the RSSDM. The RADAR location system by Micorsoft Research [10] is one of the first and most comprehensive studies of 801.11 localization using the radio signal spatial distribution. Several improved power attenuation models are introduced in [11] which considers wall and floor effects.

The fingerprint technique provides a method for mitigating non line-of-sight (NLOS) effects, given an appropriate sample grid size during the offline training stage. However, the training process requires a heavy working-load typically due to the dense sample points. Further, frequent training is necessary for acceptable location accuracy in dynamic propagation environments.

The channel impulse response (CIR) is also adopted in identifying a MS's position [25]. Estimation of the CIR is implemented by the demodulator of the receiver designed for mitigating the effect imposed by wireless channel upon received radio signal. This brings the main advantage of using CIR as a location signature since it does not need any significant hardware modification to the current existing wireless communication system. Firmware is modified to feed the CIR information from physical layer to application layer. With comparison to RSS, CIR has a greater ability in determining a geographical position uniquely since it records the multipath profile of wireless channel specific to a location. These advantages of CIR as location fingerprint make it possible to design a location system with less BSs.

Recently WiMAX (World Interoperability for Microwave Access), has drawn much attention of researchers, service providers and manufacturers. It is based on the *IEEE* 802.16X standard and is expected to enable true broadband speeds over wireless networks at a cost point to enable mass market adoption. There are two WiMAX applications: fixed and mobile. Fixed WiMAX applications are point-to-multipoint enabling broadband access to homes and businesses. In this type of fixed wireless networks (FWN), each BS has a wide coverage. In current standard a BS covers a region with radius of almost 10 *km*. ref here! This makes it hard to estimate a MS's position with the information sharing of multiple BSs. On the other hand, one feature of FWN is there are a number of fixed users in FWN with their positions known. The CIR vectors from these users could be reckoned as natural sample instances to set up the RSSDM, which saves much effort.

We intend to take advantage of this feature of FWN and design a novel localization system for FWN in this chapter. We will introduce a fingerprint location method based on CIR only. This method has minimum requirement for the number of RPs, which is one. General algorithms and support vector machine (SVM) will be applied in location estimation. The remainder of this chapter is arranged as follows. In section 5.2 CIR models are given as preliminaries and "CIR" distance is defined. Section 5.3 provides general algorithms and SVM for location in FWN. Rule of thumb in tuning SVM is presented in detail. Section 5.4 shows how to implement CIR measurements to have training and testing data sets using *R*adioplan. Performance of different algorithms is also given. The last section is devoted to conclusion and discussion of future work.

Table 5.1: Fingerprint Data Format

Position	Path Index	$|\alpha|$	$\widehat{\alpha}$	Delay	AoA
	Path Index	$|\alpha|$	$\widehat{\alpha}$	Delay	AoA

5.2 CIR Model and "CIR Distance" Calculation

One CIR model is the tapped-delayed-line model which utilizes a tapped-delay-filter to represent multipath channel as

$$h(t) = \sum_{l=1}^{L} \alpha_l \delta(t - T_l).$$

Here l is the multipath index and there are L multipaths in total. α_l is the complex gain of the lth path, T_l is the relative time delay relative to the first path ($T_0 = 0$). This filter structure describes the multipath profile (MP) of radio signal coming from a source position.

There is an improved spatial tapped-delayed-line channel model which includes the radio signal incident bearing Φ_l of the lth propagation path [62].

$$h(t, \varphi) = \sum_{l=1}^{L} \alpha_l \delta(t - T_l) \delta(\varphi - \Phi_l).$$

The data structure is shown in Table 5.1, where $|\alpha|$ and $\widehat{\alpha}$ are α's magnitude and phase, respectively. We consider this structure as a matrix corresponding to a source position, namely the location signature of the position. The number of rows of the matrix is the number of multipaths of the target position's MP. $\mathbf{c}$ and $\mathbf{C}$ are assumed to be the CIR matrix of two positions. The generalized "CIR distance" between them is

$$D_p = \left(\sum_{i=1}^{m} \sum_{j=1}^{n} |\mathbf{c}_{i,j} - \mathbf{C}_{i,j}|^p \right)^{\frac{1}{p}} \tag{5.1}$$

where m and n are the CIR matrix row and column dimensions. p is set to 1 if we use Manhattan distance and p is equal to 2 when Euclidean distance is adopted.

The phase term of the received signal suffers from small scale fading and we will omit $\widehat{\alpha}$ when calculating CIR distance.

5.3   Location Algorithms for FWN

The fingerprint method involves two stages: an offline training stage and a later online estimation stage.

In the training stage, a training data set is gathered by a field survey which contains a number of data instances. Each instance contains one pair: the "target value" and the corresponding "attributes" (features) vector. During the online stage, it is requested to estimate the target value with respect to a measured attribute vector, based on information in the training data set solely. To solve this problem, estimation algorithms may approximate the target value implicitly or construct an explicit description of the target value and its attribute vector.

In our case, the target value is the MS's geometrical position and attribute vector has the CIR parameters as its components, such as time of delay, angle of arrival and signal attenuation, etc.

Instance-based learning algorithms can approximate the target's value by simply storing the training data set, such as the k-nearest neighbors learning the locally weighted regression and radial basis functions [63]. Each time a new instance is encountered, its relationship to the stored data set is examined in order to assign a target value for the new instance. On the other hand, the SVM constructs explicit functions to describe the target value and its attribute vector of the training data instances. The arbitrary learning ability of the SVM makes it a powerful tool for solving both pattern recognition and regression problems. SVM has wide applications including in computational biology, intrusion detection, generalized predictive control, dynamic reconstruction of chaotic systems and modeling of seismic liquefaction potentials.

We will give mathematical descriptions for the algorithms indicated above in the following sections.

5.3.1   Instance-Based Learning Algorithms

Instance-based learning algorithms are available in estimating the location of the MS by searching in the training database, and include algorithms such as nearest neighbor (NN), K-nearest neighbor (KNN) and K-weighted nearest neighbor (KWNN).

To find the location regarding to a given CIR vector in the testing set, we calculate "distance" between this CIR with all instances in the training set. For the algorithm of nearest-neighbor (NN), the instance with smallest distance in training set is selected and its target value is considered as the most possible position of the

testing set.

One problem is that we need to build the training set with dense enough spatial sample points in order to achieve a satisfactory location accuracy. Sparse sample points may lead to significant location errors.

One mitigating solution is to estimate the target by combining several close neighbors. This is referred as the K-nearest neighbor (KNN) [53]. The target's position is the "averaged" position of the neighbors, weighted by inverse of their relative "CIR distance".

The vector difference between measured CIR and CIR in the database is calculated. The position of the nearest neighbor in the database is reckoned as the target position. For KNN, we like to take into account more neighbors around the nearest neighbor, the estimate of the MS position is the averaged coordinates of the total K neighbors, as in (5.2):

$$\widehat{\mathbf{X}}_T = \frac{\sum_{i=1}^{N} \mathbf{X}_i}{N} \qquad . \tag{5.2}$$

where $\mathbf{X}_i$ $(i = 1, \ldots, N)$ are the N neighbors. Performance achieved by this method is not satisfactory since the relative "CIR distance" has no direct relation with geographical distance.

KNN is a special case of KWNN, with the weight to each neighbor is equal. In KWNN, the MS position is estimated by the weighted average of the coordinates of the K-neighbors (5.3).

$$\widehat{\mathbf{X}}_T = \frac{\sum_{i=1}^{N} w_i \mathbf{X}_i}{\sum_{i=1}^{N} w_i} \tag{5.3}$$

The weight is selected to achieve better performance. In our case the weight is equal to inverse of the CIR vector/matrix distance.

[The above listed methods are not accurate models.] The "CIR distance" between the target and a RP has no simple relation with their geographical distance. The hidden relationship is dominated by the specified radio wave propagation environment. We intend to employ a more powerful tool — support vector machine to learn this hidden relation.

5.3.2   Support Vector Machine

The support vector machine (SVM) is a category of universal feed-forward networks, pioneered by Vapnik [47, p.318]. SVM has been widely applied in pattern classification and nonlinear regression.

We start from classifying a number of l training instances. Each instance consists of a pair: an input vector $\boldsymbol{x}_i \in \mathbb{R}^d$, $i = 1, \cdots, l$ and the associated pattern label y_i, where in a simple case $y_i = 1$ or -1. The task is to construct a hyperplane to separate the positive samples with label $y_i = 1$ from those negative ones with $y_i = 0$. In case of linear SVM, the points $\boldsymbol{x} \in \mathbb{R}^d$ in the hyperplane satisfies $\boldsymbol{w} \cdot \boldsymbol{x} + b = 0$ where $\boldsymbol{w} \in \mathbb{R}^d$ is unknown and normal to the hyperplane. The optimal $\boldsymbol{w}$ and b determine the hyperplane.

The training instances satisfy the following constraints:

$$\boldsymbol{x}_i \cdot \boldsymbol{w} + b \geq +1 \quad for \ y_i = +1 \tag{5.4}$$

$$\boldsymbol{x}_i \cdot \boldsymbol{w} + b \leq -1 \quad for \ y_i = -1 \tag{5.5}$$

Combining the above two equations we have:

$$y_i(\boldsymbol{x}_i \cdot \boldsymbol{w} + b) - 1 \geq 0 \quad \forall i \in 1, 2, \ldots, l \tag{5.6}$$

In pattern classification one key principle is to make the margin of separation between positive and negative examples maximized. It is known that the margin is $2/\|\boldsymbol{w}\|$ [64]. Now the problem is formulated as to minimize $\|\boldsymbol{w}\|$ for inequality constraints in (5.6). This is a constrained optimization problem and solvable by Lagrangian method, where each of the inequality constraints (5.6) is assigned a nonnegative Lagrange multiplier, α_i, $i = 1, \ldots, l \geq 0$.

The Lagrangian is given by:

$$L_P(\boldsymbol{w}, b, \alpha_i) = \frac{1}{2}\|\boldsymbol{w}\|^2 - \sum_{i=1}^{l} \alpha_i[y_i(\boldsymbol{x}_i \cdot \boldsymbol{w} + b) - 1]$$

$$= \frac{1}{2}\|\boldsymbol{w}\|^2 - \sum_{i=1}^{l} \alpha_i y_i(\boldsymbol{x}_i \cdot \boldsymbol{w} + b) + \sum_{i=1}^{l} \alpha_i \tag{5.7}$$

This constructs the primal problem. There is a saddle point with regard to $\boldsymbol{w}$, b and α_i. At the point of optimality,

$$\min_{\boldsymbol{w}, b} \max_{\alpha_i} L_P = \max_{\alpha_i} \min_{\boldsymbol{w}, b} L_P. \tag{5.8}$$

It is more often that the positive and negative samples are mixed together, a non-separable case. To generalize the optimal separating hyperplane algorithm, [65] introduced non-negative slack variables, $\xi_i \geq 0$ for measuring the misclassification errors: for an error to occur, the corresponding ξ_i must exceeds unity. $\sum_i \xi_i$ is an

upper bound on the number of training errors. The constraints in (5.4) and (5.5) are modified for the non-separable case to

$$x_i \cdot w + b \geq +1 - \xi_i \quad for \ y_i = +1 \tag{5.9}$$

$$x_i \cdot w + b \leq -1 + \xi_i \quad for \ y_i = -1 \tag{5.10}$$

$$\xi_i \geq 0 \quad \forall i \tag{5.11}$$

The generalized separating hyperplane is determined by the vector w, that minimize the functional,

$$\Phi(w, \xi) = \frac{1}{2}\|w\|^2 + C\sum_i \xi_i \tag{5.12}$$

where C is a parameter dominating the higher or less penalty to errors.

The *primal* Lagrangian is

$$L_P = \frac{1}{2}\|w\|^2 + C\sum_i \xi_i - \sum_i \alpha_i\{y_i(x_i \cdot w + b) - 1 + \xi_i\} - \sum_i \mu_i \xi_i \tag{5.13}$$

where the α_i and μ_i are the Lagrangian multipliers.

Applying the Karush-Kuhn-Tucker (KKT) conditions for the primal problem, the Wolfe dual problem [66] becomes to maximize

$$L_D = \sum_i \alpha_i - \frac{1}{2}\sum_{i,j} \alpha_i \alpha_j y_i y_j x_i \cdot x_j \tag{5.14}$$

subject to

$$0 \leq \alpha_i \leq C, \tag{5.15}$$

$$\sum_i \alpha_i y_i = 0. \tag{5.16}$$

The solution is given by

$$w = \sum_{j=1}^{N_S} \alpha_j y_j x_j \tag{5.17}$$

where N_S is the number of strict positive elements in the Lagrangian multipliers set: $\alpha_i, \quad i = 1, \ldots, l$. The training instances whose corresponding Lagrangian multiplier are positive are so called "support vectors". They are the critical instances in determining the separating plane.

There is no guarantee that linear decision function can separate instances satis-

factorily. Here comes the most interesting part of SVM, which is to preprocess the data instances to map the attribute space into a higher dimension Euclidean space, $\mathcal{H}$. With an appropriate mapping $\Phi : \mathbb{R}^d \rightarrow \mathcal{H}$ to a sufficiently high dimension, instances from two categories can always be separated by a hyperplane.

Equation (5.14) provides a hint that the algorithm would only depend on two arbitrary instances x_i and x_j through their dot product $x_i \cdot x_j$. This generates a method to rely on $\Phi(x_i) \cdot \Phi(x_j)$ in space $\mathcal{H}$. To be specific, at online estimation stage SVM computes dot products of a new instance x by computing the sign of

$$f(x) = \sum_{i=1}^{N_S} \alpha_i y_i \Phi(s_i) \cdot \Phi(x) + b \qquad (5.18)$$

where the s_i is the support vector.

If a "kernel function" K is defined as $K(x_i, x_j) = \Phi(x_i) \cdot \Phi(x_j)$, we may use the kernel function $K(\cdot)$ in both the training and predicting stages without knowledge of what the explicit form of Φ is:

$$f(x) = \sum_{i=1}^{N_S} \alpha_i y_i K(s_i, x) + b \qquad (5.19)$$

The SVM has been extended to solve regression problem by introducing a loss function [67]. Similar to pattern classification problem, we are given a number of l training samples. Each sample consists of a pair: an input vector $x_i \in \mathbb{R}^d$, $i = 1, \cdots, l$ and the associated label (function value) y_i is not constrained to $\{+1, -1\}$ but can take any arbitrary value. The goal is to find a function $f(x)$ to approximate the relation inherited from the training data set. Loss function $\mathcal{L}(y, f(x))$ is used to evaluate how the estimated value $f(x)$ deviated from the real value y. Many forms for loss function can be found in the literature such as linear, quadratic loss function, exponential, etc. In this chapter, we intend to obtain a sparse set of support vectors and Vapnik's loss function is adopted, which is also known as ϵ-insensitive loss function:

$$\mathcal{L}(y, f(x)) = \begin{cases} 0 & \text{if } |y - f(x)| \leq \epsilon \\ |y - f(x)| & \text{otherwise} \end{cases}$$

where $\epsilon > 0$ is a predefined constant which controls the noise tolerance. The form

of support vector regression [67] algorithm is presented as:

$$\min_{w,b,\xi,\xi^*} \quad \frac{1}{2}w^T w + C\sum_{i=1}^{l}(\xi_i + \xi_i^*)$$

$$subject\ to \quad w^T \Phi(x_i) + b - d_i \leq \epsilon + \xi_i,$$

$$d_i - w^T \Phi(x_i) - b \leq \epsilon + \xi_i^*,$$

$$\xi_i, \xi_i^* \geq 0, \quad i = 1, 2 \ldots, l. \tag{5.20}$$

The dual problem is:

$$\min_{\alpha,\alpha^*} \quad \frac{1}{2}(\alpha - \alpha^*)^T Q(\alpha - \alpha^*)$$

$$+\epsilon \sum_{i=1}^{l}(\alpha_i + \alpha_i^*) + \sum_{i=1}^{l}(\alpha_i - \alpha_i^*)$$

$$subject\ to \quad \sum_{i=1}^{l}(\alpha_i - \alpha_i^*) = 0,$$

$$0 \leq \alpha_i, \alpha_i^* \leq C, i = 1, 2 \ldots, l. \tag{5.21}$$

where the component of Q at the ith row and jth column, $Q_{ij} = K(x_i, x_j) \triangleq \Phi(x_i)^T \Phi(x_j)$. The approximation function is

$$f(x) = \sum_{i=1}^{l}(-\alpha_i + \alpha_i^*)K(x_i, x) + b.$$

In our application, the goal is to learn the properties of a wireless radio wave propagation environment from the data instances in the training set. It requires a high dimensional mapping to learn the complex relation within the pairs of CIR and geographical location. Furthermore, the kernel function encapsulates the inner products of arbitrary two data instances and avoids knowing the mapping explicitly. The most popular four kernels are

- linear: $K(x_i, x_j) = x_i^T x_j$.

- polynomial: $K(x_i, x_j) = (\gamma x_i^T x_j + r)^d, \gamma > 0$.

- radial basis function (RBF): $K(x_i, x_j) = exp(-\gamma)\|x_i - x_j\|^2), \gamma > 0$

- sigmoid: $K(x_i, x_j) = tanh(\gamma x_i^T x_j + r)$.

where γ, r and d are kennel parameters. We note the RBF kernel can handle the nonlinear relation between attributes and regression value due to its nonlinearity.

It is suggested as the first choice in general. There are three parameters while using RBF kernels: C, ϵ and γ. When applying SVM in learning the relation between MS position and CIR vector, it is non-trivial to find appropriate (C, ϵ, γ) such that the machine can accurately predict unknown positions regarding to a testing data instance. The performance of a SVM is measured by its prediction accuracy but not its fitness to training data set. In order to achieve better prediction accuracy and avoid over-fitting, a N-fold cross validation strategy [68] is applied in training our SVM. Namely, the training set is divided into N subsets. Sequentially one subset is tested using the machine trained on the remaining $N-1$ subsets. The training accuracy is accessed by the averaged "prediction" accuracy when each of the N subsects is used as the testing set sequentially.

We use a combinational grid search method to find appropriate (C, ϵ, γ). A coarse search is implemented by the winSVM program [69]. Different kernel types and values of parameters are tried by the program and the corresponding mean square training error are recorded. We select tuples of (C, ϵ, γ) with reasonable small training error as the staring point for the 5-fold cross-validation process. Since C, ϵ and γ are independent, it is possible to do grid-search in parallel which saves much training time. The search record is recorded and the set of parameters with least validation error is taken to train our SVM.

Before starting the training of SVM, it is important to scale the attributes' numerical range for better prediction accuracy. The reasons are similar to those when training Neural Networks, mainly to reduce effect of attributes with large numeric value range on small ones.

5.4   Simulation Setup and Results

We use the *Radiowave Propagation Simulator* (RPS) to implement the algorithms. RPS is a radio coverage and performance planning and automatic optimization system [70] issued by *Radioplan* in Dresden, Germany. It utilises either $3D/2.5D$ ray tracing engine or empirical propagation engine to model radio wave propagation in a wide range of propagation environments, such as in indoor or outdoor, urban or rural areas. RPS provides accurate channel impulse response information such as power attenuation, phase, time delay, azimuth and elevation of incoming or outgoing rays of at a per-path basis at receiver or transmitter.

Before launching the radio propagation simulation, a propagation environment needs to be generated by the integrated environment editor. In our simulation we use a modified urban outdoor environment. The original environment comes with
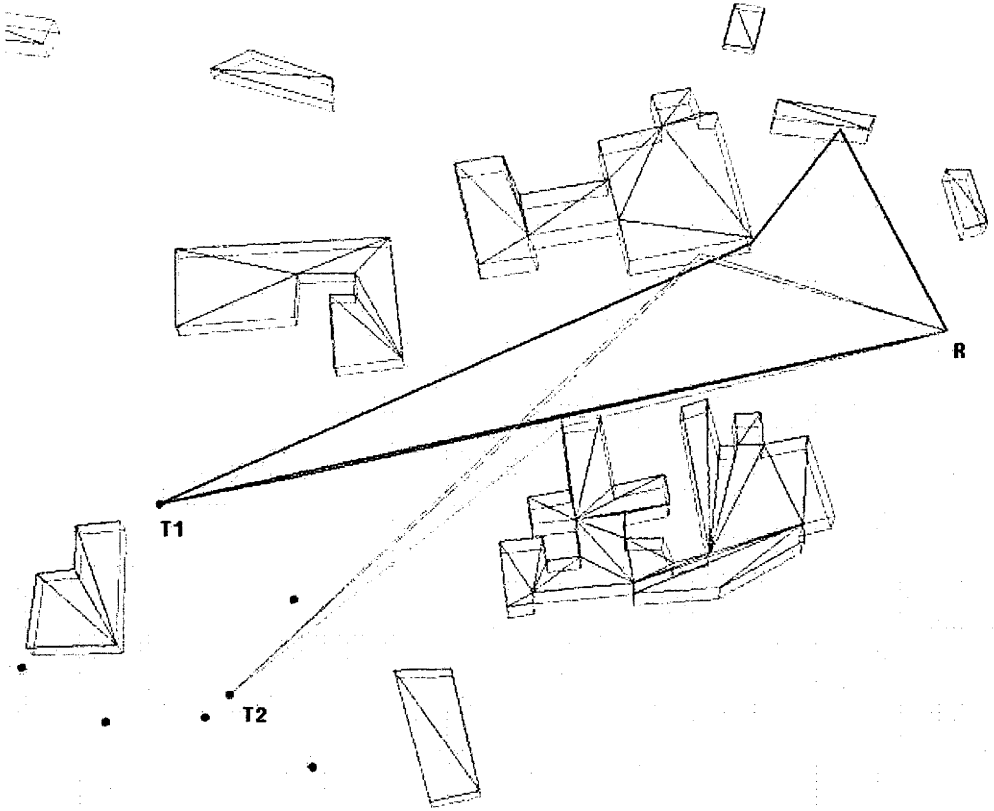
Figure 5.1: RPS Plot

RPS version 5.2 (trial version) example library. The size of the propagation region is $1000 \times 800\ m^2$ with around 30 buildings inside. Part of the simulation environment is shown in Figure 5.1, demonstrating radio wave rays reflected, refracted and diffracted in the environment. There are two emitters (T_1, T_2) and one receiver (R) in this figure. To gather the training data set, the region is separated into square blocks with grid length equal to 20m. At the centre of each block there is a transmitter deployed with isotropical antenna. The transmit power is 33dBm. The receiver is deployed at the up-right part of the area and installed with an isotropic antenna.

We also deploy numerous test points where each CIR vector and its location is gathered. The instance-based algorithms and SVM are applied in analyzing the localisation accuracy.

The error distance is defined as the distance between an estimated position and true position of a test instance. The probability distribution and cumulative distribution of estimation error for the above methods are shown in Figure 5.2 and Figure 5.3. It is shown that the performance of 4NN, 4WNN and SVM have no apparent difference: The average error distances are 53.3m, 43.4m and 49.6m,
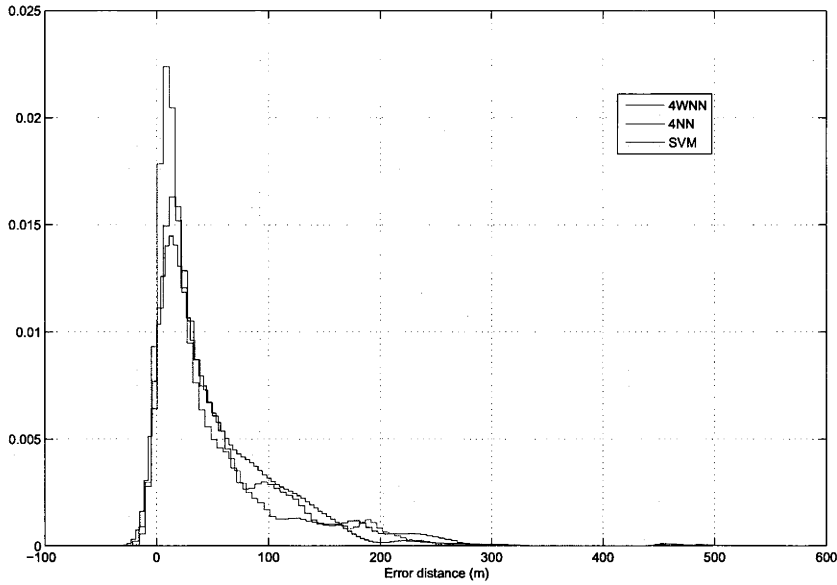
Figure 5.2: Probability distribution of error distance, 4NN stands for 4-nearest neighbor, 4WNN stands for 4-weighted nearest neighbor

respectively. SVM and 4WNN have almost the same 90% error distance, which is around 120m.

5.5   Contributions

The technical contributions of this chapter were:

1. To propose algorithms suitable for locating multiple users in parallel in a fixed wireless network. Unlike methods presented by [25], the pattern matching technology does not need to keep record of the target's moving trajectory while still capable of providing fairly good accuracy.

2. To interpret the inherent reason why SVM only provides similar location accuracy as the general methods. This indicates we cannot have further performance gain from the computational effort we spend in training SVM. To our understanding, this is due to the "small scale" spatial distribution characteristic of CIR, acting as the location signature. "Small scale fading" in wireless wave propagation is well known. Similarly, the parameters of CIR, such as amplitude, DoA and delay, fluctuate rapidly over a short period of geographical distance. Since we use parameters of CIR as the input vector x and the corresponding position as output y, the output hyperplane is a
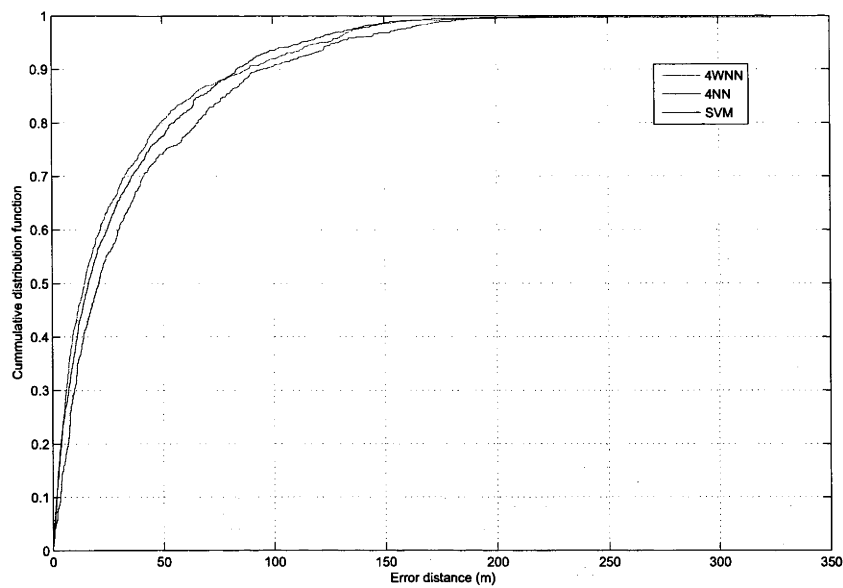
Figure 5.3: umulative distribution of error distance, 4NN stands for 4-nearest neighbor, 4WNN stands for 4-weighted nearest neighbor

non-smooth, or even a nearly discontinuous surface due to the "small scale" characteristic of CIR. This non-smoothness/discontinuity prevents the SVM having better performance than the general KWNN methods. The above also explains the similar performance of KWNN, Bayesian modeling, multi-layer perceptrons and SVM, using radio signal strength as location fingerprint in [53].

Chapter 6

Conclusions

6.1   Summary and Generalization

How to increase location accuracy is the major concern in wireless location research. The multipath propagation nature of wireless waves not only introduces inter-symbol interference to the receiver in a communication system but also brings difficulty in estimating target's location. Many solutions in literature provide limited effect in conquering the location ambiguity caused by multipath.

On the other side, wireless waves arrives in the receiver through different incoming azimuth and elevations in space. This propagation has a wider occupancy of space and therefore has its own spatial diversity compared to less number of arrival paths. This consideration intrigues us to study the unexposed potential beneficiary of multipath on location accuracy. We develop a model for generating random wavefields according to a given angular correlation characteristic which permits a numerical investigation into the effects of correlated incoming wavefield modeling. Not surprising, our numerical results show that richer multipath in a wireless terminal's spatial region can be beneficial to improving the location resolution. To make this conclusion it is critical to satisfy the following conditions:

- the incoming multipaths are correlated in angle;

- and the total energy of wavefields in an aperture-limited receiver region are identical in different richness multipath.

The first condition is a reasonable assumption since in reality multipath waves generated by same scatterer or reflector are correlated to each other. The second is essential in understanding the location accuracy of line-of-sight scenario, which is beyond of the scope of the study of this thesis. The reason is line-of-sight wave has significant more energy than normal multipath waves.

81

To develop a wireless location system practically, we give out a "virtual" radio wave propagation model for predicting the spatial distribution of the radio signal. We proposed an adaptive algorithm to learn this "virtual" environment based on the wireless signal strength measured in actual field measurements. Also, we introduced a Channel Impulse Response (CIR) fingerprint location solution, which takes advantages of the features of fixed wireless network. A practical solution is determined for the location problem using pattern matching technique.

6.2   Future Work

6.2.1   Essential Sensor Number and Sensor Positions for Sampling

One interesting problem is to address the necessary sensor number and positions to have optimal spatial sampling for wavefield coupled to a region. The effect of optimal sampling can be defined in terms of reproducing the coupled wavefield with least error and without significant sensor deployment redundancy. Optimal sampling is vital in wireless communications and/or signal processing. Potential applications include reproduce a 3D high-fidelity sound field, such as a concert, in a most efficient and economical way to let the sensor network to be as simple as possible. The optimal sensor number is addressed in [29] as the problem of numbers of receiver antennas. It is shown the number of critical antennas deployed in a 2D disk region of R is the dimensionality of the region, D_R^{2D}, assuming the antennas are smartly displaced. More antennas are superfluous — that is, they contribute little or no additional information.

6.2.2   Iterative Searching Algorithm

In this thesis we are challenged to solve the problem that how to find the smart positions of the D_R^{2D} sensors in the region of R. We start from a simple case by assuming that scattering from one azimuth is independent from another, namely an angular uncorrelated scatterer gain $A(\phi)$. Consider $Q = D_R^{2D}$ antennas in a region $\|x \le R\|$ at distinct locations $x_1, x_2, \ldots, x_Q$ for snatching up as much information as possible in the multipath field of the region. The Q antennas may be placed in the region randomly without overlapping in the region at the initial stage. We then start an iterative process to find the near-optimal positions of the Q antennas. Let $q_Q^{(i)}$ denote the sensor set of sensors $1, 2, \ldots, Q$ excluding sensor i. The region R is evenly divided into numerous small sections. The central location of each section

is used to mark the section. The number of the sections should be big enough thus the Q antennas stay in Q different sections at least. In every iteration there would Q sub-iterations. We try to find the sub-optimal position of the first antenna in the first sub-iteration. Assume there are totally M sections in the region. The sub-optimal position of the first antenna is searched through the complementary sections occupied by the $q_Q^{(1)}$ antenna set in the total M section space, while keeping the $q_Q^{(1)}$ antennas' position fixed. This means antenna 1 has $M - Q + 1$ potential sub-optimal positions. But, how to justify which position is the best one in the $M - Q + 1$ candidates? A spatial correlation matrix, denoted as $\mathcal{R}$, for the Q antennas is proposed where the element in the ith row and jth column is defined as

$$r_{i,j} = \rho(\boldsymbol{x}_i, \boldsymbol{x}_j) \qquad i, j = 1, 2 \ldots Q \tag{6.1}$$

Every time antenna 1 is moved to a new position/section we will have a matrix $\mathcal{R}$. We calculate the Q eigenvalues and store the summation of them. Once antenna 1 has traveled all the $M - Q + 1$ sections we will have $M - Q + 1$ summation results. The section with the biggest eigenvalue summation is considered as the sub-optimal position of antenna 1 in this sub-iteration. In a similar way all the other antennas' positions are sub-optimised in the first iteration by moving one antenna only during one sub-iteration while keeping all others fixed. The next iteration is simply a repetitive one of the first iteration. This problem is proposed to solve a global convergence problem in our future work.

6.2.3   Tracking Maneuvering Target

Kalman filtering is widely used in tracking linear trajectory with Gaussian noise for its economical calculation complexity. With the development of more powerful embedded computation units, particle filtering is widely adopted for its adaptivity to non-linear state evolution model under non-Gaussian noise environments. We intend to exploit the tracking performance of particle filtering while maintaining the computation complexity relatively low. In detail, we would adopt more realistic dynamic model for the target since current existing models are very limited in describing and predicting target's next position. For example, in indoor WLAN localisation system, particles are constrained to lie within a room. Our new model is designed to solve this problem and borrowed the ideas from Robot Simultaneous Localisation and Mapping. We would study the particle filtering re-sample rate for different radio propagation environment. The purpose for resampling is to remove those particles with a very low weight. However, this causes loss of particle

diversity. This motivates us to do future study on the optimal threshold in deciding when to do resampling.

6.2.4   RSSDM Optimal Updating

One disadvantage of fingerprint location technology is updating the Radio Signal Spatial Distribution Map once the radio propagation environment is changed. In future research we will analyze the optimal updating period and strategy in updating the RSSDM in wireless communication system.

6.2.5   Optimal Spatial Sample Density for Fingerprint Technology

Fingerprint location requires large amount of sample points for reliable localisation accuracy, especially in high dense multipath propagation environment. However, there is performance improvement ceil as the the sample density increases. This motives our future research to discover the relationship between sample density and location accuracy. According to our understanding, this issue is related with the radio signal spatial distribution. The spatial varying rate dominates the best sampling rate.

Bibliography

[1] J. Caffery and G. Stüber, "Vehicle location and tracking for IVHS in CDMA microcells," in *IEEE Personal Indoor Mobile Radio Conference*, 1994.

[2] J. J. Caffery and G. Stüber, "Subscriber location in CDMA cellular networks," *IEEE Transactions on Vehicular Technology*, vol. 47, pp. 406–416, May 1998.

[3] G. Sun, J. Chen, W. Guo, and K. J. R. Liu, "Signal processing techniques in network-aided positioning," *IEEE Signal Processing Mag.*, vol. 22, no. 4, pp. 12–23, July 2005.

[4] J. J. Caffery and G. Stüber, "Overview of radiolocation in CDMA cellular systems," *IEEE Commun. Mag.*, vol. 36, no. 4, pp. 38–45, Apr. 1998.

[5] C. Drane, M. Macnaughtan, and C. Scott, "Positioning GSM telephones," *IEEE Commun. Mag.*, vol. 36, no. 4, pp. 46–54, Apr. 1998.

[6] Y. Zhao, "Standardization of mobile phone positioning for 3G systems," *IEEE Commun. Mag.*, vol. 40, pp. 108–116, Jul. 2002.

[7] J. J. Liberti and T. Rappaport, *Smart Antenna for Wireless Communications: IS-95 and Third Generation CDMA Applications*. Upper Saddle River, NJ: Prentice Hall PTR, 1999.

[8] H. Krim and M. Viberg, "Two decades of array signal processing research: The parametric approach," *IEEE Signal Processing Mag.*, vol. 13, no. 4, pp. 67–94, July 1996.

[9] M. Williams, G. Dickins, R. A. Kennedy, and T. D. Abhayapala, "Spatial limits on the performance of direction of arrival estimation," in *Proc. 6th Australian Communication Theory Workshop AusCTW05*, vol. 40, Feb. 2005, pp. 175–179.

[10] P. Bahl and V. N. Padmanabhan, "Radar: An in-building RF-based user location and tracking system," in *IEEE Infocom.*, vol. 2, Mar. 2000, pp. 775–784.

[11] P. Bahl, V. N. Padmanabhan, and A. Balachandran, "Enhancements to the radar user location and tracking system," Microsoft, Tech. Rep. MSR-TR-00-12, Feb. 2000.

[12] M. Brunato and K. K. Csaba, "Transparent location fingerprinting for wireless services," in *in Proceedings of Med-Hoc-Net 2002*, 2002.

[13] J. Krumm and J. Platt, "Minimizing calibration effort for an indoor 802.11 device location measurement system," Microsoft, Tech. Rep. MSR-TR-2003-82, Nov. 2003.

[14] J. Abel and J. Smith, "Source range and depth estimation from multipath range difference measurements," *IEEE Transactions on Acoustics, Speech, and Signal Processing*, vol. 37, no. 8, pp. 1157–1165, Aug. 1989.

[15] W. H. Foy, "Position-location solutions by Taylor-series estimation," *IEEE Trans. Aerosp. Electron. Syst.*, vol. AES-12, pp. 187–194, Mar. 1976.

[16] Y. Chan and K. Ho, "A simple and efficient estimator for hyperbolic location," *IEEE Trans. Signal Processing*, vol. 42, no. 8, pp. 1905–1915, August 1994.

[17] J. J. Caffery Jr., "A new approach to the geometry of TOA location," in *IEEE Vehicular Technology Conference Fall, 52nd*, vol. 4, Sep. 2000, pp. 1943–1949.

[18] J. Mendel, *Lessions in Estimation Theory for Signal Processing, Communications, and Control.* New Jersey, USA: Prentice Hall, 1995.

[19] S. Al-Jazzar and J. Caffery, "Ml and bayesian toa location estimators for NLOS environments," in *IEEE Vehicular Technology Conference Fall, Vancouver, BC*, vol. 1, Sep. 2002, pp. 316–320.

[20] E. D. D. Claudio, R. Parisi, and G. Orlandi, "A clustering approach to multi-source localization in reverberant rooms," in *Proc. of the First IEEE Sensor Array and Multichannel Signal Processing Workshop*, Boston Marriott Cambridge, Cambridge, MA, USA, 2000, pp. 198 – 201.

[21] D. B. Ward, E. A. Lehmann, and R. C. Williamson, "Particle filtering algorithms for tracking an acoustic source in a reverberant environment," *IEEE Trans. Speech Audio*, vol. 11, no. 6, pp. 826 – 836, 2003.

[22] S. S. Woo, H. R. You, and L. S. Koh, "The NLOS mitigation technique for postition location using IS-95 CDMA networks," in *Proc. IEEE Veh. Technol. Conf.*, vol. 4, Feb. 2000, pp. 2556–2560.

[23] X. Wang, Z. Wang, and B. O'Dea, "A TOA-based location algorithm reducing the errors due to non-line-of-sight (NLOS) propagation," in *Proc. IEEE Veh. Technol. Conf.*, vol. 1, no. 54, 2001, pp. 97–100.

[24] J. Riba and A. Urruela, "A non-line-of-sight mitigation technique based on ML detection," in *Proc. International Conference on Acoustics, Speech and Signal Processing (ICASSP)*, Montreal, Quebec, Canada, May 2004, pp. 153–156.

[25] T. Nypan, K. Gade, and O. Hallingstad, "Vehicle positoning by database comparison using the box-cox metric and kalman filtering," in *VTC Spring*, AL, USA, May 2002.

[26] T. Rappaport, *Wireless Communications, Principles and Practice*, 2nd ed. Upper Saddle River: Prentice Hall, 2002.

[27] H. M. Jones, R. A. Kennedy, and T. D. Abhayapala, "On dimensionality of multipath fields: spatial extent and richness," in *Proc. IEEE International Conference on Acoustics, Speech and Signal Processing*, vol. III, 2002, pp. 2837–2840.

[28] R. A. Kennedy and T. D. Abhayapala, "Spatial concentration of wave-fields: Towards spatial information content in arbitrary multipath scattering," in *Proc. 4th Australian Communications Theory Workshop, AusCTW'2003*, Melbourne, Feb. 2003, pp. 38–45.

[29] R. A. Kennedy, P. Sadeghi, T. D. Abhayapala, and H. Jones, "Intrinsic limits of dimensionality and richness in random multipath fields," *IEEE Trans. Signal Processing*, 2007 (to appear).

[30] D. Colton and R. Kress, *Inverse Acoustic and Electromagnetic Scattering Theory*, 2nd ed. Berlin, Germany: Springer-Verlag, 1998.

[31] L. J. Ziomek, *Fundamentals of Acoustic Field Theory and Space-Time Signal Processing*. Boca Raton: CRC Press, 1995.

[32] N. McLachlan, *Bessel Functions for Engineers*, 2nd ed. London: Oxford Univeristy Press, 1961.

[33] P. Teal, T. D. Abahayapala, and R. Kennedy, "Spatial correlation for general distribution of scatterers," *IEEE Signal Processing Letter.*, vol. 9, no. 10, pp. 305–308, Oct. 2002.

[34] K. Pedersen and B. Fleury, "A versatile spatio-temporal correlation funciton for mobile fading channels with non-isotropic scatterers," in *Proc. IEEE Workshop Statistical Signal Processing*, Pocono Manor, PA, 2000, pp. 58–62.

[35] C. Meyer, *Matrix Analysis and Applied Linear Algebra.* Philadelphia, USA: SIAM: Society for Industrial and Applied Mathematics, 2000.

[36] J. Beran, *Statistics for Long-Memory Processes.* New York, NY: CHAPMAN & Hall, 1994.

[37] Z. Chen, H. L. Bertoni, and A. Delis, "Progressive and approximate techniques in ray-tracing-based radio wave propagation prediction models," *IEEE Transactions on Antennas and Propagation*, vol. 52, no. 1, pp. 240–251, Jan. 2004.

[38] S. Y. Seidel, T. S. Rappaport, S. Jain, M. L. Loar, and R. Singh, "Path loss, scattering, and multipath delay statistics in four european cities for digital cellular and microcellular radiotelephone," *IEEE Trans. Veh. Technol.*, vol. 40, pp. 721–730, Jan. 1991.

[39] G. L. Turin, F. D. Clapp, T. L. Johnston, S. B. Fine, and D. Lavry, "A statistical model of urban multipath propagation," *IEEE Trans. Veh. Technol.*, vol. 21, pp. 1–9, Feb. 1972.

[40] F. Ikegami, T. Takeuchi, and S. Yoshida, "A theoretical prediction of mean field strength for urban mobile radio," *IEEE Trans. Antennas Propagat.*, vol. 39, pp. 299–302, Mar. 1991.

[41] R. A. Serway, *Physics for Scientists and Engineers, with Modern Physics*, 3rd ed. New York, USA: Saunders College Publishing, 1992.

[42] S. Coco, A. Laudani, and L. Mazzurco, "A novel 2-d ray tracing procedure for the localization of EM field sources in urban environment," *IEEE Transactions on Magnetics*, vol. 40, no. 2, pp. 1132–1135, Mar. 2004.

[43] S. J. Fortune, D. H. Gay, B. W. Kernighan, O. Landron, R. A. Valenzuela, and M. Wright, "WiSE design of indoor wireless systems: Practical computation and optimization," *IEEE Comput. Sci. Eng.*, vol. 2, pp. 58–68, Mar. 1995.

[44] P. D. Teal and R. A. Kennedy, "Bounds on extrapolation of field knowledge for long-range prediction of mobile signals," *IEEE Trans. Wireless Commun.*, vol. 3, no. 2, pp. 672–676, Mar. 2004.

[45] J. G. Proakis, *Digital Communications*, 2nd ed. New York, USA: Computer Science Series, McGraw-Hill, 1989.

[46] B. Sklar, "Rayleigh fading channels in mobile digital communication systems part i: Characterization," *IEEE Commun. Mag.*, pp. 93–103, July 1997.

[47] S. Haykin, *Neural Networks: A Comprehensive Foundation*, 2nd ed. Upper Saddle River, NJ, USA: Prentice-Hall, 1999.

[48] "Related sites on neural networks and machine learning," University of Florence. [Online]. Available: http://www.dsi.unifi.it/neural/w3-sites.html

[49] D. Jiang and J. Wang, "A recurrent neural network for on-line design of robust optimal filters," *IEEE Transactions on Circuits and Systems - Part I: Fundamental Theory and Applications*, vol. 47, no. 6, pp. 921–926, 2000.

[50] ——, "On-line learning of dynamic systems in the presence of model mismatch and disturbance," *IEEE Transactions on Neural Networks*, vol. 11, no. 6, pp. 1272–1283, 2000.

[51] R. Battiti, R. Battiti, T. L. Nhat, T. L. Nhat, R. Villani, and R. Villani, "Location-aware computing: a neural network model for determining location in wireless lans," Technical Report DIT-5, Universita di Trent, Tech. Rep., 2002.

[52] X. Nguyen, M. Jordan, and B. Sinopoli, "A kernel-based learning approach to ad hoc sensor network localization," *ACM Transactions on Sensor Networks (TOSN)*, vol. 1, no. 1, pp. 134–152, 2005.

[53] R. Battiti, M. Brunato, and A. Villani, "Statistical learning theory for location fingerprinting in wireless LANs." [Online]. Available: http://citeseer.ist.psu.edu/battiti02statistical.html

[54] A. J. Motley and J. M. P. Keenan, "Personel communication radio coverage in buildings at 900 MHz and 1700 MHz," *Electronics Letters*, vol. 24, no. 12, pp. 763–764, 1988.

[55] "Orinoco 11b-pcard technical report." [Online]. Available: http://www.proxim.com/products/wifi/client/11bpccard/index.html

[56] D. Gibson, "Orinoco driver, technical report." [Online]. Available: http://ozlabs.org/people/dgibson/dldwd/

[57] J. Tourrilhes, "Orinoco information, technical report." [Online]. Available: http://www.hpl.hp.com/personal/Jean_Tourrilhes/Linux/Orinoco.html

[58] P. Roskin, "Scanning patch for v.13-d, technical report." [Online]. Available: http://www.hpl.hp.com/personal/Jean_Tourrilhes/Linux/Orinoco.html

[59] J. Tourrilhes, "Wireless tools for linux, technical report." [Online]. Available: http://www.hpl.hp.com/personal/Jean_Tourrilhes/Linux/Tools.html

[60] Z. Shen, J. Andrews, and B. Evans, "Short range wireless channel prediction using local information," in *The Thirty-Seventh Asilomar Conference on Signals, Systems and Computers*, vol. 1, Nov. 2003, pp. 1147–1151.

[61] J. Tourrilhes, "Introduction to monte carlo methods, computational science education project." [Online]. Available: http://csep1.phy.ornl.gov/mc/mc.html

[62] E. S. Skafidas, T. Pollock, C. A. Liu, and K. Saleem, "Proposed channel model and measurements," IEEE P802.15 Wireless Personal Area Networks Standards.

[63] T. M. Mitchell, *Machine Learning*. USA: Computer Science Series, McGraw-Hill, 1997.

[64] C. J. C. Burges, "http://www.springerlink.com/content/q87856173126771q/A Tutorial on Support Vector Machines for Pattern Recognition," *Data Mining and Knowledge Discovery*, vol. 2, no. 2, pp. 121–167, Jun. 1998.

[65] C. Cortes and V. Vapnik, "http://www.springerlink.com/content/k238jx04hm87j80g/Suppo Vector Networks," *Machine Learning*, vol. 20, no. 3, pp. 273–297, Sep. 1995.

[66] R. Fletcher, *Practical Methods of Optimization*, 2nd ed. John Wiley and Sons, Inc., 1987.

[67] V. Vapnik, *Statistical Learning Theory*. New York, NJ, USA: Wiley, 2001.

[68] C.-W. Hsu, C.-C. Chang, and C.-J. Lin, "A practical guide to support vector classification." [Online]. Available: http://www.csie.ntu.edu.tw/ cjlin/libsvm/

[69] M. Sewell, http://www.cs.ucl.ac.uk/staff/M.Sewell/winsvm/, 2005.

[70] Radioplan, "RPS User Manual 5.2."